REAL-TIME CONTROL AND VIBRATIONS ANALYSIS OF A COMPLETELY AUTOMATED MINIATURIZED RIG

A Thesis

by

ENRIQUE ZARATE LOSOYA

Submitted to the Office of Graduate and Professional Studies of
Texas A&M University
in partial fulfillment of the requirement for the degree of

MASTER OF SCIENCE

Chair of Committee,	Eduardo Gildin
Co-Chair of Committee,	Samuel Noynaert
Committee Members,	Prabhakar Pagilla
Head of Department,	A. Daniel Hill

December 2016

Major Subject: Petroleum Engineering

ABSTRACT

Drilling Automation has become an important research effort in the Oil and Gas Industry since the fall of Oil prices in 2008. The cyclical nature of our industry and the fierce competition is pushing operators and drilling service companies to either be more efficient, or fade.

A miniaturized autonomous drilling machine was built for the Society of Petroleum Engineering – (SPE) DSATS 2016 Drillbotics™ International Competition with the objective of performing optimal operations in terms of rate of penetration and energy efficiency. The miniaturized rig uses state-of-the-art sensors, control algorithms, and innovative instrumentation solutions, leading to a significant amount of data to be analyzed in real-time. High-frequency data was acquired using LabVIEW and analyzed in real-time using the MATLAB programming environment. The results of the analysis are used in a closed-loop control algorithm to optimize the rate of penetration, energy efficiency and mitigate drilling equipment failures. Using real-time instrumentation data an automated step-test procedure was implemented to optimize drilling parameters on the fly. Remote control and surveillance is possible through an in-house developed web server and smartphone app. During the initial testing phase, vibration-induced dysfunctions were mitigated and a 110% rate of penetration improvement was observed compared to initial tests. In addition, control structure was enhanced with stand-alone micro controller driven controllers that improved weight on bit (WOB) and RPM control accuracy by 305%.

To God, my little sisters Jessica, Jocelyn, Gaby and to my beloved parents.

You have raised us throughout times of hardship but never gave up the hope of a better future. Your selfless acts are the real source of my conviction and impulse. Even in the distance, you supported me with prayers and reassuring words that gave me the strength to make this illusion a reality. I'm profoundly grateful for everything you have committed to us.

I also dedicate this thesis to every person that has placed their trust and love in me.

ACKNOWLEDGMENTS

I would like to thank my advisors Dr. Eduardo Gildin and Dr. Samuel Noynaert for their willingness, insight, and sharpness. The assistance and mentorship of Dr. Eduardo Gildin who has always been welcoming and available to answer my inquiries. Working within his research group at Texas A&M University has been an amazingly enjoyable experience.

I was very lucky to have excellent advisors. I would also like to extend my gratitude to Dr. Sam Noynaert, for being so involved in the project and provide invaluable suggestions and insight. Also, I would like to thank Dr. Pagilla his patience and for teaching me control theory through is excellent graduate level course.

Lastly, I thank everyone that was involved in the development of this project, my teammates Revanth Dusi & Mengke Liu for their hard work and commitment. Prof. Fred Dupriest for his invaluable input on drilling limiters. Mr. Maldonado for his dedication and support through the project. Dr. Won-Jong Kim for accepting me under his guidance over the Summer of 2014, an experience that ultimately led me to pursue a Graduate Degree. David Brooks from Pason Systems for going above and beyond with his interest and support. Fred Florence from RigOps for his resolute support towards drilling automation. My office mates for creating an excellent work environment and Francisco Coral for every long conversation and support while living away from our families.

CONTRIBUTORS AND FUNDING SOURCES

This work was supervised by a thesis committee consisting of Professors Dr. Eduardo Gildin [advisor] and Dr. Samuel Noynaert [co-advisor] of the Department of Petroleum Engineering and Dr. Prabhakar Pagilla of the Department of Mechanical Engineering. Funding for research expenditures was provided by the Department of Petroleum Engineering at the Dwight Look College of Engineering in Texas A&M University.

The MATLAB® code used for the analyses depicted in section 3.2 were conducted in part by Revanth Dusi of the Department of Industrial Engineering in collaboration with Mengke Liu of the Department of Mechanical Engineering. All other work for the thesis was completed by the student.

This work was made possible in part by the Mexican National Council of Science and Technology (CONACYT) under Grant number 572036/400250. Its contents are solely the responsibility of the author and do not necessarily represent the official views of the Mexican National Council of Science and Technology.

NOMENCLATURE

WOB	Weight On Bit
ROP	Rate of Penetration
RPM	Revolutions Per Minute
MSE	Mechanical Specific Energy
DOC	Depth Of Cut
MPD	Managed Pressure Drilling
BHA	Bottom-Hole Assembly
MWD	Measurement While Drilling
PDC	Polycrystalline Diamond Compact
NI	National Instruments
cDAQ	Compact Data Acquisition
VI	Virtual Instrument
DAC	Digital Analog Converter
BLE	Bluetooth Low Energy
GATT	Generic Attribute Profile
SPE	Society of Petroleum Engineers
DSATS	Drilling Systems Automation Technical Section
IADC	International Association of Drilling Contractors

LOA	Levels Of Automation
P_{Hy}	Hydrostatic Pressure
V	Voltage
I	Current
K	Controller Gain
τ	Torsional Stress
I_p	Polar Moment of Inertia
ω_n	Natural Frequency
ζ	Damping Ratio
Ω	Electrical Resistance in Ohms
SISO	Single Input Single Output
PID	Proportional Integral Derivative
PWM	Pulse Width Modulation
IC	Integrated Circuit
OP-AMP	Operational Amplifier
I^2C	Inter-Integrated Circuit Protocol
SoC	System On a Chip
UUID	Universally Unique Identifier
RSSI	Received Signal Strength Indicator
HSE	Health, Safety and Environment

f_n	Natural Frequency
T_g	Braking Torque
PHP	Hypertext Preprocessor
CSS	Cascading Style Sheets
HTML	HyperText Markup Language
CSV	Comma Separated Value
API	Application Program Interface
AI-AO	Analog Input or Output
DI-DO	Digital Input or Output
MOSFET	Metal–Oxide–Semiconductor Field-Effect Transistor
TRIAC	Triode for Alternating Current
DHC	Doghouse Computer
DHC WKSTN	Doghouse Computer Workstation

TABLE OF CONTENTS

LIST OF FIGURES

LIST OF TABLES

1 INTRODUCTION AND LITERATURE REVIEW

1.1 Introduction

Automation adoption in our industry has been behind other industries where the automation track has proved positive improvements. Several operators and service companies have expressed the need for an uptake in drilling systems automation since they see an alternative to handle the uncertainties in the current price scenario. The word automation was mentioned in more than half of the technical talks presented at the last 2016 SPE Drilling Conference in Fort Worth. The Society of Petroleum Engineers' Drilling Systems Automation Technical Section is pushing the edges to make robust automation a reality in the next ten years [1].

Since 1960 to date there have been around 43,000 patents awarded to individuals within the Oil and Gas industry. However, this number looks pale when knowing that it is the same amount of patents in the telecommunication industry awarded just over the 2015 fiscal year. The need to adopt or develop new technological devices for automation is remarkable.

Drilling automation in the Oil & Gas industry has been a topic of interest for several years from the first coined "systems concept" approach to building drilling rigs e.g. electrical, hydraulic and electronics systems [2] to advanced machine learning and artificial Intelligence drilling advisory systems [3]. An accelerating pace of change in the industry, coupled with exponential growth in computer power

and efficiency per calculation [4], along with new data analysis techniques over the last decade will inevitably lead us to the advent of fully automated drilling systems.

The profitability of any development depends on the price of a barrel of oil, the costs of and productivity of new wells. Drilling a well is considered to be one of the most expensive operations within the Oil and Gas Industry. Thus, any gain in efficiency is crucial under tight economic conditions. According to a U.S. Energy Information Administration study on upstream costs from March 2016 [5], the average drilling and completions cost per well in five onshore areas in the U.S. were up to 30% below than the mean in 2012 when they were at its highest point over the last decade at $8.5 million. A keen interest in drilling automation as a viable technology to keep this efficiency gain trend is seen today as the industry is operating on narrower economic margins since the fall of the oil prices in 2014 as shown in Fig. 1.1. This thesis proves that Automation of the drilling operation is technically and technological feasible, by providing an example of a completely automated lab-scale drilling rig that implements real-time data analysis and optimization algorithms.

1.2 A Brief History of Drilling Automation

Automation in the oil and gas industry have been aimed mostly towards the mechanization of discrete drilling processes such as rotary speeds, weight on bit, and pipe-handling control. Eustes highlights relevant early work at automating drilling operations. Drilling automation started with the invention of the first rotat-

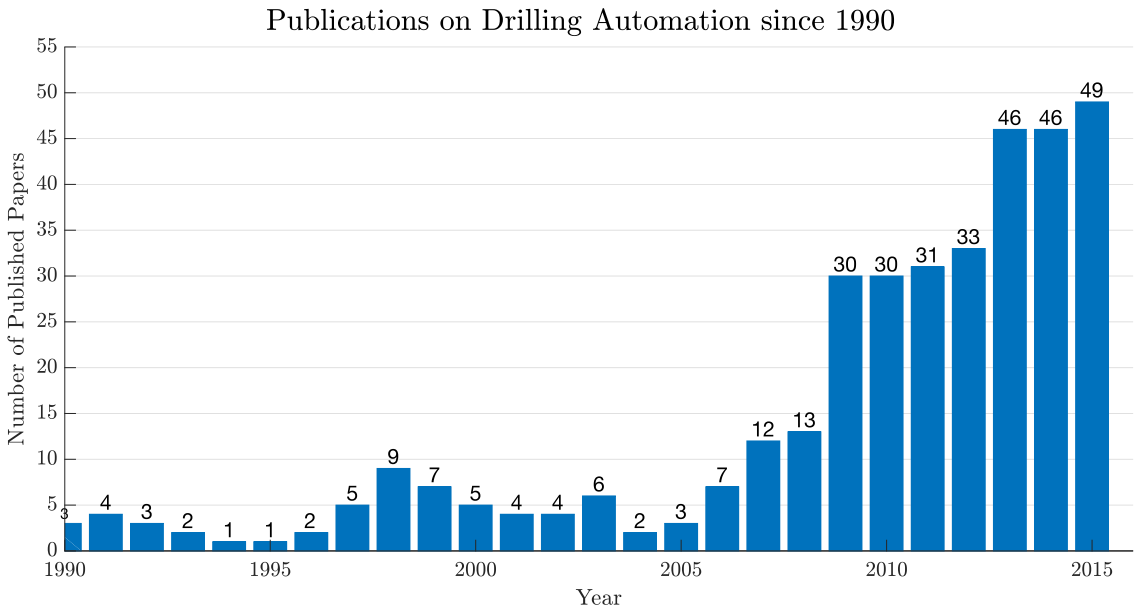

Figure 1.1: Published papers on drilling automation since 1990. *Data from OnePetro.org*

ing diamond bit feed system used for drilling tunnels by Rodolphe Leschot of Frace in 1860 [6]. The notion of weight on bit as we know it today was proposed in 1923 as noted by the patent filed by Hild Frederic W in 1927 [7]. However, its importance became popular within the industry until late 1927 as many other inventors and companies started to improve the performance of several draw-works designs which began from rudimentary metallic breaks, replaced by hydraulic-controlled machines followed by pneumatic, and electrical systems.

Today's draw-works systems are usually electronically controlled AC or DC motors with a gearbox design, sometimes coupled with an electro-hydraulic system. Recent advances on Variable Frequency Drives (VFD) and Permanent Magnet (PM) or Brushless motor drives [8] has led to the rise of such technologies within the

industry due to its improved efficiency, precision, and controllability. This change is univocally beneficial for Drilling Automation as the further reliability and repeatability of an operation the "*easier*" is to implement an automated system to perform it.

One remarkable example of an early computer controlled system developed for the drilling industry was done in 1969 [9]. The system ran on a $28,500 USD 3C DDP-16 16-bit minicomputer with limited processing performance with a memory size of 4k and a speed of 0.240 million instructions per second (MIPS). [10], which was blazingly fast at the time but pale to the 238,310 MIPS of a modern high-end personal computer and the 100 MIPS of a cheap microcontroller like the $8.3 USD 32-bit ARM® Cortex® -M3 RISC [11] . Computer-controlled systems have become a norm in industrial applications. Current common solutions include Industrial Control Systems (ICS), Supervisory Control and Data Acquisition (SCADA), Distributed Control Systems (DCS) and programmable logic controllers (PLC). In 1983, Varco designed and developed its Derrick Drilling Machine which was introduced to the market a year later. This invention is now commonly known as a TopDrive System. A summary is described in Section 1.3.

A conceptual development on an offshore rig was achieved by Japan Ocean Industries in the early 90s. The company field-tested some prototypes of improved mud pulse MWD, pipe handling, and top drive systems. [12]. Although the machine was never completed and tested offshore, it lay down the foundations

of what is now a common modern drilling rig setup in the Industry. A timeline showing the most remarkable achievements of automation in the Oil and Gas Industry is shown in Fig. 1.2 and 1.3.

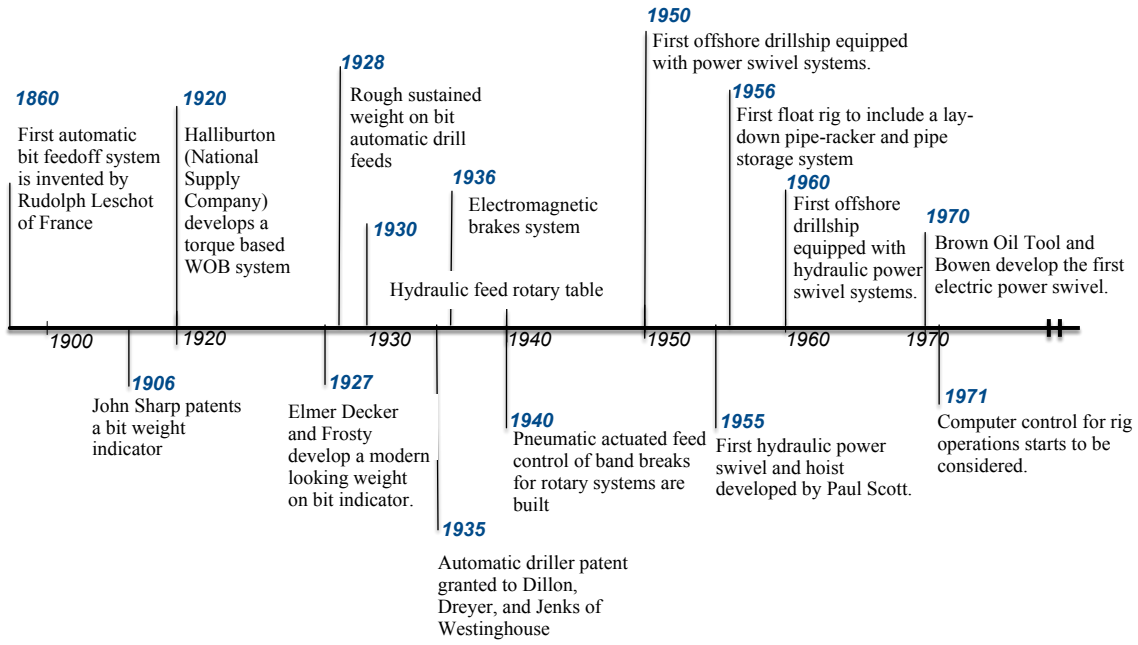

Figure 1.2: Advances on drilling automation timeline

The modern Rotary Steerable System (RSS) was developed in 1995 replacing mud motors as the best choice for directional drilling. Rotating while building curve was now possible, with the advent of measuring while drilling tools (MWD) and downhole to surface communication via mud-pulse telemetry, directional drilling became more affordable and safer. A significant increase in horizontal wells activity was seen in 1996. Today, the industry relies on this technology to access previously inaccessible formations.

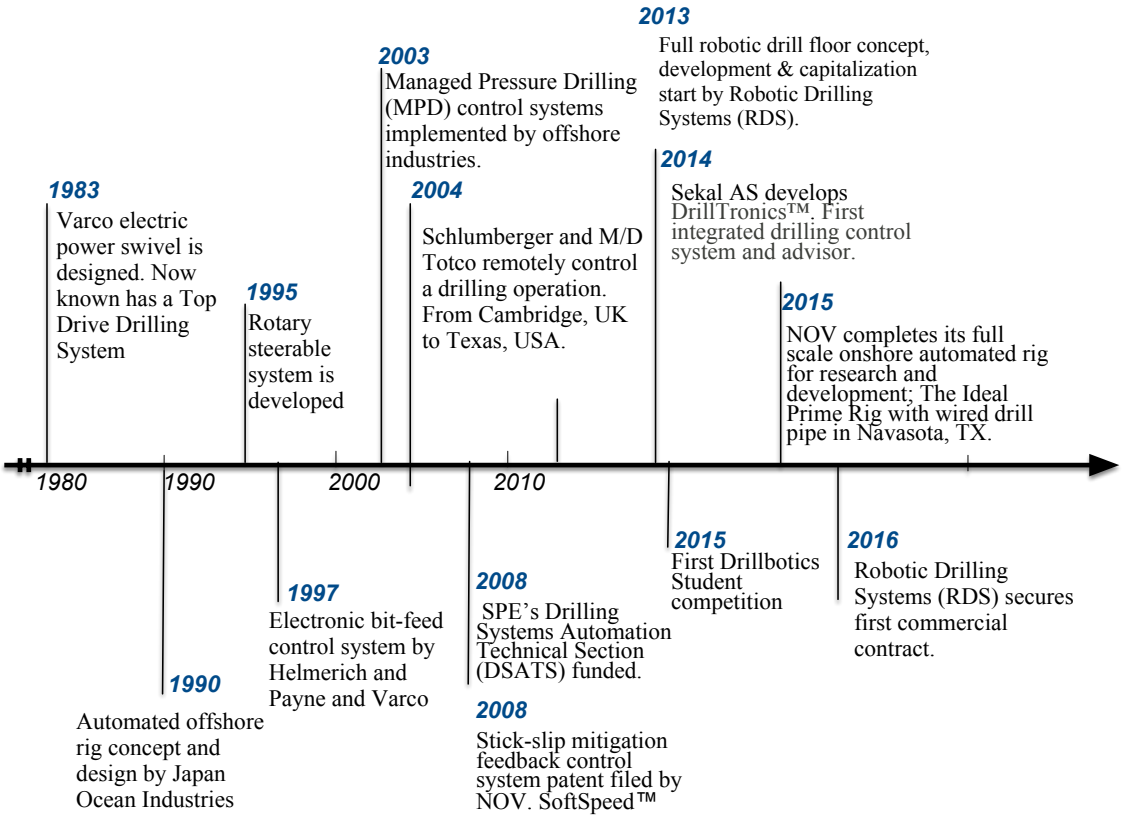

Figure 1.3: Advances on drilling automation timeline, continued.

Over the last twenty years, some of the most successful industry examples of autonomous systems are the TopDrive, Managed Pressure Drilling and SoftSpeed™ systems. A description of such systems is given in Chapter 1.3 . Followed by the current challenges and initiatives to encourage drilling automation adoption in our industry (1.6) and future development (1.5).

1.3 Successful Automated Systems in the Drilling Industry

A basic description of some of the most successful automated systems currently used in our Industry will be briefly discussed in this subchapter as each major technology deserves a complete document on its own.

Managed Pressure Drilling

The official technical definition given by the International Association of Drilling Contractors (IADC) is as "*An adaptive drilling process used to precisely control the annular pressure profile throughout the wellbore. The objectives are to ascertain the downhole pressure environment limits and to manage the annular hydraulic pressure profile accordingly*".

MPD technology is usually applied offshore, where more complex extended reach wells and formation pressures regimes are found.

Traditional drilling techniques control the hydrostatic pressure regime of the well to avoid taking an influx into the wellbore or breaking the formation by controlling the Equivalent Circulating Density (ECD) which is the effective mud

density as a function of the mud rheology and annular friction pressure losses. Hence, the Bottom Hole Pressure (BHP) must be greater than the formation pore pressure but lower than the fracture pressure for a given depth. Drillers often use the term 'The Drilling Window' or for this relationship. Narrow 'Drilling Windows' wells are challenging to drill if not impossible. The operating windows for current technologies are shown in Fig. 1.4.

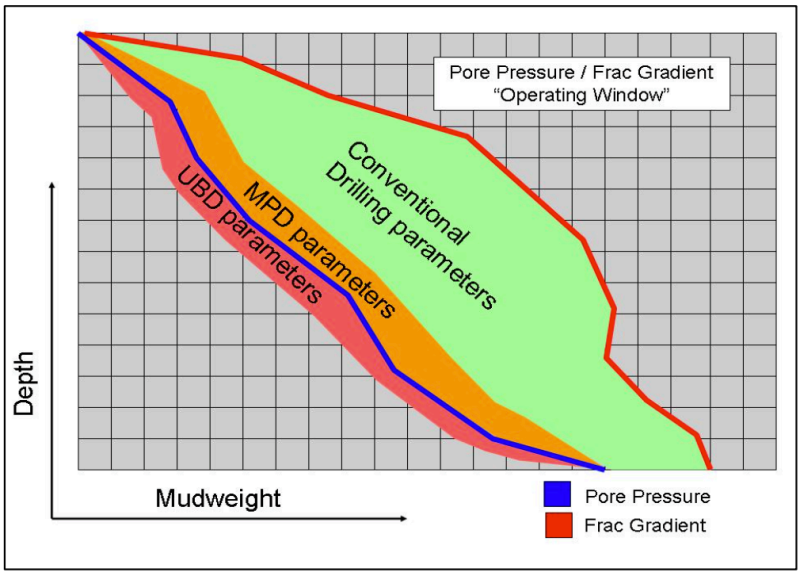

Figure 1.4: Drilling windows *after [13]*

Using traditional drilling practices the Bottom Hole Pressure (BHP) is determined by:

$$BHP = \begin{cases} P_{Hy} + ECD & \text{when circulating} \\ P_{Hy} & \text{under static conditions} \end{cases} \tag{1.1}$$

A MPD system completely isolates the wellbore from surface conditions, creating a controlled atmosphere for the complete annulus. A closed-loop system is continuously measuring pressures and depth to control a surface choke or rotating control device that adjusts the flow rate and pressure of the entire wellbore. Thus, adding a back pressure term to Eq. 1.3 so that the BHP is given by:

$$BHP = \begin{cases} P_{Hy} + ECD + Backpressure & \text{when circulating} \\ P_{Hy} + Backpressure & \text{under static conditions} \end{cases} \tag{1.2}$$

An excellent detailed description of each variant is found in *Mæland [14]*. There are four major variants of MPD:

- HSE method or Return Flow Control (RFCD)
- Constant Bottom Hole Pressure Profile (CBHP)
- Mud Cap Drilling (MCD)
- Dual Gradient Drilling (DGD)

MPD systems dynamically adjust the backpressure term to compensate for any frictional pressure loss, i.e., when making connections. The system allows drilling under very narrow drilling windows so that ambitious extended reach wells become feasible under better safety conditions as well as improving well completion time by reducing the required number of casing sets. Advanced MPD systems include kick detection, mud density instrumentation, and advisory systems. However, the minimum necessary equipment for a MPD system remains the same which is usually

composed of a variable choke, pressure transducers and a controller implemented on a PLC device, as shown in Fig. 1.5.

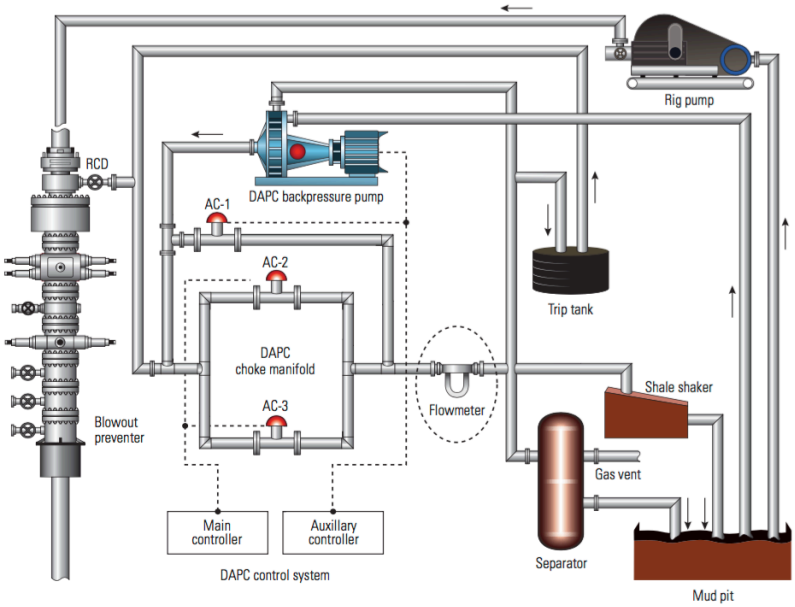

Figure 1.5: Managed pressure drilling system diagram.
From Dave 2011[15]

The Top Drive System

The Top Drive system is considered to be one of the most revolutionary technology in the Oil and Gas industry since the invention of the rotary table [18]. The system replaces the kelly and rotary table of previous rigs designs. It is composed of several electric motors coupled with some hydraulic mechanisms to automatically connect stands; modern top drive systems use DC or VFD AC motors, which makes it compatible with advanced controllers to mitigate Stick-slip such as SoftSpeed ™. In addition to providing the rotary force for drilling. A TopDrive system has the following advantages:

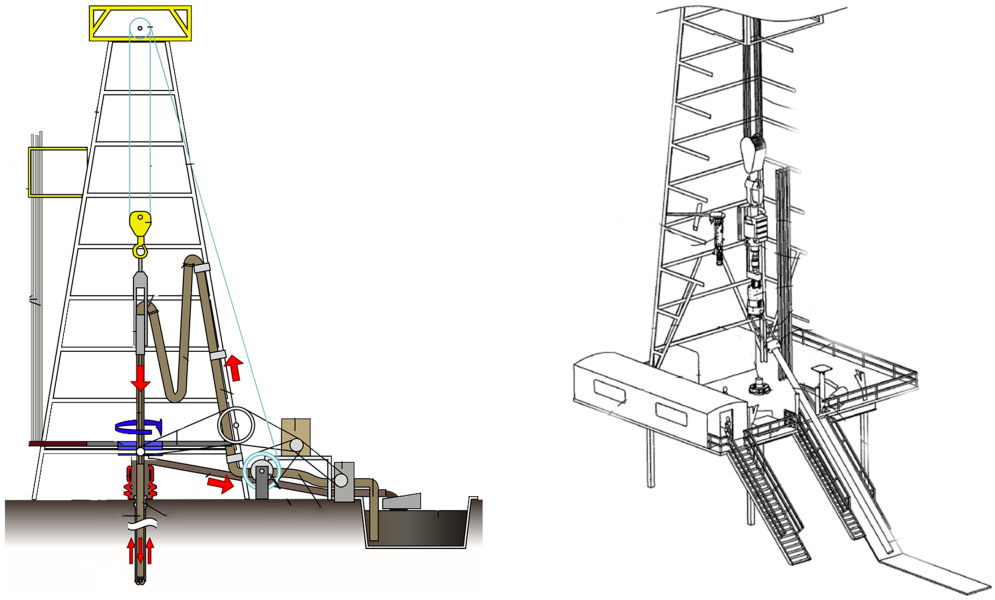

Figure 1.6: Kelly and rotary table and top drive diagram. *Adapted from Malyszkz [16] and Boutwell [17].*

- Increased efficiency and performance over the Kelly bushing system
- Compatible with advanced control systems, modern systems provide useful real-time feedback data such as torque, power consumption, and rotary speed.
- Increased safety of workers
- Decreased stuck pipe frequency
- Faster pumps response time
- Extends the life of drill pipes
- Preferred in horizontal wells as better control of the drill string is needed.

Softspeed™

Power electronic devices such as switches and semiconductors over the past decade have considerably become more affordable and dependable; this has driven the introduction of more efficient AC motor controllers such as the variable-frequency drive (VFD). Modern TopDrives systems utilize this technology which allows controlling an electric motor behavior precisely by varying the frequency and voltage feed into it. VFD have several advantages; the most important are the availability of accurate real-time feedback information such as Torque, Voltage and rotation speed without any instrumentation in place. This has led to the development of new control techniques such as NOV ™ SoftSpeed ™ to mitigate bit dysfunctions such as stick-slip. [19]. A field case example of the implementation of such system is shown in Fig. 1.7.

According to NOV's patent by Nessjoen [20]. The system is a closed-loop proportional-integral (PI) controller that 'reacts' to torque oscillations on a limited frequency band typical of the Stick-Slip dysfunction while drilling. A new version of the system released in 2010, is an adaptation of a classic PID (Proportional Integral Derivative) controller. A "PIJ" controller that is essentially a classical PI controller with an inertia compensation J-term that is proportional to the difference in measured acceleration only. The J-term increases the controller frequency spectrum to compensate for second mode Stick-slip modes. The system is also capable of auto-tunning the parameters as a function of the drill string length [21].

Advanced higher order controllers derived from Lyapunov analyses have been proposed to mitigate stick-slip and drill string vibrations while further rejecting external disturbances. Even though their simulation provides a better controller response in most cases, the complexity of such robust controllers and plant limitations of industrial actuators drastically limit the implementation of such methods in a practice. Graphical comparisons and simulations of such alternatives are available in *[22]*.

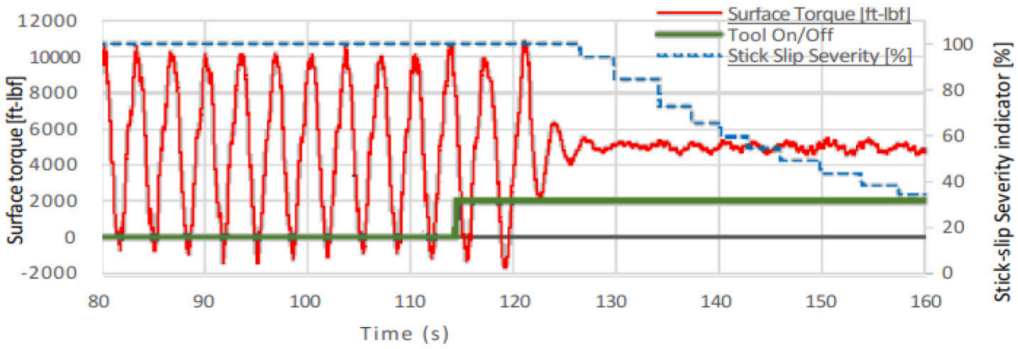

Figure 1.7: Active torsional dampening stick-slip mitigation system. *After Vogel et al. 2016 [23]*

.

1.4 Why Drilling Automation?

Automation has proved remarkable improvements in other industries, such as the manufacturing or aviation industry where automated systems compose a higher stake in daily operations. Increased performance, efficiency, reliability and safety of well designed autonomous systems are the primary motivation for a drilling automation uptake within the Oil & Gas Industry. Macpherson [24] categorizes some of the major drivers for automation where automated systems can effectively mitigate or improve current solutions and the technology needed to address each one of these drivers is now available.

1. ***Increased well complexity and excessive Non-Productive Time (NPT).***

   Multi-Directional extended reach wells are becoming more common especially in the offshore business. Ambitious projects with narrower pressure margins, complex trajectories and uncertainties must rely on robust automated systems in the future to achieve extended distances while mitigating costs, risks while reducing NPT.

2. ***Data overload.***

   Modern computer systems are capable of crushing vast amounts of data; from acquiring, storing, categorizing and interpreting it in a relatively short period. Automated systems will be able to run local optimizations based on history or model-based data that will either take control of drilling parameters or advise the driller accordingly. The system should be able to predict, determine and

intervene to avoid any significant failure occurrence.

3. ***Knowledge transfer.***

   Skilled and experienced employees will eventually exit the industry, leaving their roles to younger professionals. This loss in expertise can be reduced using autonomous systems.

4. ***HSE reasons.***

   Safety has always been the top priority for companies where dangerous working and extreme conditions are common, such as the Oil and Gas industry. Also, strict environmental regulations must be followed to avoid serious negative consequences to the ecosystem and the health of collaborators. Automated systems will decrease the number of people working in hazardous zones, as well as improve the HSE monitoring processes currently in place.

5. ***Economic drivers.***

   The economic drivers for automation are tangible. According to the Det Norske Veritas Germanischer Lloyd (DNV GL) Technology Outlook 2015 [25] Drilling Automation and smart well technology could decrease CAPEX drilling costs by 30-50% compared with traditional rigs. The BP™ 2015 Technology Outlook estimates that *"advances in technology could reduce industry extraction costs by approximately 25% by 2050 "* [26]. Some operators have heavily invested on drilling automation development projects to commercialize autonomous robotic systems. Such as a rig floor robotic pipe handler developed

by Norway's Robotic Drilling Systems AS (RDS) that has signed a contract with Nabors Industries (NYSE: NBR) for it first delivery in 2016 [27].

Modern automated optimization algorithms have been tested in the field, improvements of 10% to 80% in the rate of penetration (ROP) over a human driven rotary drilling rig have been observed. As well as when building and steering wells with an 80% improvement while sliding. The promise for substantial savings is not only attainable but certain ([28][29][30][31][32][33][34]).

1.5 The Future of Drilling Automation

Drilling Systems Automation Technical Section

The Society of Petroleum Engineers (SPE) started an industry technical section focused on Automation technology applied to the drilling industry, the Drilling Systems Automation Technical Section (DSATS)[1]. The purpose of DSATS is to accelerate the development and implementation of automated systems in the Oil & Gas Drilling industry. The group has been one of the most active technical sections within SPE.

In the Summer of 2013, DSATS launched the Drilling Systems Automation Roadmap initiative joint industry project (JIP) affiliated with the International Association of Drilling Contractors (IADC), and the Association for Unmanned Vehicle Systems International (AUVSI). The objective is to promote a well-defined system

roadmap target for an integrated industry development to enable the interoperability needed for the implementation of new robust autonomous systems. Some advances in the proposed metadata structure, OPAC standards have been made with the participation of industry operators and services companies such as Shell, NOV and Baker Hughes is tangible, the detailed proposal and updated status is available at *de Wardt 2015 [32]*.

DSATS has been actively encouraging initiatives to promote the participation of automation in the industry. The section has held workshops, forums, lectures and scientific publications to communicate new technology developments, recommended practices and the standardization of drilling data nomenclature [1]. DSATS has also drawn the attention of other industries by promoting the inclusion of experts from industries where systems automation is more advanced.

1.6 Drilling System Automation Challenges

Even though the interest for Drilling Automation within the industry is higher than it has ever been, and the number of professionals working on research and commercialization of automated solutions has increased over the last decade, fully automated drilling systems face significant challenges that limit the development and application of robust automated solutions.

Instrumentation Inaccuracies and Variability

There are many vendors of data acquisition and instrumentation that provide a sundry array of electronic device recorders (EDR) and data acquisition services to operators. Unfortunately, it is common practice to assume the accuracy of the instrumentation technology they provide without any deterministic study on the physical to electrical signal conversion performance, and the technical accuracy of the calibration procedures used by the service provider. Another important aspect is the low-frequency measurements EDR service companies currently offer. Commonly at around 1-Hz ([35]) which is insufficient for any high-speed autonomous system.

Sensors require rigorous calibration procedures and periodic maintenance to maintain it is reliability over time. A process that is often taken lightly in daily operations. Sensors are responsible for providing the necessary surface measurements information used for observation, monitoring, and control of any drilling operation; they provide vital readings such as hook load, drill string revolutions per minute (RPM), surface torque, pump pressure and rate. Nevertheless, cumbersome measurements errors have been observed in the field [36], such field - observed errors are shown in Table 1.1.

Variable	Field Observed Max. Error	Derivative variable error	Small Error	Consequence	Large Error	Consequence	Worst Case Scenario
Torque	*>100%*	MSE / Rig State	*5% - 10%*	Sub-optimal drilling analysis, planning and execution. Inadequate MUT limit	*>20%*	$\pm 5,000 ft*lb$ error for most TDS-11 drives. Bit, Motor, MWD, Tubular or Vibration-Induced Failure.	Loss of Drill String
RPM	*>100%*	MSE / Rig State	*2% - 10%*	Sub-optimal drilling. Improper feedback loop to the TopDrive. Poor Anti-Stick-Slip performance.	*>20%*	Bit or MWD Failure, Vibration dysfunction. Poor Drilling Performance	Loss of Drill String
Hookload	*>100%*	WOB / MSE / Bit Depth / Rig State	*2% - 5%*	Sub-optimal drilling. Improper WOB feedback loop to the draw-works.	*>10%*	$\pm$ 50,000lb for most sensors	Loss of Drill String
Block Position	*>25%*	Bit Depth / ROP	*1% - 2%*	Block position error is cumulative. Incorrect MD/TVD/Survey Measurements.	*>5%*	10ft error per joint pipe drilled. Significant survey errors and severely compromised TD.	Wellbore intersection
Flow Out	>100%	Rig State / Kick Detection	*5% - 10%*	Poor well control. Poor stuck pipe/pack off detection.	*>20%*	Inability to detect kicks, packs offs or other problems.	Blowout
Pit Volume	*>5%*	Δ Pit Volume. Kick size/density.	*1% - 2%*	Poor well control. Poor kick detection/performance.	*>5%*	5 bbl could be 100% error in well control calculations.	Blowout
Pump Pressure	>100%	ΔP / MSE Rig State	2% - 5 %	Poor managed pressure performance. Poor well control. Wear/damage to downhole motors/turbines.	>10%	500 - 750 psi error could lead to potential damage to motors/turbines/MWD tools. Potential for kicks/fracturing when operating near pore pressure/narrow fracture gradient.	Blowout
Pump Rate	>100%	MSE / Rig State	2% - 5%	Poor Diagnostic ability with tracers. Poor hole cleaning. Wear/damage to downhole motors/turbines.	>10%	10 Strokes/min error could significantly affect well control or managed pressure scenarios.	Blowout

Table 1.1: Common instrumentation errors found in the field. *After Behounek 2015 [36] & Zenero et al. 2016 [37].*

An experienced human driller could easily detect a significant anomaly in any reading on the fly and act accordingly. Nonetheless, this may not hold true for small but essential instrumentation anomalies. The driller would make decisions based on inaccurate data. Furthermore, reliable instrumentation data is vital for any closed loop autonomous system, without robust redundancy. A closed loop system will just follow the difference between the input and feedback output of the controlled plant to compute an appropriate controller gain, which can lead to a significant inaccurate response, that could potentially cause hazardous disruptions[38].

The basic instrumentation data is used to calculate outstanding optimization derivatives variables such as Mechanical Specific Energy (MSE), Weight on Bit (WOB), and Rate of Penetration (ROP); carrying and increasing the error margin. Improved algorithms coupled with instrumentation redundancy and data analysis are being developed to mitigate control or surveillance errors ([39] [40] [41]). The current situation with rig instrumentation data represents an obstacle to drilling automation systems. High speed, reliable and accurate measurements are needed.

In 2014, more than thirty operators formed the DSTAS Operator's Group on Drilling Data Quality (OGDDQ) to study and address drilling data quality issues. The group purpose is to change the industry's standards for instrumentation data quality [42]. OGDDQ is currently analyzing the effects of fundamental sensor's measurements inaccuracies and the consequences. Small errors may only cause sub-optimal drilling, analysis, and planning but significant errors could be catas-

trophic [43]. Operators realized that many of their own rigs surface sensors are not very accurate which leads to unreliable analysis results of such findings are shown in Table 1.1. OGDDQ will develop specifications for drilling tools, machines, and instruments based on the desired outcomes of operating companies; accuracy, precision, resolution, repeatability, reliability, safety, environmental, form factor, usability cost, and other process needs. As well as the development of recommended practices for field verification of drilling instrumentation equipment [43] [37].

Drilling Data

Drilling Data is composed of the following main areas and applicability examples according to DSATS Data Quality Assurance Subcommittee [1]:

1. ***Surface and Downhole Measurements made at a rig***.
    - High and Low-Frequency Instrumentation Data & Every Sub-System Measurement.
2. ***Metadata describing those measurements***.
    - Accuracy, Calibration, Resolution, Drifting, Location, Manufacturer , Time-Zone, Temperature, Working Hours...
3. ***Derived variables from these measurements.***
    - Mechanical Specific Energy (MSE), Measured Depth (MD), True Vertical Depth (TVD, Rate of Penetration (ROP), Weight on Bit (WOB), Stick-Slip Percentage, Drill Joint Number...
4. ***Contextual and situational data that describe the environment within***

which a measurement is made.

- Flow Off annular Pressure, Flow On Annular Pressure, Swabbing, Tripping In/Out, Drilling, Making a Connection, Setting Casing...

5. ***Data generated by real-time applications.***
    - Physics-based Models, Data Driven Models, Recommended WOB for an interval...
6. ***Data about the performance specifications of drilling devices.***
    - Mud Pumps, Shakers, Motors, Top Drives, Pressure Transducers, Drawworks...
7. ***Historical data conceivably used in automation tasks.***
    - Offset wells, Equipment Configuration, Performance Limiters, Historic pump pressure, Dangerous interval observed in offset wells...

Surface-Downhole Data Link

Surface and downhole readings are important for drilling optimization, from the development of dynamic simulation models to the real-time analysis and decision loop. [44][35]. Unfortunately, the current mud-pulse telemetry system widely used in the industry to communicate downhole data to the surface is extremely bandwidth limited in addition to its inherent lag. Data rates usually vary from 3 bits per second (bps) to 20 bps depending on depth.[45], this limited bandwidth forbids high-rates data transmission from any downhole tool and therefore vanishes any sophisticated real-time drilling optimization autonomous system.

Modern downhole tools are almost entirely autonomous [46]. For example, measurement while drilling and rotary steerable tools. Those tools encapsulate many electronic components that are isolated from surface conditions and feedback which makes much higher logging rates possible; the data is used on their separate closed loop controllers without any reliance on surface measurements to make the right changes. High speed logged data is usually stored internally and recovered after the bit has been taken back to the surface then it is analyzed and used for drilling optimization purposes, in preparation for the next well. Downhole-Logging and post analysis can be very expensive and time-consuming, most operators today do not log and store data on a routine basis.

To overcome the limited bandwidth of current telemetry systems wired drill pipe had been developed [47]. Transfer rates offered by this solution is orders of

magnitude higher than traditional mud pulse telemetry. Wired drill pipe is capable of transferring data at 57,600 bps, without significant signal attenuation or noise caused by changes in depth, fluid properties or formation resistivity. Transmitting every single filtered high-speed measurement from downhole tools in real-time is now possible. Several fields tested cases highlighting the advantages of wired pipe technology are available in the literature [48][49][50][51] [52][53].

Data Standardization and Liability Issues

Several different companies are involved in the process of any drilling operation today. Operators, drilling contractors, and service companies usually employ proprietary hardware with unique communication protocols to provide any service. The current business structure drives the isolation of sub-systems and alienates the inherent benefits of the data. The fragmented ecosystem is detrimental to the adoption of drilling automation as a viable path. Instrumentation data must be redundant, accurate and wholly available to be successfully used in any reliable automated process [54].

The discrepancy between data owners, creators and those who will ultimately benefit from the data generated by any operation must be addressed to let autonomous systems thrive. Nevertheless, this problem is not unique to the Oil and Gas industry itself; other industries have faced this puzzle of proprietary data. The solution was not a fundamental change in the way those companies handled their business processes but to how the compilation of data occurred, several standards

were developed and enforced by the interested industry or government [55].

Different standards development organizations exist, these organizations develop, support and promote consensus between companies. Examples of traditional International regulatory bodies are the Organization for Standardization (ISO), the Society of Automation (ISA), and the Electrotechnical Commission (IEC). The traditional consensus and implementation of a new standard is usually very time-consuming, in addition, the use and application of such standards require payment of patent licensing fees [56]. Because of this, several open-source standards processes have emerged. The main difference from traditional standardization is that those standards are regularly developed, maintained and freely published by an industry consortium. Furthermore, the ownership remains a public trust and are freely open to interested participants. Lu 2016 [55] thoroughly explain the current state of data standards for smart manufacturing, where the implementation of automated systems is far more advanced than the Drilling Industry.

Several industry operators have proposed the adoption and implementation of open standards, due to the faster adoption rate and license-free nature. DSATS is currently encouraging the development of an OLE for Process Control (Object Linking and Embedding for Process Control) standard crafted for the Drilling Industry. The group has proposed an early draft of the guidelines for the Drilling Industry and is actively working on finalizing it to start with the implementation. The proposed data acquisition and distribution levels are shown in Fig. 1.8.

OPC is an open source communication structure that defines a standard protocol that can be used by any company to link Human Machine Interfaces (HMI) with hardware such as PLC or DCS or other software interfaces. OPC is a composite of several sub-standards for specific applications such as data events, alarms or historical data.

An Open Standard, it means lower costs for services companies and flexibility for clients. Hardware and software companies just need to provide an OPC server on their solutions to communicate with any other OPC compatible client. A standard like OPC specially designed for the Drilling Industry will allow the implementation of more automated systems in the industry, better calibration procedures and provide more valuable information of every sensor's data acquired.

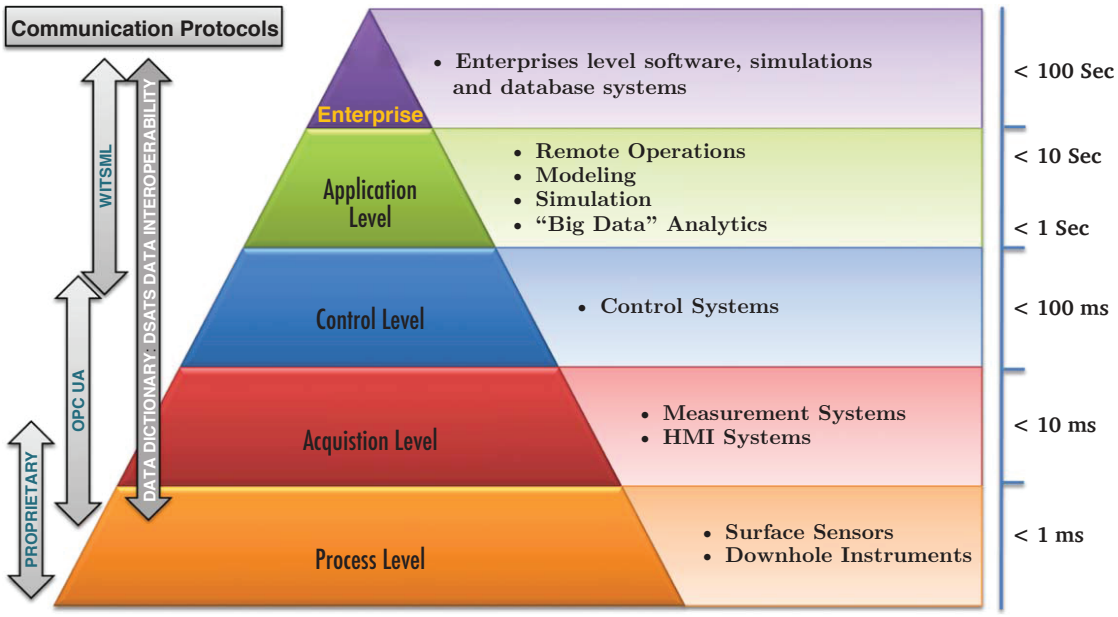

Figure 1.8: Proposed DSATS™ communication levels. *After Vogel et al. 2016 [23].*

1.7 Levels of Automation

Different levels of automation (LOA) have been proposed in the literature to classify an automated process from completely manual to fully autonomous. Endsley and Kaber[57] produced a ten level LOA taxonomy to designate functions to human and computer systems. The duties were monitoring, generating options, selecting, and implementing a response. Endsley's Levels of Automation are shown in Table. 1.2. It should be noted that removing the human factor from a high cognitive level process with limited physical understanding or modeling is detrimental to the performance of any automated system A. Vera [58] [57]. Parasuraman et al. [59] proposed a four-stage model of human-automation interaction design that defines a recommended level of automation for each the four basic operations previously discussed, the author highlights that human involvement in any automated process becomes more significant as higher-risk decision making is required.

Level of Automation	Monitoring	Generating	Selecting	Implementing
1.- Manual Control	Human	Human	Human	Human
2.- Action Support	Human/Computer	Human	Human	Human/Computer
3.- Batch Processing	Human/Computer	Human	Human	Computer
4.- Shared Control	Human/Computer	Human/Computer	Human	Human/Computer
5.- Decision Support	Human/Computer	Human/Computer	Human	Computer
6.- Blended Decision	Human/Computer	Human/Computer	Human/Computer	Computer
7.- Rigid System	Human/Computer	Computer	Human	Computer
8.- Automated Decision	Human/Computer	Human/Computer	Computer	Computer
9.- Supervisory Control	Human/Computer	Computer	Computer	Computer
10.- Full Automation	Computer	Computer	Computer	Computer

Table 1.2: Levels of automation. *After Endsley & Kaber 1999 [57].*

The miniature rig used in the study is ranked at level 8-9 because human interaction is required to monitor the drilling process and take action in case of a major emergency. The system monitors and analyzes acquired data to generate possible choices, then selects and executes any change, a fully Autonomous operation with supervision control. Human-Machine-Designs models were used in the development of emergency systems, high-risk decision-making procedures, and user-friendly GUI.

Thorogood et al. 2010 [60] ranks the overall status automated systems in the drilling Industry from LOA 1 - 4, with the exception of some downhole tools classified as LOA 9. The classification of some of the current drilling commercial solutions based on their LOA scale is seen in Fig. 1.9

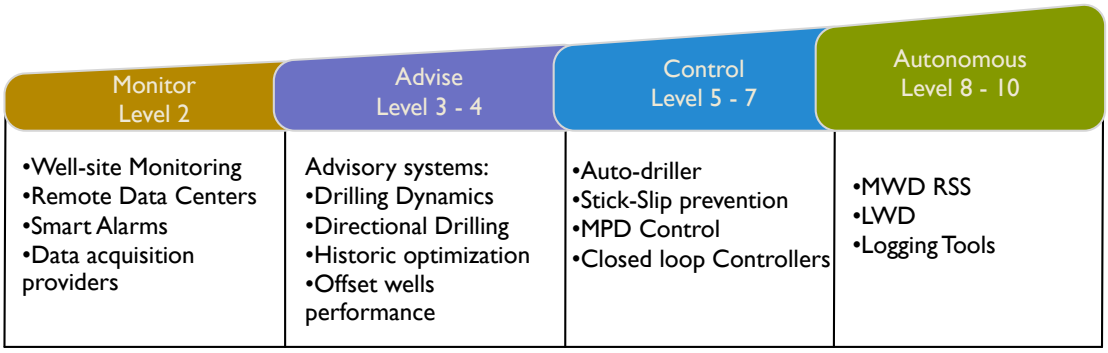

Figure 1.9: Examples of available drilling automation solutions. *Adapted from Macpherson et al. 2013 [24].*

1.8 Scope of Thesis

In this study, A miniaturized autonomous drilling machine was built for the Society of Petroleum Engineering – (SPE) DSATS 2016 Drillbotics ™ International Competition with the objective of performing optimal operations in terms of rate of penetration and energy efficiency. The miniaturized rig uses state-of-the-art sensors, control algorithms, and innovative instrumentation solutions, leading to a significant amount of data to be analyzed in real-time. An Gain-Scheduled-PID controller for Real-time WOB control was modeled, simulated and implemented, increasing the performance of the drilling process. Downhole sensor and module were designed and manufactured to acquire high-frequency data in near real-time. High-frequency data was acquired using LABView® and analyzed in real-time using the MATLAB® programming environment. 130 Million raw data points were collected, filtered and averaged at each run. In addition, the system includes the following new functionalities:

- Wireless downhole sensors
- Remote data visualization and cloud-storage
- Signal filtering, redundancy reduction, and instrumentation data.
- System identification, modeling, and simulation.
- Stand-alone micro-controller driven scheduled gain Proportional Integral Derivative (PID) controller.

- Improved Weight on Bit (WOB) and RPM control
- Pason's Electronic Drilling Recorder (EDR) integration
- Real-time Rate of Penetration(ROP) and Mechanical Specific Energy (MSE) optimization.
- Active torque surveillance safety system
- User-Friendly Human Machine Interaction and GUI

This thesis details the design, development, and testing of such improvements to allow further research collaboration and continuity of the project. The system will be later used for educational and research purposes in the Department of Petroleum Engineering at Texas A&M.

1.9 Thesis Organization

This thesis is organized as follows. Chapter 1 consists of a brief history of drilling automation and some remarkable examples of successful drilling automated systems, followed by the discussion of some of the most important boundaries that hinder the development of new robust automated solutions in 1.5. Chapter 2 highlights the mechanical structure of the miniaturized drilling rig built and used in this study, including but not limited to the main components, instrumentation, and significant control variables parameters. Chapter 3 describes some drilling fundamental concepts used in the development of the rate of penetration optimization algorithm (ROP) as well as the characteristic of the drilling components and rock formation samples. In addition, part of the software developed for the downhole sensor, iOS app, LabVIEW and MATLAB loop is discussed. Chapter 4 describes the system dynamics model and the results of its simulation as well as the mechanical limits and natural frequencies of the major components. Lastly, Chapter 5 shows some relevant results of the performed drilling experiments.

2 AUTOMATED MINIATURIZED RIG

This Chapter highlights the mechanical structure of the miniaturized drilling rig built for the development of this experiment based on the Drillbotics competition guidelines [61]. This section discusses the main mechanical components such as the hoisting system, Top Drive motor, and drawworks structure. The sensors used for instrumentation purposes and the important control parameters they provide followed by a description of the safety systems in place.

2.1 The Drillbotics™ Competition

Drilling automation is the use of computer-assisted devices in drilling a wellbore. It involves a considerable amount of technology, from accurate and redundant instrumentation, downhole drilling tools to sophisticated control algorithms. Some previous successful examples of automation in today's industry are the top drive, managed pressure drilling systems, and NOV's SoftSpeed™ controllers. The economic drivers for automation are increasing complexity, data overwhelm, efficient drilling operations, and safety.

Automated systems and equipment for drilling are under development by equipment providers, service companies, and operators. Interested members of these companies have formed a consortium in 2008, the SPE Drilling Systems Automation Technical Section (DSATS) which believes that automation will have a

long-term positive influence in the industry. DSATS is promoting the adoption of new technologies, research funding and advocating the use of open data standards within service operators.

In the fall of 2014, DSATS launched the Drillbotics™ International Competition [62] to build a laboratory-scale drilling rig and automatically drill through a sample of challenging rock formation with unknown rock layers and inclination angles. One $0.375x0.035$ aluminum tube is used as the system's drill-pipe to increase the level of difficulty. Texas A& M and other universities around the world competed building a miniaturized drilling rig in the Spring of 2015. The system successfully drilled autonomous through a rock sample. Texas A&M University placed second in the 2015 edition, a detailed description of the instrumentation and mechanical system is described [61].

The design and construction of the winner drilling machine are detailed in [63]. The competition encourages the design, creation, and implementation of new tools and algorithms to improve the performance of a completely automated drilling machine. Also, a multidisciplinary and collaborative effort is needed to archive the level of competency required. For the 2016 competition, several performance and systems improvements have been made.

2.2 Mechanical Specifications

The mechanical structure of the miniaturized rig is shown in Fig. 2.1.

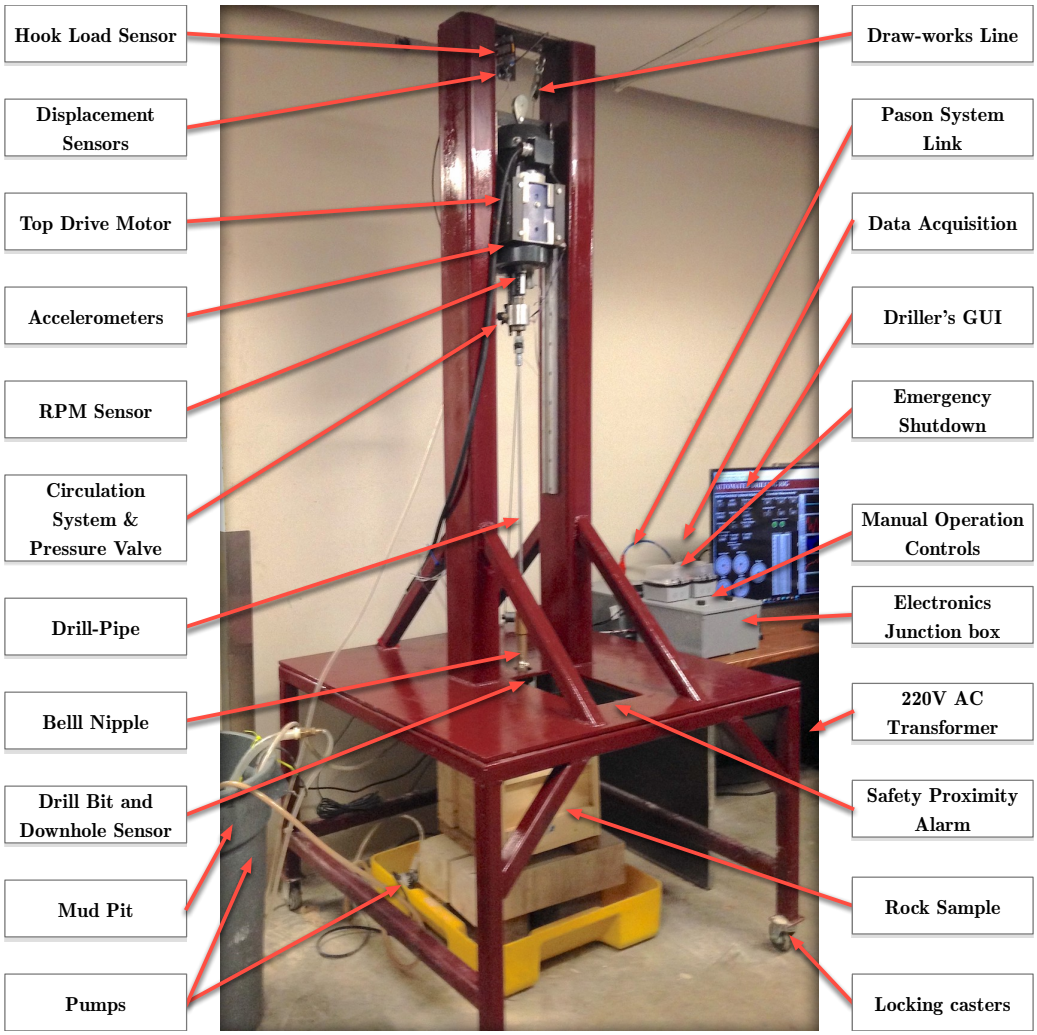

Figure 2.1: Miniaturized drilling rig main components

System Limitations

The limitations of the system are apparent as the hoisting system is not capable of making connections and laying down the drilling strings, which is ignored

because of the experiment primary focus the development and understanding of an automated drilling system with emphasis on bit-rock interaction and ROP optimization. The rig needs to drill through a $1 ft^3$ formation block with a 1.125-in. Diameter PDC micro-bit. The power system is limited for safety reasons to the civilian power grid with a two phase 220V AC and a maximum power rating of 2.5-HP. Setting casing is not considered in the design either.

Hoisting System

The hoisting system includes the derrick, Top Drive, Drawworks motor and tension line. Two steel support columns with I-Beams, guide the TopDrive along the derrick structure. A classic pulley system was used to provide a more accurate control of both, the top drive position and the applied Weight on Bit.

Locking Casters

The drilling rig for this project was designed after a modern portable onshore drilling rig as a model. The rig structure is supported by four steel pipes with casters that are used to provide support and mobility to the rig. The system can be transported from one location to another with ease.

Top Drive's Motor

The Top Drive provides the rotational speed and torque forces to the drilling string and the drill bit. The system was designed with different drill pipe materials and specifications in mind. A 2.0 HP OMPM-DC Series permanent magnet 220V DC

motor was chosen for this purpose; the motor is capable of driving torque forces of up to 70 $lbf \cdot in$ at a rotation speed of up to 1,800 RPM. The engine is hinged to a carriage connected to the guide rails; the motor moves along this rail when drilling.

Drilling Fluid Circulation System

The fluid circulation system is essential for well stability, it removes rock cuttings, cools the drill bit, and lubricate components. Fluid is injected through the drill pipe at high pressures; bit nozzles control the pressure differential at the bit and regulate the fluid velocity to remove cuttings while drilling. Cuttings are carried through the annulus back to the surface, where a mud filtering and cleaning system is in place. Fluid is then reinjected back into the wellbore in a closed-loop fashion. If inadequate mud properties or flow pressures are used, the drilling process becomes inefficient and could potentially be dangerous.

The closed-loop circulation system in this system is composed of two mud pumps, with a filtering mechanism. Rock cuttings are discharged into a mud pit, where they settle at the bottom. A second water pump is located at the very top of the pit container to ensure cleaner fluid and avoid clogging. An inline valve controls the fluid velocity and pressure drop. Fluid is injected trough a swivel located between the Top Drive and Drill pipe. A bell nipple with a rubber gasket on the bottom, a welded flange on top with a flow outline is used to carry cuttings back to the surface of the hole. Lastly, the main water pump is capable of varying the fluid velocity at command, for most of the tests, a pump speed of 70% was adequate to

remove rock cuttings without leaks or clogging.

Drawworks System

A pulley system with a tension line coupled to a gear motor is used to control an adequate hook load, that is the difference between the total weight of the motor and drilling string, and the measured axial force in the tension line determines the amount of weight on bit (WOB) that is being applied to the bit. The gear motor operates at a maximum rotational speed of 7.9 RPM at 12V DC with a gear ratio of 386:1.

Circuits Junction Boxes

All the electrical circuits, power supplies, and analog signal filters are safely located inside a separate Junction box to guarantee their safety and proper performance. The junction boxes isolate sensitive electronics from ambiance moisture and unwanted external factors.

Emergency Shutdown

A redundant emergency shutdown system is used, a mechanical switch is located on top of the junction boxes to shut down the Drawworks Motor, Water Pumps, the Top Drive Motor or all systems in a single action. The arrangement is color coded and readily available to the driller. As with industrial standards, this operation is independent of any software computation; it directly cuts the power supplied to the system .

Safety Ultrasonic Alarm System

A proximity perimeter alarm is automatically activated once the drilling process starts, the perimeter is delimited using ultrasonic distance sensors and a microcontroller. If there's any violation to the safety perimeter the system activates a sound alarm, as well as visual physical lights and communicates the status to the main Graphical User Interface. The driller can also set up an automatic shutdown of the drilling operation if needed.

2.3 Instrumentation

The most important instrumentation sensors used in the development of this project will be discussed in this section. Some measurements are derived variables of fundamentals readings such as Torque, Weight on Bit, Vibration, Temperature, and Downhole Data acquisition is discussed. A list of the technical details of each sensor and results of the sensor calibration procedure used are shown in Table 2.1.

Revolutions per Minute

In order to measure RPM, an optical tachometer made with an optoelectronic circuit composed of an infrared emitter (IR) diode coupled with a photo-resistor and a transistor, is used to generate pulses at each revolution. The IR diode shoots light to the motor shaft where a light reflecting tape is placed; then the photo resistor excites a transistor base to generate a voltage pulse. The signal is discretized based on a voltage cutoff, and it is used to evaluate its frequency. The frequency

corresponds to the shaft rotational speed. The principle of operation is shown in Fig. 2.2.

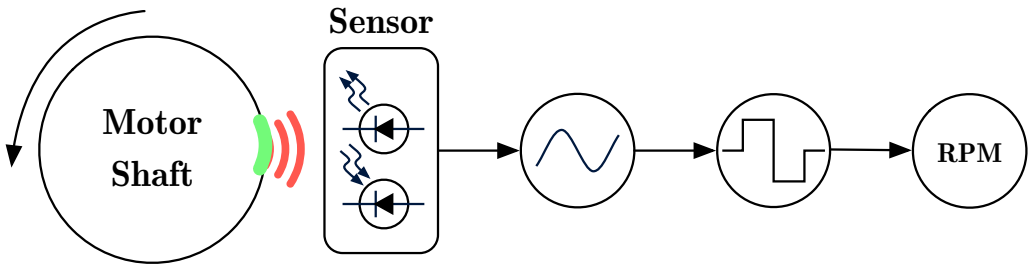

Figure 2.2: Optical tachometer

The motor rotational speed is controlled by adjusting the voltage supplied to the coils. An industrial motor driver is used to control it accurately.

Weight on Bit

An industrial FUTEK LSB300 S-Beam LoadCell (*Fig. 2.3*) is located at the top of the Top Drive drilling line; the sensor is a balanced and calibrated Wheatstone bridge electrical circuit.

Figure 2.3: Futek load cell

Weight on Bit is measured indirectly, and this measurement is based on the hook load tension at the Top Drive carrier. A full-Wheatstone bridge load cell is used to gauge the tension along the drill line. The amount of force applied to the drilling string in the axial direction will be inversely proportional to the hook line tension. The Weight on Bit is the difference between the total weight of the top drive structure with the drill string components and the measured hook load tension.

Weight on Bit is an extremely important measurement because it greatly influences borehole quality, bit dysfunctions and the rate of penetration of a drilling operation. An adequate WOB control is essential to improve drilling performance. In this study, an Gain-Scheduled PID controller was developed to guarantee WOB control.

A Wheatstone bridge is an electrical circuit configuration that is used to measure small changes in the electrical resistance of an unknown transducer usually a strain gauge by comparing it the known gauges resistance values. The unknown transducer will change its resistance value due to several factors such as pressure, force, and temperature. A current is applied to the circuit input to provide voltage. The output voltage resulting from the imbalance caused by any deformation on the strain-gage bridge determines the magnitude of the force acting on the bridge. The usual electrical circuit configuration is shown in Fig. 2.4.

From Fig. 2.4. The output relationship given by this Wheatstone bridge circuit is:

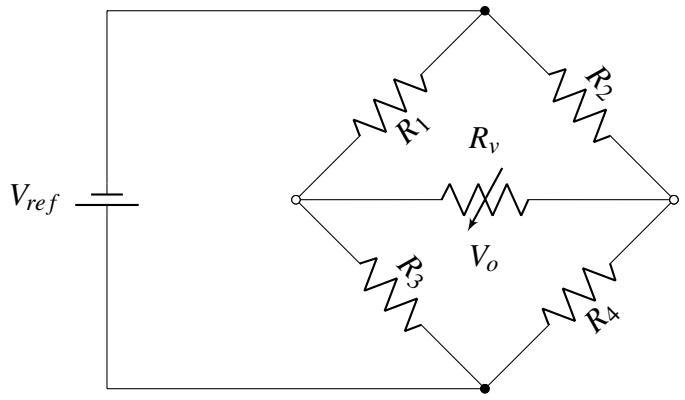

Figure 2.4: Wheatstone bridge circuit

$$V_o = \frac{R_3 \cdot V_{ref}}{R_3 + R_1} - \frac{R_4 \cdot V_{ref}}{R_4 + R_2} = \frac{R_3 \cdot R_2 - R_1 \cdot R_4}{(R_3 + R1)(R_4 + R_2)} \cdot V_{ref} \tag{2.1}$$

If the voltage output is zero, the Wheatstone bridge is said to be balanced.

$$\frac{R_3}{R_1} = \frac{R_4}{R_2} \tag{2.2}$$

The sensitivity of the bridge output to changes at the four resistors must be known. This is determined by the rate of change between the voltage difference with the reference voltage input, and is described by:

$$\frac{\delta V_o}{V_{ref}} = \frac{R_1 \delta R_3 - R_3 \delta R_1}{(R_3 + R_1)^2} - \frac{R_2 \delta R_4 - R_4 \delta R_2}{(R_4 + R_2)^2} \tag{2.3}$$

Heat causes the atoms of materials to vibrate, the higher the amount of heat the more violently atoms collide. Materials are classified as conductors if their internal resistance increases with temperature or insulators if it decreases as temperature increases. This is one of the reasons why electronic sensors exhibit measure-

ment drift errors, even after calibration, unless the drifting coefficient as a function of temperature is known and used to correct the measured value. Drifting errors could be diminished by conducting frequent calibrations or by maintaining a stable temperature during a measurement.

The gauge strains on a Wheatstone bridge are susceptible to this physical law. If all resistors are physically identical, the amount of change in resistance due to ambient effects such as temperature, atmospheric pressure, cancel out among the first order terms ($\delta R_1, \delta R_2, \delta R_3, \delta R_4$), producing no net effect on the output voltage from the bridge. Thus, only the adjacent pair of resistors have to be identical to archive environmental compensation, which is achieved if R_2 and R_4 or if R_1 and R_3 have the same temperature coefficient [64].

In our case, the sensor has a nominal bridge resistance value of $1K\Omega$ with a non-linearity response of $\pm 0.05\%$ and a calibrated temperature compensation from 15 to 72 C $\pm 0.0008\%$. The sensor was calibrated with an excitation voltage (V_{ref}) of 1.0 VDC giving a rated output of 1.9085 $mV/V@200lbf$. The rated output has been verified during the calibration procedure and tests.

Torque

Torque measuring is of vital importance for this project. Knowing the current, and the voltage driving the DC motors is critical for control purposes and safety monitoring. A non-intrusive method is employed.

Current is measured using an industrial grade high-performance current trans-

ducer. The amount of torque at a given time applied to the drill string is calculated as a function of the rotational speed, the motor efficiency factor, and the voltage & current across the motor coils. Manufacturer's information was used to calibrate the measured torque.

An AcuAMP® DC current sensor capable of sensing up to 200A is placed at the TopDrive motor power input to measure its current flow. The sensor is based on the Hall effect phenomena, which is the result of a voltage difference (Hall potential) across an electrical conductor, this potential is proportional to the current flowing through the conductor, and the flux density or magnetic induction perpendicular to the conductor. The industrial grade AcuAMP ® Current transducer uses both parameters, the Hall potential and the magnitude of the magnetic field, to generate a proportional signal response through a signal conditioner. The generated signal usually complies with the Industrial Standard $4-20mA$ current loop.

Measuring the electrical potential difference between two nodes in an electrical circuit or voltage through an electric circuit is a passive activity and can be done using any multimeter or electronic sensor. The voltage applied to the Top Drive motor as a function of the desired revolutions per minute was calculated based on the manufacturer's specifications and calibrated with real measurements taken during the calibration procedures applied to this project.

DC motors convert electrical power to mechanical power. In any energy conversion process, an efficiency factor is implied. Energy loss could occur due to sev-

eral factors such as heat dissipation, friction, or external forces acting on a given system.

$$Power_{in} = Power_{Out} + Power_{Loss} \tag{2.4}$$

Ohm's law asserts that the current through a conductor is directly proportional to the voltage across it. The common mathematical equation that describes this relationship is given by:

$$I = V \cdot A = \frac{V}{R} \tag{2.5}$$

A Watt is defined as rate of energy conversion with respect to time, which in electromagnetism terms a watt equals the rate of work that is used when an ampere (A) of current flows through an electrical potential difference of one volt (V) this is:

$$W = \frac{V^2}{\Omega} \tag{2.6}$$

This relationship can given by the voltage supplied to the motor (V_{in}), is the back Electromotive Force (EMF, V_{EMF}) produced, the electric resistance of the armature (R_m), and the current flowing through the coils (I_m) as:

$$I_m \cdot V_{in} = V_{EMF} \cdot I_m + R_m \cdot I_m^2 \tag{2.7}$$

Clearly, I_m^2 corresponds to the energy loss term, and it is attributed due

to heat losses within the armature coils. The mechanical power needed to drive the motor is related to the electromagnetic torque (T_G) and the rotational speed ω ($radians/second$) which is given by:

$$P_m = V_{EMF} \cdot I_m = T_g \cdot \omega \tag{2.8}$$

It is useful to recall that ω equals:

$$\omega \frac{rads}{sec} = \frac{2\pi \cdot N}{60} RPM_s \tag{2.9}$$

This expression can also be expressed in simpler terms to get a useful torque equation using the number of poles (P), parallel paths (Z), the current flux per pole (φ), the number of conductors and the rotating speed of the motor (RPM) as:

$$T_g = \frac{P \cdot Z \cdot I_m \cdot \varphi}{2 \cdot \pi \cdot A} \tag{2.10}$$

Alternatively, it is possible to relate the motor efficiency factor, this is, the mechanical output force of the motor divided by the required electric energy input. To estimate the torque at a given time, we use:

$$T_g = \frac{I \cdot V \cdot E_f \cdot 60}{RPM \cdot 2\pi} \tag{2.11}$$

However, the torque, power, and the efficiency motors are not constant. The manufacturer usually provides a table of technical specifications and laboratory re-

sults from which several assumptions are taken to facilitate the implementation. In this case, the motor is rated with a full-load torque of 5.84 lb-ft and an armature current of 9.8A with an 85% efficiency factor. Finally, we can calculate the running torque from remembering that one horsepower equals 743Watts or $33,0000 lb/ft$, from Ohm's law we can calculate the power consumption from the voltage and current drawn to compute the Torque in lbf/ft as:

$$T_g = \frac{HP \cdot 33,000 \cdot E_f}{RPM \cdot 2\pi} \tag{2.12}$$

Or alternatively:

$$T_g = \frac{I \cdot V \cdot E_f \cdot 60}{RPM \cdot 2\pi \cdot 0.737562149} \tag{2.13}$$

Which is the same equation as Equation 2.11.

A simplified full braking torque relationship as function of the Top Drive RPM is plotted in Fig. 2.5, the Torque capacity decreases with higher revolutions per minute, but the current consumption increases with Torque and voltage.

Vibrations

Vibrations are performance limiters in drilling operations; ROP could be drastically impacted by bit dysfunctions caused by excessive vibrations along the drill string. To measure vibrations, high-performance 9DOF accelerometer, gyroscope and magnetometer are used. The sensors are placed on top of the motor, right

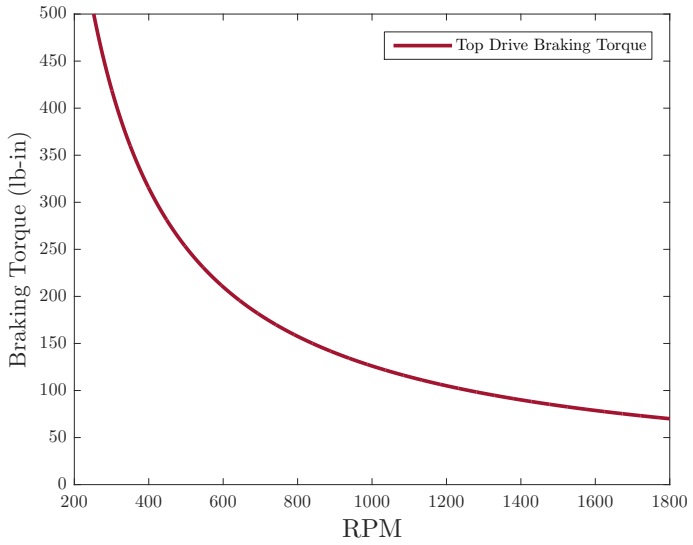

Figure 2.5: Top drive motor braking torque vs RPM

below the fluid swivel and downhole, next to the bit. These readings are used to analyze and optimize ROP performance.

Temperature

Temperature is measured for monitoring processes, equipment such as the Top Drive and Drawworks motors, and the drilling string can overheat, this can lead to mechanical failures and safety hazards. The system activates the safety alarms to alert the driller of potential issue if high temperatures are detected. The temperature is acquired through resistance thermometers (RTD).

Sensor's Calibration Procedure and Accuracy

The technology defines the capability of any transducer to convert physical characteristics into electrical systems. Accuracy is the amount of uncertainty in a measurement. Instrumentation manufacturers specify the range, sensitivity, preci-

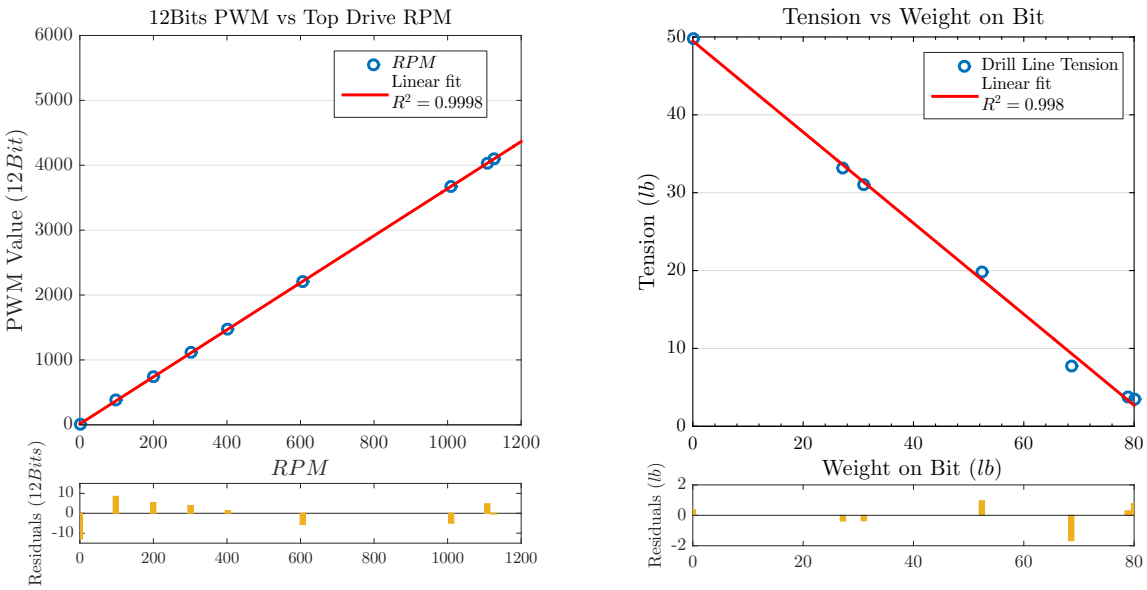

(a) PWM to RPM Calibration

(b) Hook load tension to WOB

Figure 2.6: Real measurements vs intrumented readings calibration

sion, resolution, linearity, etc. of a device. Nevertheless, those specifications can greatly vary from one to another. Sensors must be calibrated and corrected periodically to assess its performance.

The manufacturer specifications were followed to quantify the precision of each sensor used in the control algorithm. The physical to electrical signal conversion error as an absolute percentage is given in Table 2.1. Calibration procedures were carried to verify the linearly of transducers and the amount of error for a given reading. An example of the calibration procedure is seen in Fig. 2.6, and Fig. 2.7.

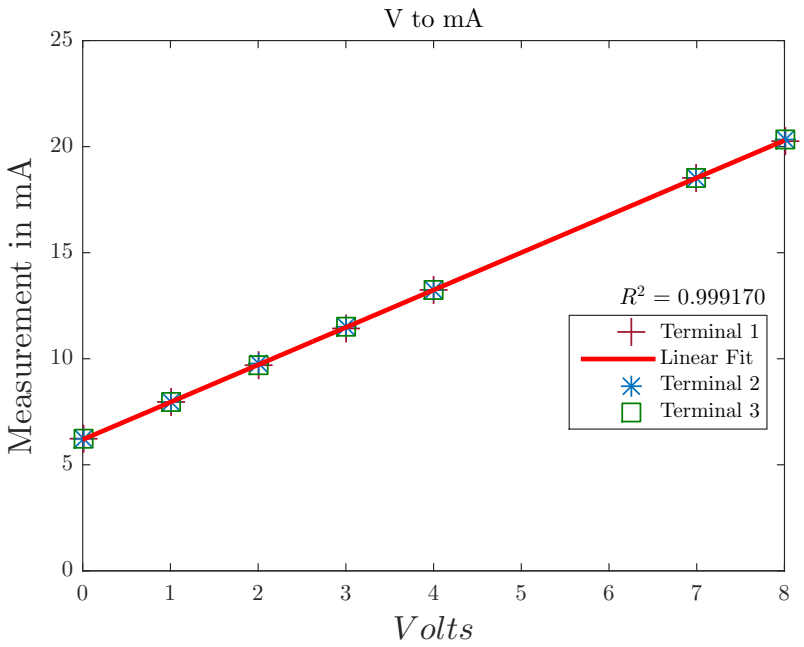

Figure 2.7: Voltage to current loop conversion and calibration

Measurement	Sensor Type	Sensor	Accuracy	Linear R^2
WOB	Full Wheatstone Bridge	Futek LSB300	*0.05 %*	*99.984 %*
ROP	Laser Distance	OPT2011	*1.0 %*	*98.332 %*
ROP 2	String Linear Displacement	UniMeasure LX-PA	*0.03 %*	*99.912 %*
RPM	Infrared Digital	Self Made	*0.01 %*	*99.998 %*
Top Drive Current	DC Hall Effect Magnetic	DCT100-42	*1.0 %*	*99.854 %*
Top Drive Current 2	Hall Effect IC	ACS712	*1.5 %*	*99.000 %*
Drawworks Current	Intrusive Integrated Circuit	VH5019	*10 %*	*92.143 %*
Surface Temperature	RTD	TEMP112	*0.6 %*	*97.321 %*
Surface Vibrations	$\pm 3G$ *AO* Accelerometers	Shock Resistance	*0.3 %*	*100.00 %*
Alarm System	Ultrasonic Sensors	MaxSonar	*5.0 %*	*95.00 %*
Downhole Vibrations	Low Energy Module	Digital Nano LIS3DH	*0.00062%*	*100.00 %*
Downhole Temperature	Low Energy Module	Digital TEMP112	*0.6 %*	*100.00 %*
Flow Velocity	Pump Controller	Speed Regulator FB	*10 %*	*98.720 %*

Table 2.1: Instrumentation accuracy and calibration results

3 SYSTEM INFRASTRUCTURE

Some important drilling fundamental concepts such as bit dysfunctions and their relationship with mechanical specific energy are explained and discussed in this section. Followed by the description of the rock formations, drill pipe, bits and downhole sensors used during on drilling experiments. Finally, an overview of how data was handled, saved and visualized as well as the loop structure that was developed and used on each run is discussed.

3.1 Drilling Fundamentals

Drilling is the removal of rock material by either ductile or brittle failure of the rock by indenting and sliding with a bit cutter. Weight on bit (WOB) increases the indentation magnitude while the RPM produce the sliding force and distance to remove rock particles. The two motions are independent. For instance, if we maintain a given WOB the indentation depth will remain constant no matter how fast we rotate. This implies that the rate of penetration (ROP) is independently linear with both Revolutions per minute (RPM) and Weight on bit (WOB) [65].

Several factors can affect the drilling performance, either on a linearly or non-linearly fashion. These factors are called drilling limiters; they reduce the efficiency of the overall drilling operation while increasing the amount of wear of drilling equipment. Some factors that affect ROP linearly are (1) weight on bit, (2) rotary

speed, (3) bit aggressiveness (bit Coefficient of friction), (4) bit dulling, (5) ductile vs brittle failure mechanism and (6) rock strength. In addition several non linear effects can occur, such as (7) bit balling, (8) bottom hole balling, (9) vibrations and (10) interfacial severity.

The linear relationship between WOB and RPM is because drilling bits indent until the vertical contact area is such that the force per area is less than the rock strength. If the rock strength is higher the amount of force needed to offset the loss of force per area will increase, therefore ROP will decrease.

ROP increases with RPM because the sliding distance per period for each PDC cutter increases the amount of drilled rock. Lastly, measured torque will increase linearly with Depth of Cut (DOC) due to its natural relationship with force per unit area required to fracture the rock exposed to the cutter face.

Mechanical Specific Energy

Mechanical Specific Energy (MSE) is the energy used per volume of rock drilled. As important as it is, a specific relationship of the energy used to 'crush' rock for a specified unit of volume of rock was nonexistent until 1965 when Teal derived it [66]. He proposed an interesting approach to model the drilling process in excavation/mining operations as a crushing process in which bigger volumes of rock are fragmented into much smaller pieces that allow recovering the material economically.

Teal derived a relationship to correlate the amount of work used in rotary

drilling from relating trust and rotary components on a given cross-sectional area from which rock is being removed [66]. He recognizes that no single value of MSE can be used as an index for a given time due to variations in rock homogeneity, percussion frequency, and other complex drilling dynamics variables. However, an average over a homogeneous section of rock was determined to be enough to calculate, model and predict drilling specific energy performance. Mean MSE values were obtained for different drilling operations configurations for a given bit and formation type.

Basically, the MSE model calculates the rotational and axial work to the volume of rock drilled. Plotting the results, we can observe a strong relationship to rock compressive strength and the energy used to remove a certain volume of rock. Essentially, an efficiency index is calculated which states that if the bit is 100% efficient, the Mechanical Specific Energy will equal the rock compressive strength.

The ratio of measured MSE to rock strength has then been used since 1965 in lab environments to measure rock cutting efficiency. The development of both the concept and idealization of Mechanical Specific Energy (MSE) has become a valuable parameter for drilling engineers to improve drilling performance and efficiency.

The MSE equation without a correction factor is:

$$MSE_{psi} = \frac{480 \cdot T \cdot RPM}{OD^2 \cdot ROP} + \frac{4 \cdot WOB}{\pi \cdot OD^2} \tag{3.1}$$

MSE tends to increase, decrease or remain constant depending on bit dysfunctions and the overall drilling efficiency. Different types of dysfunctions are encountered in the wellbore, and each dysfunction has a particular control response necessary to mitigate as shown in Fig. 3.1.

The advantages of using real-time tracking of Mechanical Specific Energy has been reported to archive remarkable improvements in drilling efficiencies. Drilling performance is difficult to be equitably measured and compared from well to well, because many performance indexes that are used as correlation factors, are based on data from offsets wells and different rig configurations, or wellbore trajectories. Therefore, a new approach was taken by an operator and a pilot program in 2003 was established to verify the usefulness of onsite MSE tracking first displayed as a rig site surveillance tool in 2003 [67].

Results were better than expected on almost every site surveyed, showing significant improvements on rate of penetration (ROP) as well as increasing bit efficiency. The operators were able to detect several common causes of MSE inefficiencies causes in which the transfer of energy from the bit to the rock is constrained such as bit balling, bottom hole balling, and vibrations.

MSE was found to improve the overall performance of many drilling parameters such as ROP, bit life and even detect dysfunctions quickly on real-time. This initial approach was carried over a niche of pilot operation and then enforced as

part of the operator's drilling practices.

Nevertheless, one downside of MSE surveillance is that several real-time parameters are needed to perform this type of analysis as Depth, ROP, RPM, WOB, Mud Weight, Torque, Downhole Accelerometer, Expected Rock strength and Gamma Ray for proper correlation. Still, with the advent of instrumented rigs and more advanced data acquisition service companies, many operators now employ this type of surveillance tools to assess and optimize drilling performance while drilling. It's becoming a common drilling practice [68].

ROP should conceptually respond linearly to the applied WOB or RPM. The point when the relationship becomes non-linear is called the founder point. Several factors can influence the location of the founder point for a given set point of WOB/RPM such as rock strength, hole size or pressure conditions. However, the MSE relationship will remain equal to rock strength being drilled if being efficient; in practice the driller has to determine the only one trend line and correlate it with parameter changes, making the real-time MSE readings a stronger parameter to watch while drilling.

A step test is a method widely used in the drilling industry to estimate the efficiency and causes of possible dysfunctions or inefficient drilling conditions based on mechanical specific energy (MSE). The method takes into consideration the linear relationship between ROP WOB and RPM to allow drillers to make changes over drilling parameters to determine if the operation is being carried efficiently or not.

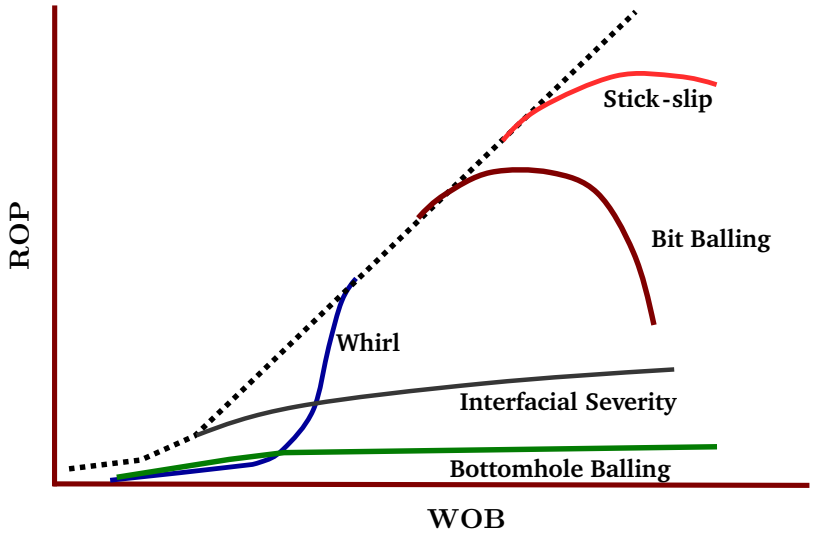

Figure 3.1: Mechanical specific energy concept

Fig. 3.1. defines the relationship between commonly found bit dysfunctions and the response usually seen on ROP [67].

3.2 Platform Design and Operation

The automated rig algorithm presented in this study operates and changes important drilling parameters autonomously based on both MSE and ROP. The algorithm is executed on every loop while analyzing the previous 30 seconds data available. First it calculates the Mechanical Specific Energy (MSE) of the drilling operation, then calculates the average Rate of Penetration for a given time interval. Followed by a linear regression to automatically weight out outliers and fit a linear function along ROP trend to compute a prediction interval to estimate the bounds of an interval in along which future displacement data points will fall with a 95% probability.

The prediction interval allows the algorithm to determine if the operation is being executed efficiently as well as determining when a new formation is being drilled. If WOB and RPM remain constant, the slope for a given ROP should remain, if the slope changes we are either drilling through a new rock strength or having dysfunctions. In addition, if MSE changes dramatically over a short interval of time a major dysfunction or failure is occurring and the algorithm has to act accordingly. Lastly, the loop will try to maximize both drilling parameters within previously established limits by implementing an automated step test to determine the founder point, this is, the point where the operation stops being efficient and a non-linear response against ROP is seen due to a major dysfunction such as whirl. The machine will gradually increase RPM and WOB and assess the response. If there is an unexpected drop in ROP the previously 'safe' drilling combinations will be used as starting points for a new step test. A flow chart describing the simplified MATLAB linear regression algorithm and automated step test response is shown in Fig. 3.2 .

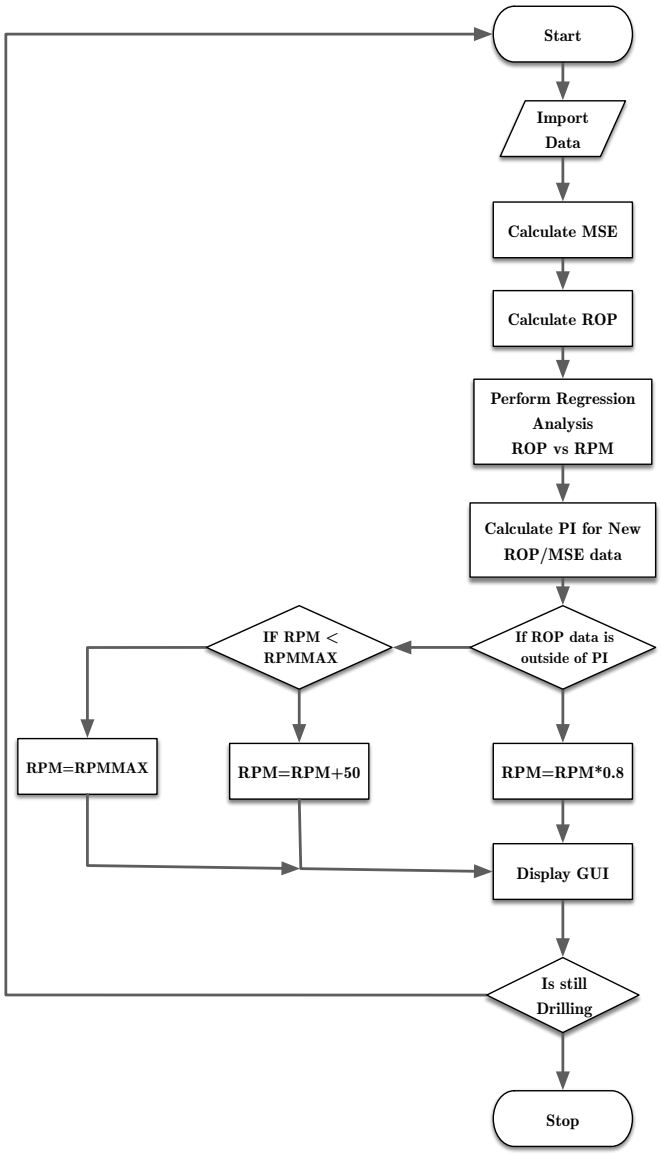

Figure 3.2: Automated ROP/MSE optimization flow chart

Drill Pipe and Bit

Baker Hughes™ provided a special fixed cutter PDC bit used in this experiment through the Drillbotics™ Competition. The 1.125-inch OD bit has two 0.529 inch PDC cutters with a 20-degree back rake and two nozzles of 0.093-inch diameter. Several other PDC bits were manufactured and imported to be used in sub sequential experiments, a total of 19 custom made bits were utilized in the project. With an outer diameter (OD) varying from 1-1.42 inches. The bits are shown in Fig. 3.4 and Fig. 3.3.

Figure 3.3: Baker Hughes™ PDC Bit

Both bit types use the same polycrystalline diamond compact (PDC) material as real size drilling bits. Drilling occurs through indentation of the rock and shearing. The magnitude of indentation is called Depth of Cut, and it increases proportionally to the applied weight on bit and the rotational speed of the drill

string. The bit cutters also have a small chamfer which leads to inadequate drilling performance if low weight on bit is applied; bit aggressiveness decreases when drilling on the chamfer. The efficiency of a drilling operation changes for a given WOB and ROP when the chamfer is entirely buried and the face of the cutter makes contact with the rock surface.

Figure 3.4: Custom-built PDC drilling bits

Rock Samples

Rock cubes with different formations and dips were manufactured to test and validate models; the rocks were $1-4ft^3$ and primarily composed of sandstone, granite, cement, hard cement and carbonated rocks. The rocks are mostly composed of sandstone/siltstone with a compressive strength of $2,000psi$ to $8,000psi$. Granite layers of around $19,000psi$, and soft and hard commercial cement/concrete of

around $2,000psi - 7,000psi$. Each rock sample was drilled at least four times and data was logged. The samples are shown in Fig. 3.5 and Fig. 3.6.

Drilling occurs due to ductile or brittle failure of the rock. Each formation has an unique rock strength and material properties that affect drilling performance. In addition, several inclination angles and dips per formation were introduced to assess the time response of the drilling operation.

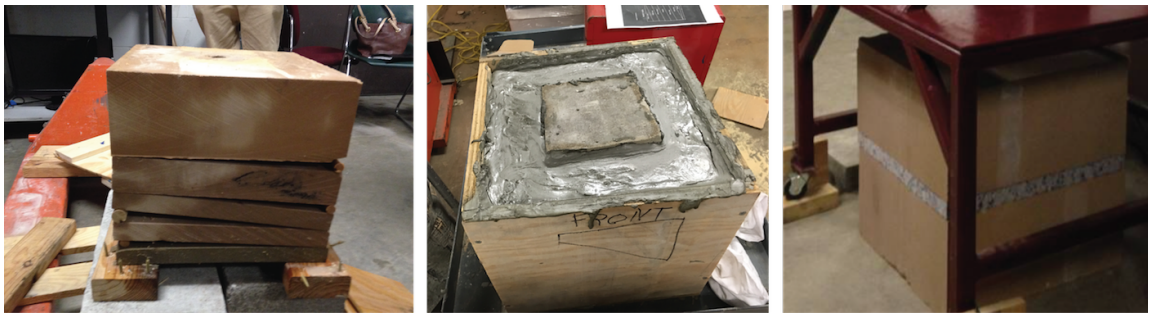

Figure 3.5: Rock-samples

A digram of the different rock cube configurations used to determine optimal drilling parameters and test the controllers response while drilling are shown below:

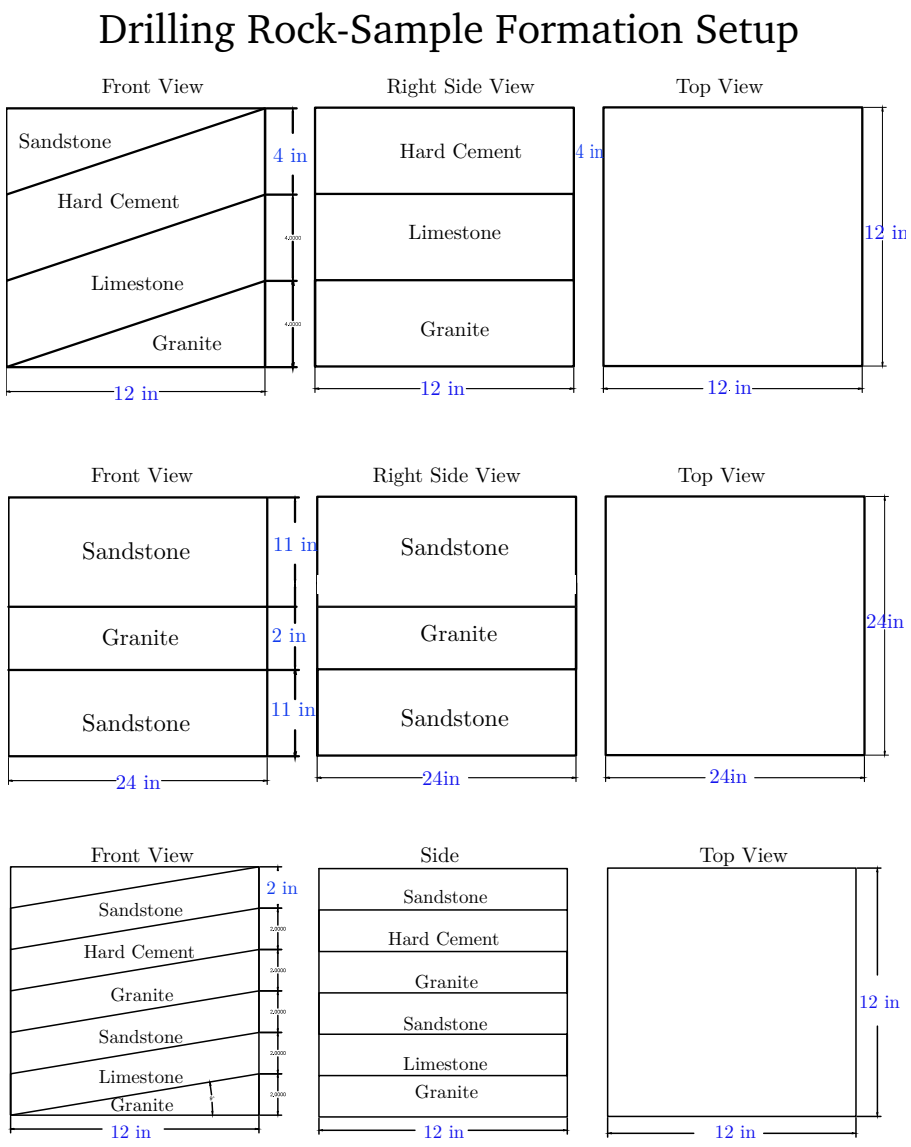

Figure 3.6: Custom built rock samples used for drilling experiments

The average rate of penetration for a given WOB and RPM was automatically computed and compared, in addition, the characteristic slope response was used to

determine if the machine was drilling over a new formation layer or a dysfunction was present.

3.3 System Hardware and Software

Data Acquisition and Control Computer

Measurements are taken via electronic transducers or sensors that translate physical characteristics into a quantifiable value proportional to the magnitude of what is being observed. The rig is instrumented with several sensors that translate physical measurements into electrical signals. The raw signal generated by any sensor is always filled with random fluctuations, often referred as electrical noise, the magnitude and causes of those fluctuations vary. Different methods to reduce the amount of noise in a signal and isolate a solid representation of the original exists in the realm of signal processing [69][70].

A digital data acquisition system is composed of four main steps, first, a sensor measure and transmit a proper electrical signal; secondly, this signal is filtered to reduce the amount of noise in it; third, the signal is digitalized via an analog-digital converter; and lastly, signals are acquired in digital form and stored in a computer or any Integrated Chip (IC) to be analyzed and used for different proposes.

Sensors

Sensors or transducers are devices responsible for taking measurements of physical systems and translate the response to an electrical signal. The output of

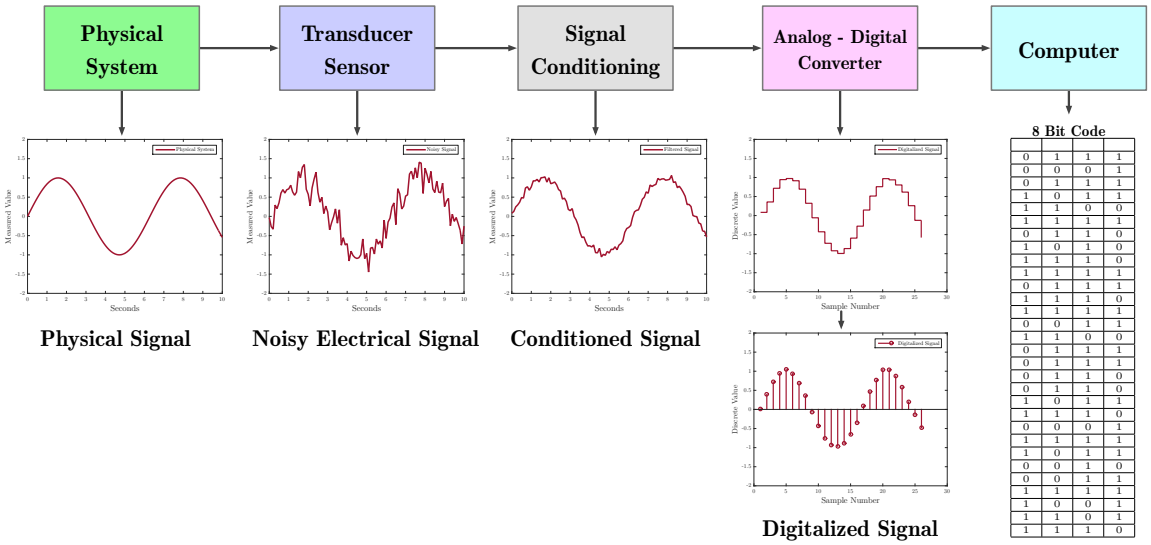

Figure 3.7: Digital data acquisition system block diagram. Adapted from [71]

the sensor depends on what kind of phenomenon is measured, the environmental conditions and the level of accuracy required. Typically, an electrical voltage or current output is employed. Sensors may require discrete components or electronics circuits to generate a signal correctly.

DAC & ADC

A Digital to Analog converter (DAC) or an Analog Digital Converter (ADC) are devices used to convert continuous time domain signals into digital bits, or vice-versa. There are a collection of DAC architectures and systems such as switch, the kelvin divider or string DAC, fully decoded DAC, quad cascaded switches each with their own special applicability and limitations [72]. However, depending on the application, the most important characteristics of a DAC are power consump-

tion, resolution, sampling frequency, accuracy, and cost. This conversion is usually implemented by integrated circuits called ICs at very high speeds. The DAC can degrade a signal informational value, so a proper DAC signal with high resolution and repeatability should be chosen for critical applications such as real-time control systems.

A digital acquisition system usually has the necessary electrical circuits to isolate, digitalize and condition signals in a safe manner. National Instruments Data Acquisition Industrial System [73] was chosen to acquire and measure instrumentation signals from the rig because the cDAQ modules and solutions offer a seamless integration with the G graphical parallel programming environment NI LabVIEW software. That provides a single programming interface to and from multiple DAQ devices and allows the creation of advanced Graphical User Interfaces. It is easier to implement an automated system to acquire, filter and display data in real time. The driller's GUI was developed in LabVIEW® to monitor and implement manual of the drilling process. The main Data Acquisition devices are presented in Table 3.1 :

Compact Data Acquisition Devices
cDAQTM-9174
NI 9201 ±10 V, Analog Input, 500 kS/s, 8 Ch Module
NI 9401 Bidirectional Digital I/O 8Ch
NI 9263 ±10 V, Analog Output, 100 kS/s, 4 Ch Module
NI 9219 Universal Analog Input Module

Table 3.1: Compact digital data acquisition modules

3.4 Downhole Sensor

Downhole vibrations are crucial to acquire and analyze in real time. Having a downhole size of just 1.125” proved challenging for the implementation of a downhole sensor in the design. The downhole sensor platform module shown in FIG. 3.8 is based on the stand-alone Bluetooth low energy (Bluetooth Smart) Ublox cB-OLP425 which is based on a High-Performance and Low-Power 8051 microcontroller Core (32Mhz) System on a Chip(SoC) solution from Texas Instruments, the CC2504 SoC. Combining a 2.4GHz transceiver, micro-controller, 256kB of in-system programmable flash memory, 8kB of RAM, in addition to the peripherals integrated into the SoC. The module includes a high resolution temperature sensor and a 3DOF digital accelerometer.

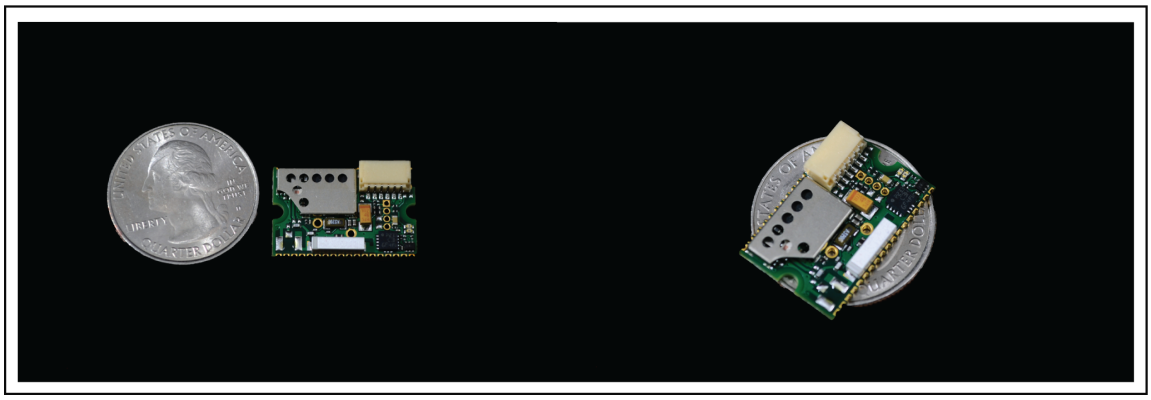

Figure 3.8: Downhole BLE sensor module

The modules support ultra low power consumption is suitable for applications using coin cell batteries, the module is capable of being on standby for years and transmitting data for months powered just by a single 2032 coin battery of about

225 mAh. It comes with a complete embedded Bluetooth stack and offers solder castellations for further hardware development. The stack includes object code compatible with the 4.0 Bluetooth low energy protocol. The module offers digital input/output GPIO, SPI, I2C, and UART interfaces as well as analog inputs. The operating temperature range is –40°C to +85°C without temperature protected encapsulation. The simplified overview is given by the block diagram depicted in Fig.3.9.

The downhole acceleration module uses a MEMS digital output motion sensor ultra low-power high-performance 3-axes nano accelerometer that has dynamically user selectable full scales of ±2g/±4g/±8g/±16g and it is capable of measuring accelerations with output data rates from 1 Hz to 5 kHz . The device may be configured to generate interrupt signals by two independent inertial wake-up/free-fall events as well as by the position of the device itself.

The Integrated Chip (IC) uses the standard I2C and SPI digital communication protocol between chips, making it perfect for modular system development, also, it supports a 16 bit resolution data output. In addition, a TMP112 High-Accuracy, Low-Power, Digital Temperature Sensor is mounted along the circuit to provide accurate downhole temperature readings.

The device firmware was modified to transmit data at higher frequencies under streaming conditions and to transmit it using a custom data structure. The IC firmware can be rewritten and read using binary ensemble code through the

cBACC73 CC Debugger Adapter Board. The code itself is debugged using the Integrated Development Environment (IDE) IAR Embedded Workbench 8051. A trial version of both systems was used to make the necessary modifications to the downhole sensor's SDK.

The module is capable of transmitting data up at 115.2 kbit/s up to 50 m using only the internal antenna and up to 200 with u. FL 6 dB external antenna attached.

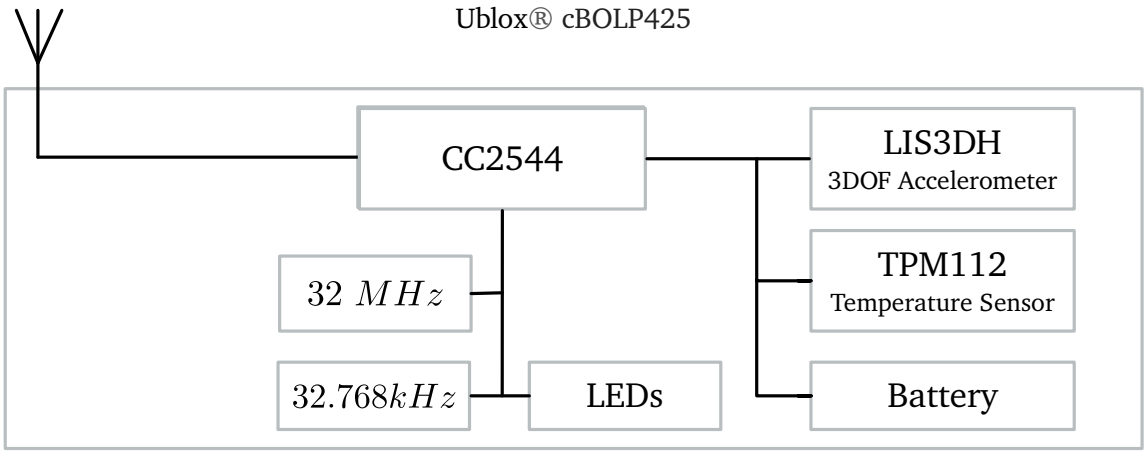

Figure 3.9: Downhole sensor simplified diagram

The application was developed using XCode 7 and Objective-C to run on the Apple iOS operating system. Ublox®provides a sample app with the minimum requirements that allows developers implement powerful capabilities faster. The App implements the BLE server role in communicating with the client. Modifications were made to both the iOS and the firmware source code, to log, encrypt and transmit data over the Internet to web server using a the secure HTTPS communication protocol. The application is shown in Fig. 3.10 and a simplified operations flow is seen in Fig. 3.11. The Universally unique identifier (UUID) for different services of

the device are:

- LED Service UUID: 0xFFD0
- Temperature Service UUID: 0xFFE0
- Accelerometer Services UUID: 0xFFA0-4

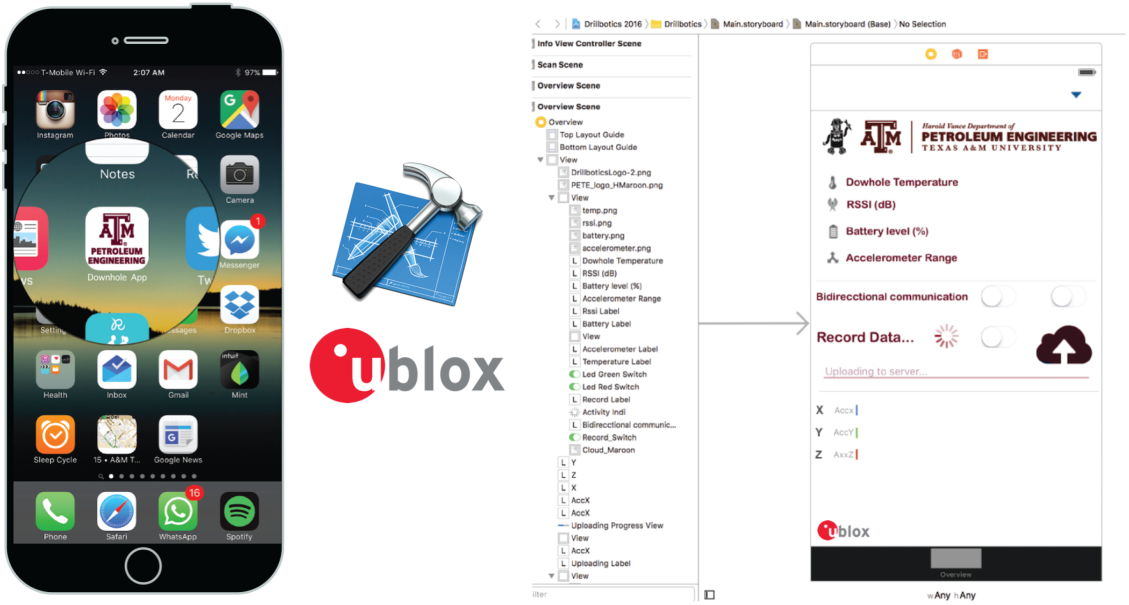

Figure 3.10: Downhole sensor IOS app

BLE Technology

Bluetooth Low Energy Technology 4.0 works under two core protocols, the Attribute Protocol (ATT) and the Generic Attribute Protocol (GATT) exclusively developed for low energy devices, every BT Low Energy client/server is expected to use them.

```
Start;
if Connection was successful then
    while Data notifications are being received do
        read current data point;
        parse data into string arrays;
        encrypt and concatenate arrays;
        write strings to internal memory log;
        if remote server is available then
            authenticate & read commands;
            retrieve last 150 data points;
            encode string array;
            upload to remote server;
        else
            return;
        end
    end
else
    return;
end
```

(a) Client app tasks

```
Start;
if Authenticated connection then
    while Data stream is being received do
        read current data point;
        parse data into string arrays;
        decrypt and concatenate array;
        write strings to SQL database;
        add metadata if available;
        write strings to CSV file;
        add missing delimiters strings to CSV file;
        if User is connected then
            retrieve last 150 data points;
            scan and split CSV columns;
            writes properly parsed file and privileges;
            use google charts API to generate plots;
        else
            return;
        end
    end
else
    wait until a new request is received;
end
```

(b) Remote server tasks

Figure 3.11: Simplified pseudocode of client-server operations

GATT Protocol

The Attribute Protocol (ATT) uses the Generic ATT data protocol to define the way that two Bluetooth Low Energy devices communicate with each other over a standardized message structure. The Generic Attributes (GATT) define a hierarchical data structure that is exposed to connected Bluetooth LE devices. GATT profiles describe on an use case, the roles, properties and general behaviors of a client. The protocol is structured through a collection of services and characteristics that define each server-client communication link. A graphical representation of this profile protocol is shown in Fig. 3.12

A profile is composed of services needed to comply with an use case; a service

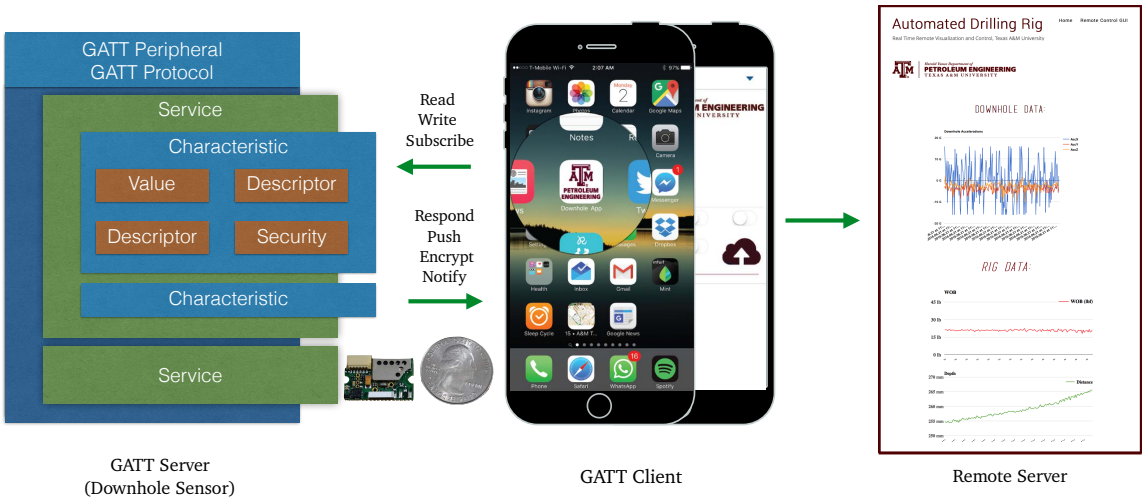

Figure 3.12: Downhole module GATT protocol diagram

conveys the characteristics or references to other services. A characteristic consist of a type represented by a universally unique identifier (UUID) value, a set of properties designates the processes the characteristic supports, as well as, a set of security permissions. An example of a characteristic includes the array of data describing the X, Y, and Z vibration response of an accelerometer chip within the downhole sensor device.

The GATT protocol classifies these services and encapsulates the function of parts of a device. This framework establishes the standards of services, their characteristics, such as discovering, reading, writing, notifying and indicating, and the broadcast configuration of each characteristic. GATT also defines client and server roles in three types: Discovery, Client-initiated, and Server initiated procedures.

The client-server relationship is defined by the GATT server which is responsible for storing and transmit data over Attribute Protocol (ATT) based on client re-

quests and confirmations. The server sends event-driven responses asynchronously to the client.

Downhole Sensor Capsule Design

The design of an adequate isolation structure was needed to place the electronics inside the stabilizer structure. The capsule was designed in a CAD commercial software, and structural simulations were carried to verify that the capsule was able to sustain acting downhole forces under the expected drilling conditions. Given the limited cross sectional area and constraints faced because of the small PDC bit diameter, metal 3D printing technology was chosen to manufacture the capsule. Fig. 3.13 shows some snapshots of the early model design, a mass distribution screen shot and the dynamic torsional simulation results as well as the final printed capsule.

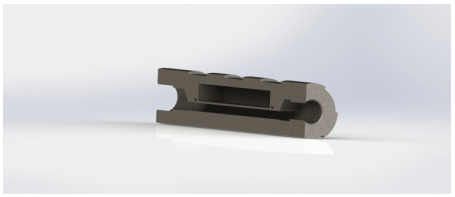

a) Downhole Capsule Cross Section View

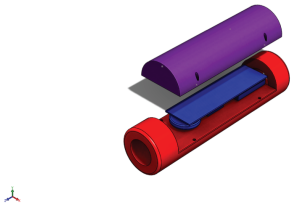

b) Density View of an Early Design

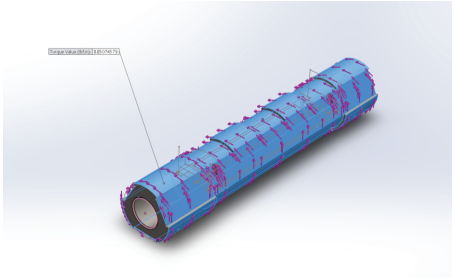

c) Mechanical Torsional Stress Simulation

d) 3D- Metal Printed Final Capsule

Figure 3.13: Downhole capsule design

3.5 Data Handling

The main data acquisition and control structure was developed in LabVIEW, MATLAB and an Arduino Due as the micro-controller where faster response times where needed. Wireless transmissions from the downhole device's sensors is directly fed to the handheld phone through the iOS App at around 100 Hz, which logs and transmit data to a remote web server using PHP commands and an SQL database. Wired instrumentation is acquired sensors along the rig via NI cDAQ hardware at around 32,000 Hz. The signals are filtered and handled in the main control computer where a discrete fast Fourier transform is performed for all the accelerometers before conditioning the signal by applying a digital filter and performing an average over each 10,000 samples to diminish noise. Spectral measurements are used later in the LabVIEW loop to both show the user the average magnitude of vibrations and to determine if the system is working within vibrational safety limit. The analog tachometer pulses are digitalized and the oscillating period is determined to get the average revolutions per minute over the previous points. Raw voltage signals are transformed to the physical parameters that each sensor is measuring using previously calibrated functions. The results of every instrumentation signal are plotted in the GUI and shown to the driller in both parameters against time or drilled depth.

At the same time, using a parallel loop, downhole data is fetched from the remote server, and locally generated data is parsed and concatenated to be saved to

a logging file and send over the internet to the remote database server. Finally, every major drilling parameter is communicated to the Pason system using a voltage to current loop converter circuit. While the previous steps are computed, the MATLAB algorithm fetches logged data and execute the analysis discussed in Section 3.2. The closed loop controllers reference points are modified through the MATLAB algorithm directly over a serial communication link.

Wired data is also being acquired independently in a faster loop within the micro-controllers responsible for controlling both the weight on bit and the revolutions per minute. The micro-controllers also perform several automated critical safety surveillance checks, such as computing and assessing the Top Drive and drawworks torque overheating limits, proximity alarms and power systems overheating while ignoring expected current spikes seen due to drilling parameters changes commanded from the Matlab algorithm.

Lastly, a virtual control room and visualization can be accessed over the internet via both using the built-in LabVIEW publishing tool using the proprietary plug-in or through a standard web page using any HTML five compatible browser where data is plotted in real time, the user is able to stop the operation remotely or change drilling parameters dynamically.

A graphical description of the data flow is shown in Fig. 3.14. In summary, we conceived the data workflow as follows:

1. Data is acquired using NI Compact Data Acquisition System (cDAQ) at a High-frequency of 32,000 Hz.
2. Data is digitally filtered, stored and transmitted through a Graphic User Interface (GUI) developed in LabVIEW® .
3. Wireless and downhole sensors transmissions are fetched from a server-based database system.
4. Data is parsed to MATLAB® and analyzed on every loop
5. The results of this analysis is used to modify fundamental drilling parameters.
6. New reference points are sent to the microcontrollers driving the PID algorithms.
7. An optimization algorithm based on the step test is implemented while no dysfunction is detected.

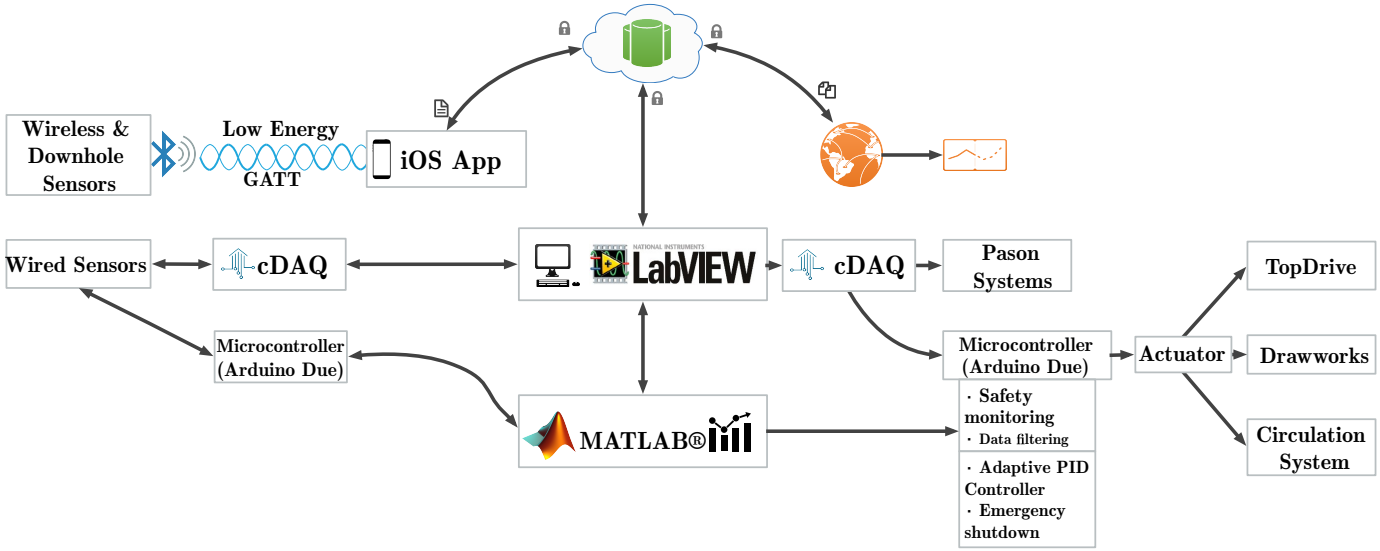

Figure 3.14: System's data loop schematic

Electronic Drilling Recorder

Pason is one of the leading service companies in the Oil and Gas drilling industry that specializes in fully integrated drilling data solutions from data acquisition, visualization, and communication. Pason EDR offers and end-to-end service portfolio to operators by providing the rig instrumentation equipment, data acquisition systems, and software that links the rig manager, operator, geologist and driller under a standard data network. The system is capable of recording data up from sensors at a sampling rate of up to 5Hz. Plotting the data in its GUI and using some industrial bus connections, in addition to some management software tools and is composed of a touch screen doghouse computer, the Rig Manager server, an electronic signal commuter router and networking connections with basic sensors that measure the depth, pump strokes, hook load, standpipe pressure, rotary torque and surface rotary RPM.

Many drillers and engineers are familiar with the company drilling graphic user interface, and options it offers. The miniaturized rig is compatible with all the crucial parameters used by the system. This will allow potential graduates to both, familiarize with the system to learn from first hand what they will be potentially using in their careers and to be able to detect and troubleshoot common errors on the fly.

4 MINIATURE DRILLING RIG DYNAMICS

A simple dynamic model of the overall mechanical structure is derived in this section. Also, the drill pipe buckling limits, fundamental frequencies, and equations of motion used in the simulated run are presented. This derivation is important because it allows simulating the dynamic response of the system over time that approximates the real behavior. Based on such simulations a control model can be derived and tuned to modify control parameters in real time. Fig. 4.1 represents a simplified free body diagram of the overall system. Translational and rotational dynamics are defined separately, also, lumped inertia and stiffness were used to reduce the order of the rotational system.

4.1 WOB System Dynamics

The displacement of the Top Drive is used to measure the drill motion in the axial direction; however, this alone does not determine the drilling performance nor the applied WOB. A calibrated high precision Wheatstone bridge is used to measure the applied force at the bit. A small misalignment or slight deviation in the axial measurement or rotational speed can create large normal and lateral forces which create excessive vibrations. This can create problems such as whirl patterns and dysfunctions that lead to poor drilling performance, excessive wear, and mechanical pipe failure.

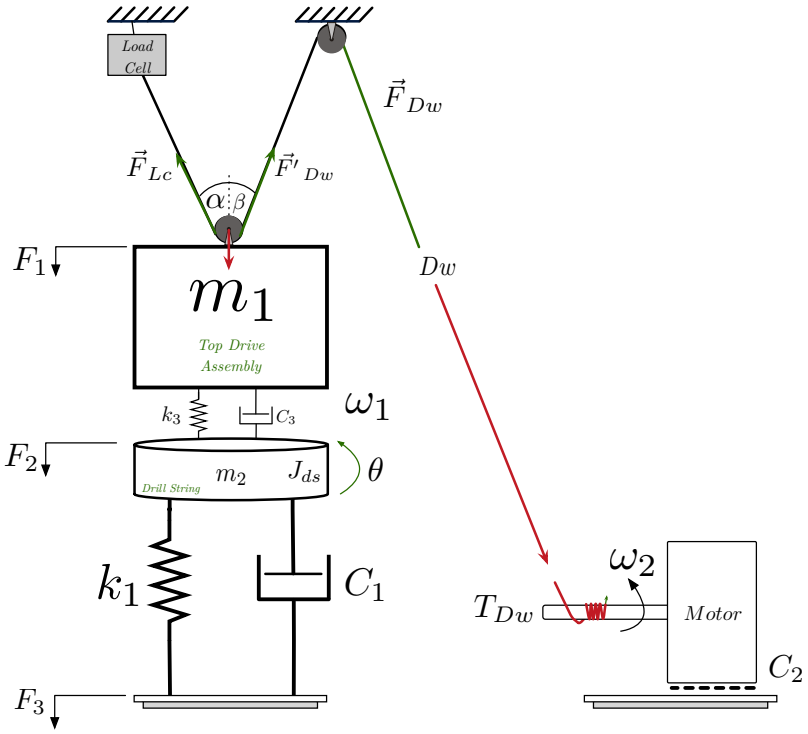

Figure 4.1: Top drive and drill string dynamic model

A simple but accurate model of the pulley system driving the Top Drive motor structure along the guide rails is presented in this section. The mechanism is coupled to a gear motor that controls the amount of force applied to the bit. This model does not take into account frictional & viscous coefficients and other non-linearities relationships. The free body diagram of the drawworks tension line configuration used in this study is seen in Fig. 4.2.

The governing system of equations of forces acting along the X and Y axis in this mechanism is given by:

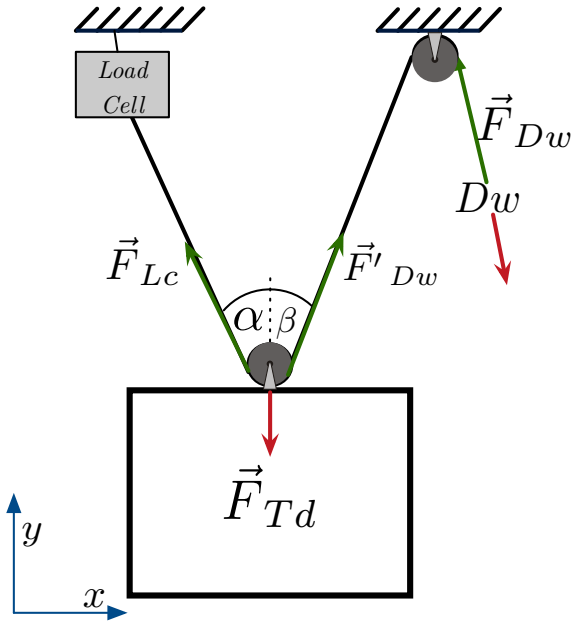

Figure 4.2: Pulley system model

$$Along \quad X = \qquad F_{Dw} \cdot \sin\beta - F_{Lc} \sin\alpha = 0 \quad (a) \tag{4.1}$$

$$Along \quad Y = \quad F_{Lc} \cdot \cos\alpha + F_{Dw} \cos\beta - F_{Td} = 0 \quad (b) \tag{4.2}$$

Where F_{Lc} is the force being applied to the LoadCell, F_{Dw} is the amount of force generated by the pulling action of the Drawworks motor, and T_Td is the amount of force exerted to both pulleys by the total weight of the Top Drive and drilling string assembly, α and β are the angles along the central pulley in degrees. Rearranging Eq. 4.1 Eq. for F_{Lc} and substituting in Equation 4.2 :

$$F_{Lc} = F_{Dw}\frac{\sin\beta}{\sin\alpha}$$

$$F_{Dw}\frac{\sin\beta}{\sin\alpha}\cdot\cos\alpha + F_{Dw}\cos\beta - F_{Td} = 0$$

Solving for F_{dw} and F_{Lc} and simplifying from equation 4.1 yields the following relationship:

$$F_{Lc} = (F_{Td} + \Delta L_w)\cdot\csc[\alpha+\beta]\sin[\beta] \tag{4.3}$$

$$F_{Dw} = (F_{Td} + \Delta L_w)\cdot\csc[\alpha+\beta]\sin[\alpha] \tag{4.4}$$

Therefore, the magnitude of the load cell tension (F_{Lc}) and the force acting on the drawworks motor shaft (F_{Dw}). It is important to highlight that actual α and β angles will change slightly depending on the Top Drive position due to non-eccentricities and manufacturing tolerances. In addition, the extra weight of the steel line ($\Delta L_w(Td_{Pos})$) has to be accounted in the calculations. Thus, those values become functions of depth in the setup i.e. $\alpha(Td_{Pos})$ and $\beta(Td_{Pos})$. These dynamic modifications were implemented into the algorithm as a function of the Top Drive assembly displacement to archive a more accurate representation of the actual force being applied to the bit.

The applied WOB is the difference over time from the original starting Top-

Drive assembly weight minus the load cell reading over the transferability ratio determined for given depth:

$$\text{Weight on Bit} = F_{TdOriginal} - \frac{F_{Lc}}{Ratio(Td_{Pos})} \tag{4.5}$$

Table 4.1 presents the results the previous equations for a given depth and original top drive assembly mass $F_{TdOrginal}$, this function was used to determine WOB at a given depth while drilling.

Variables	**Value**
α || β	22° || 23°
$\mathbf{F_{Td}}$ || $\mathbf{F_{TdOriginal}}$	$80 lbf$ || $100\ lbf$
Load Cell Ratio	0.552577
Drawworks Ratio	0.447423
LoadCell Tension	$44.2062\ lbf$
Drawworks Tension	$42.3819\ lbf$
Weight On Bit	20 lbf

Table 4.1: Analytical WOB calculation results

4.2 Top Drive Assembly Dynamics

The Top Drive assembly is composed of a 2-HP permanent magnet DC motor along with the drill string and bottom hole assembly. Figure 4.3 describes a simple electrical model for a permanent magnet DC motor. The characteristic response of such motors can be described by:

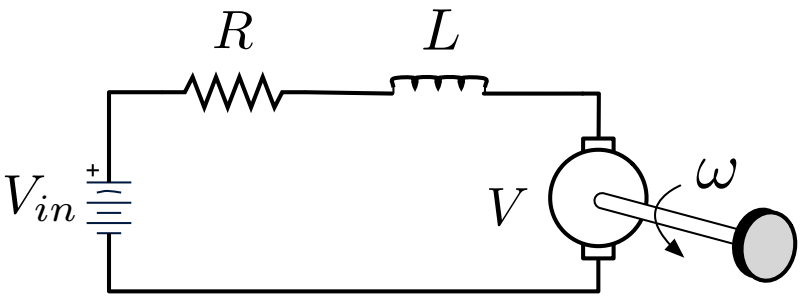

Figure 4.3: Mathematical model of an electric Motor

$$T = K_t i \tag{4.6}$$

$$V = K_e \theta = K_e \frac{d\theta}{dt} \tag{4.7}$$

Where T is the motor torque in Nm, V_{in} is the induced voltage through the coils, I is the current, θ is the rotational displacement of the motor shaft in Radians, K_t is the torque constant in Nm/A and $K_e$is the voltage constant in $V/Rad/s$. When an input voltage is applied V_{in} to the coils, the voltage equation is affected by the drop in the potential difference across the armature due to the coils electrical resistance. This relationship is given by:

$$V_{in} = R_a i + L_a \frac{di}{dt} + V \tag{4.8}$$

where R_a is the armature resistance in Ohms Ω, L_a is the armature inductance in Henry (H) and i is the electrical current in Amperes (A). The inductance resistance is usually neglected it accounts for a fraction of the armature flux and is not

used in the generation of torque. A gear motor drives a mechanical load coupled with electrical static and dynamic mechanical subsystems such as the armature, circuits, gears and shaft. The primary loads are the moment of inertia (J) and friction damping coefficient (ξ) of the motor's shaft, therefore, the varying torque is given by:

$$T = J\frac{d^2\theta}{dt^2} + \xi\frac{d\theta}{dt} + T_L$$

We can write the following relationship equations after Equation 4.2 applying Newton's and with Kirchhoff's laws :

$$K_t i = Js^2\theta + \xi\theta s$$

$$V(s) - K_t\theta s = R_a i + L_a i s$$

it can be seen that i can be expressed as:

$$i = \frac{V - K_t s\theta}{R_a + L_a s}$$

allowing to reduce equatio 4.2 to:

$$J\theta s^2 + \xi\theta s = K\frac{V - K_t\theta s}{R_a + L_a s} \tag{4.9}$$

from Eq. 4.2 the relationship between the applied voltage (V) and angular position (θ) can be derived as :

$$G_m(s) = \frac{\theta(s)}{V(s)} = \frac{V(s)}{s[(R_a + L_a s)(Js + \xi) + K_t^2]} \tag{4.10}$$

recalling that ω is the angular velocity given by $\frac{d\theta}{dt}$, equation 4.2 yields:

$$G_m(s) = \frac{\omega(s)}{V(s)} = \frac{V(s)}{[(R_a + L_a s)(Js + \xi) + K_t^2]} \tag{4.11}$$

In state-space form, the governing equations above can be expressed by choosing the rotational speed and electric current as the state variables. The permanent magnet motor used in the rig is coupled with a gear mechanism to decrease the internal rotational speed of the motor and increase the maximum torque capacity. The relationship between the internal motor speed and the outer shaft is called a gear ratio (G_r). Neglecting the inertia and friction losses of the pulley and adding the relationship of from Equation 4.1 we derive:

$$\frac{T_m(s)}{V(s)} = \frac{K_t(Js + L_a)}{G_r((\xi + Js)(L_a s + R_a) + K_t^2)} \tag{4.12}$$

which relates the torque generated by the drawworks motor and the supplied voltage

Recalling from equation 4.1 the force acting along the drawworks line (F_{Dw} is

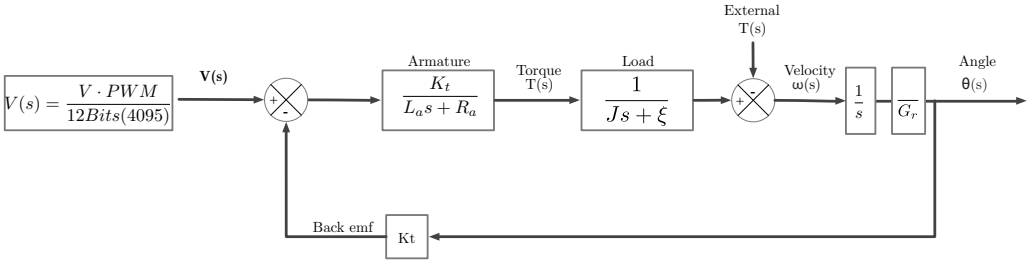

Figure 4.4: Block diagram of a DC motor

given by :

$$F_{Dw} = (F_{Td} + \Delta L_w) \cdot \csc[\alpha + \beta] \sin[\alpha] \tag{4.13}$$

Thus, the amount of torque being applied at the motor's shaft will be given by:

$$T_m(s) = F_{Dw} \cdot r \sin(\theta_2) \tag{4.14}$$

where r is the motor's shaft radius in meters and θ_2 is the angle at which force is being exerted tangentially to the motors shaft and assuming that the cable does not slip and an ideal pulley system is employed, this is, considering the friction factors and inertias negligible then the downward velocity will equal the tangential velocity of the drawworks motor shaft $\omega(s)$, and the amount of torque generated by the motor should be proportional to the force acting along the drawworks tension line. The resulting governing equation of motion assuming low spring coefficients and an over-damped response can be given by a simple second-second order transfer function.

Shear Stress and Pipe Torsional Deformation

Adequate selection and analysis of the drill string is critical to prevent performance limiters or pipe failure. Excessive vibrations can cause bit dysfunctions such as whirl, borehole patterns or stick-slip. A buckling and frequency response analysis of the drilling tube used in this study is presented in this section. The drilling string was specifically selected to increase the magnitude of vibrations and probability of failure if an inadequate control algorithm is present. The drill string chosen to run the drilling experiments discussed in this document was a 0.375”x0.035”x36” tube made of aluminum T 6061. Figure 4.5 pictures the cross section view of the aluminum pipe. Where r_1 and r_2 are the internal and external radius of the pipe respectively and τ_{max} is the maximum tangential torsional stress that the pipe can endure without failing.

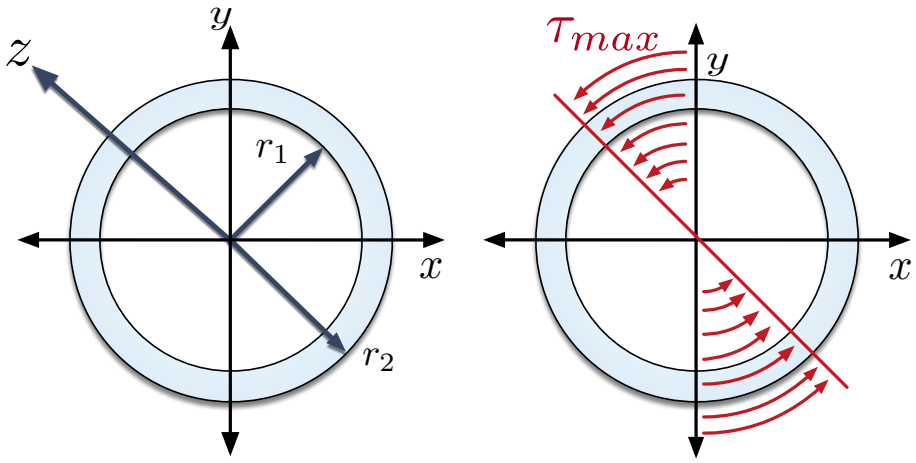

Figure 4.5: Tube cross section view

The maximum shear stress can be calculated assuming only an axial compressive force and static conditions by:

$$\tau_{max} = \frac{VQ_{max}}{I_c b} \tag{4.15}$$

Which yields a maximum torque of around 157.23 in-lb or 13.08 ft-lb incurring in an angular torsional deflection of 0.497 degrees per in-lbs of torque. Thus, a maximum torsional bending of 78.14 degrees can occur before mechanical failure.

Another approach to take into consideration both compression and torsional forces acting on the tube is given by the widely accepted yielding Von Mises yield stress criterion which is based on the maximum distortion energy theory. It relates triaxial stress to an equivalent stress that is a theoretical value to relate a generalized three-dimensional (3D) stress state and compare it with the yield strength of a uniaxial failure criterion. If the triaxial stress exceeds the yield strength, a yield failure will occur. Under this assumptions, the maximum torsional stress was found to be around 20 - 25% less than under single axial load.

The area Moment of Inertia is given by:

$$I_m = \frac{\pi}{64} \cdot (OD^4 - ID^4) = \frac{\pi}{64} \cdot (0.375in^4 - 0.305in^4) = 5.459E^{-4}in^4 J_m = \frac{m}{2} * (RO^2 + RI^2) \tag{4.16}$$

The theoretical axial spring constant for the hollow tube is given by:

$$K_c = \frac{Area \cdot E}{L} = \frac{0.00384845in^2 \cdot 10^7 psi}{36in} = 1069.01lbf/in. \tag{4.17}$$

Clearly, the theoretical stiffness of the tube will yield an over-damped system especially if an axial force is acting on it. The tube will fail at a lower compressive stress due to buckling. The drilling string first natural frequency can be derived as:

$$\omega_n = \sqrt{\frac{123.71N/m}{0.059928Kg}} = 45.4362Rad/s \tag{4.18}$$

4.3 Buckling Analysis

Buckling is a failure mode of a structural element due to high compressive stress; it is one possible cause of pipe failure and doglegs while drilling. The pipe will abruptly break when the axial compressive stress at one point is higher than the ultimate compressive stress of the material. Strength is the maximum load a material without failing and stiffness is the magnitude of deflection.

Euler's buckling theory relates the maximum axial compressive load capacity for a perfectly homogeneous and straight column. This load is referred as the critical load (F_{cr}), the maximum load causes the column to bend and be unstable, the introduction of any lateral force in this state will make the column lose its equilibrium point and fail by buckling. If an excessive load is applied significant, permanent will deformations occur if the axial compressive stress is higher than the modulus of elasticity of the material.

Bucking theory applies to long uniform columns that tend to fail by the material elastic stability limits instead of inelastic stability or strength limit. The slender ratio relates the effective length of a column to the radius of gyration of its cross section in two dimensions. The column section tends to buckle around the minimum radius of gyration given by ($r = \sqrt{\frac{I}{A}}$). The slenderness ratio is given by $\frac{L}{r}$. A column is considered long if:

$$\frac{L}{r} > (\frac{\pi}{k})\sqrt{\frac{2E}{\sigma_z}}$$

The critical compressive load that causes buckling decreases as the slenderness ratio increases. Usually, if the slenderness ratio is greater than 120, failure occurs by buckling, otherwise, failure will occur by minimum stress or inelastic stability. The critical load greatly varies depending on the imposed boundaries conditions at both ends of the column. The boundary conditions of interest are shown in Fig. 4.6.

The governing differential equation for transverse displacement where the column materially homogeneous and the load acting axially on it are considered constant given by:

$$\frac{\delta^2}{\delta y^2}[EI\frac{\delta^2}{\delta y^2}x(y,t)] - \frac{\delta}{\delta y}[P\frac{\delta}{\delta y}x(y,t)] + m\frac{\delta^2 x(y,t)}{\delta t^2} = 0 \tag{4.19}$$

Where E is the modulus of elasticity, I is the area moment of inertia, m is the

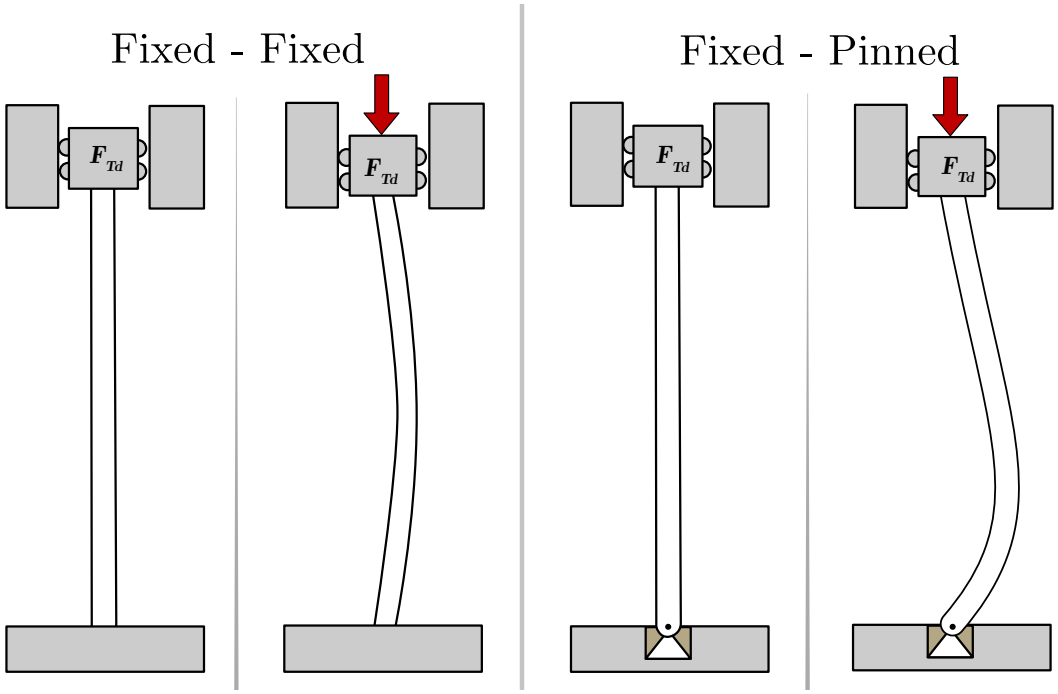

Figure 4.6: Assumed boundary conditions for Euler's buckling theory

mass per unit length, L is the tube length and P is the axial compression load *(from Han et al. 1999 [74])*.

A simplification using simply pinned boundary condition of Eq. 4.3, and solving for the column Euler's critical load is defined as:

$$F_{cr} = \frac{2.046\pi^2 EI}{L^2} \tag{4.20}$$

Consequently, increasing material stiffness or moment of inertia increases the buckling strength while the length is quadratic inversely proportional to the maximum load capacity for given material and shape.

The area moment of inertia depends only on the cross-sectional shape of the body being modeled without taking into consideration it's material properties. The

moment of inertia for a hollow circular shaft is calculated by:

$$\begin{aligned} I_x = I_y &= \frac{\pi}{4}(r_2^4 - r_1^4) \\ &= \frac{\pi}{64}(D^4 - d^4) \\ J_z &= \frac{\pi}{2}(r_2^4 - r_1^4) \end{aligned}$$

Buckling Finite Element Analysis

Buckling failure was modeled by a finite element eigenvalue-eigenvector solution. The column was discretized modifying a previously modeled FEA algorithm by Siva [75]. The model uses two nodes Euler beam elements with two degrees of freedom, i.e. axial displacement and rotation on each node with Intermediate nodal points. The eigenvalue problem is of the form $|K + \lambda mKF|\delta m = 0$ where λm is the buckling load factor, KF is the extra stiffness generated by the burden stresses, F, and δm is the buckling displacement shape for the n^{th} node. A brief description of the derivation of the geometric matrixes and fundamental application of the FEA theory is described, the reader is referred to external documentation on this amazing subject.

Usually, the number of coefficients of a displacement function equal the total number of degrees of freedom (DOF) of each discrete element. It is possible to express the displacement function as a function of the nodal displacements by evaluating the function locally at each node and solving for q_n. Interpolations func-

tions describe how the assumed displacement function changes over the region of the element. If the interpolation matrix is linear the matrix form can be given as:

$$u(x) = \begin{bmatrix} N_1 & N_2 & N_3 & N_4 \end{bmatrix} \begin{bmatrix} q_1 \\ q_2 \\ q_3 \\ q_4 \end{bmatrix} \tag{4.21}$$

The functions N_n are called interpolation functions because they describe how the assumed displacement function varies over the domain of the element [76]. In this case, the interpolation functions and the displacement function in matrix forms is:

$$N1 = 1 + \frac{4x^3}{L^3} - \frac{3x^2}{L^2} \qquad N2 = \frac{x(L-x)^2}{L^2}$$
$$N3 = \frac{x^2(3L-2x)}{L^3} \qquad N4 = \frac{x^2(x-L)}{L^2}$$

The method is valid as long as deformation occurs along the axial direction. The local stiffness matrix k is:

$$K = EI \begin{pmatrix} \frac{12}{l^2} & \frac{6}{l^2} & -\frac{12}{l^3} & \frac{6}{l^2} \\ \frac{6}{l^2} & \frac{4}{l} & -\frac{6}{l^2} & \frac{2}{l} \\ -\frac{12}{l^3} & -\frac{6}{l^2} & \frac{12}{l^3} & -\frac{6}{l^2} \\ \frac{6}{l^2} & \frac{2}{l^2} & -\frac{6}{l^2} & \frac{4}{l} \end{pmatrix}$$

The elemental kinetic energy matrix of the beam element is given by:

$$M = \int_0^l [N]^T \rho \mathrm{A}(N) dx$$

$$M = \rho A \begin{pmatrix} \frac{38l}{35} & \frac{l^2}{14} & \frac{39l}{70} & -\frac{11l^2}{140} \\ \frac{l^2}{14} & \frac{l^3}{105} & \frac{13l^2}{420} & -\frac{l^3}{140} \\ \frac{39l}{70} & \frac{13l^2}{420} & \frac{13l}{35} & -\frac{11l^2}{210} \\ -\frac{11l^2}{140} & -\frac{l^3}{140} & -\frac{11l^2}{210} & \frac{l^3}{105} \end{pmatrix}$$

Where is ρ is the mass density and A is the cross-sectional area of the column. The column is subjected to a compressive axial periodic force p(t) that is modeled by:

$$K = \int_0^l [\frac{\delta N}{\delta x}]^T [\frac{\delta N}{\delta x}] dx$$

The geometric stiffness matrix is also referred as the stability matrix is presented as:

$$K_s = \frac{1}{30l}\begin{pmatrix} 36 & 3l & 36 & 3l \\ 3l & 4l^2 & -3l & -l^2 \\ -36 & -3l & 36 & -3l \\ 3l & -l^2 & -3l & 4l^2 \end{pmatrix}$$

As discussed earlier, the Euler's buckling solution reduces to an Eigenvalue equation. To calculate the magnitude of the velocity and stiffness of the column matrix, a non-trivial solution to this system of homogeneous linear equations exists if and only if the determinant of:

$$|K - \lambda K_s| = 0$$

Where K and K_s is the stiffness matrix of the beam, the constructed geometric stiffness matrix, respectively, the Eigenvalues values corresponds to the Euler buckling load and the Eigenvectors, to the buckling mode, i.e. the shape of the column.

Drill String Natural Frequencies

The natural frequency of the column can be determined by solving the following eigenproblem:

$$|K - \lambda \omega M| = 0$$

The algorithm was run to compute both the theoretical natural frequencies of

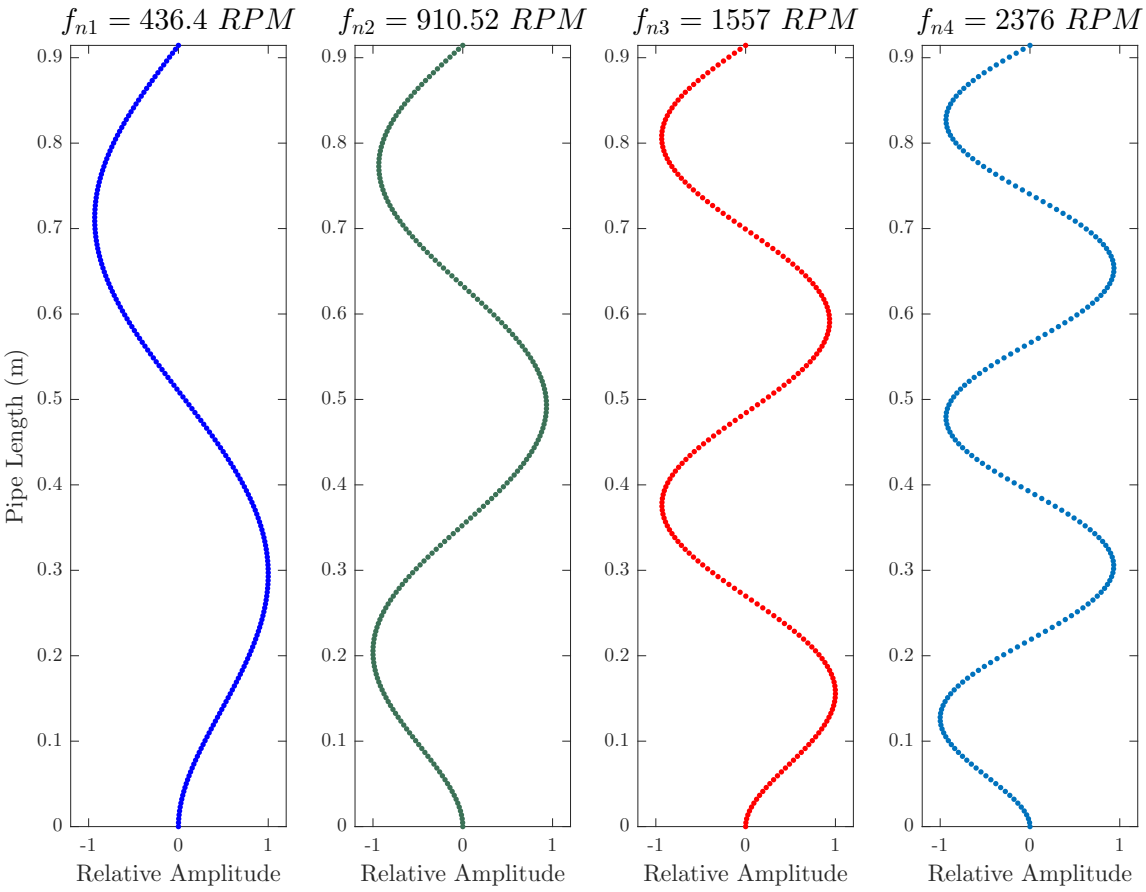

Figure 4.7: Resonant frequencies of drill pipe

the drilling pipe and the critical buckling force. The results of such computations are shown in 4.2 .

The critical buckling load for the drill pipe is shown in Fig. 4.8, the buckling results are accurate based on previous drilling tests and experience.

The natural vibrations computed by the simulation are correct and in line with the theoretical derivation of the Euler's buckling theory. However, the drilling pipe used in the experiment does not correlate well with the assumptions behind it. Furthermore, the theory does not take into consideration a dynamic or constant

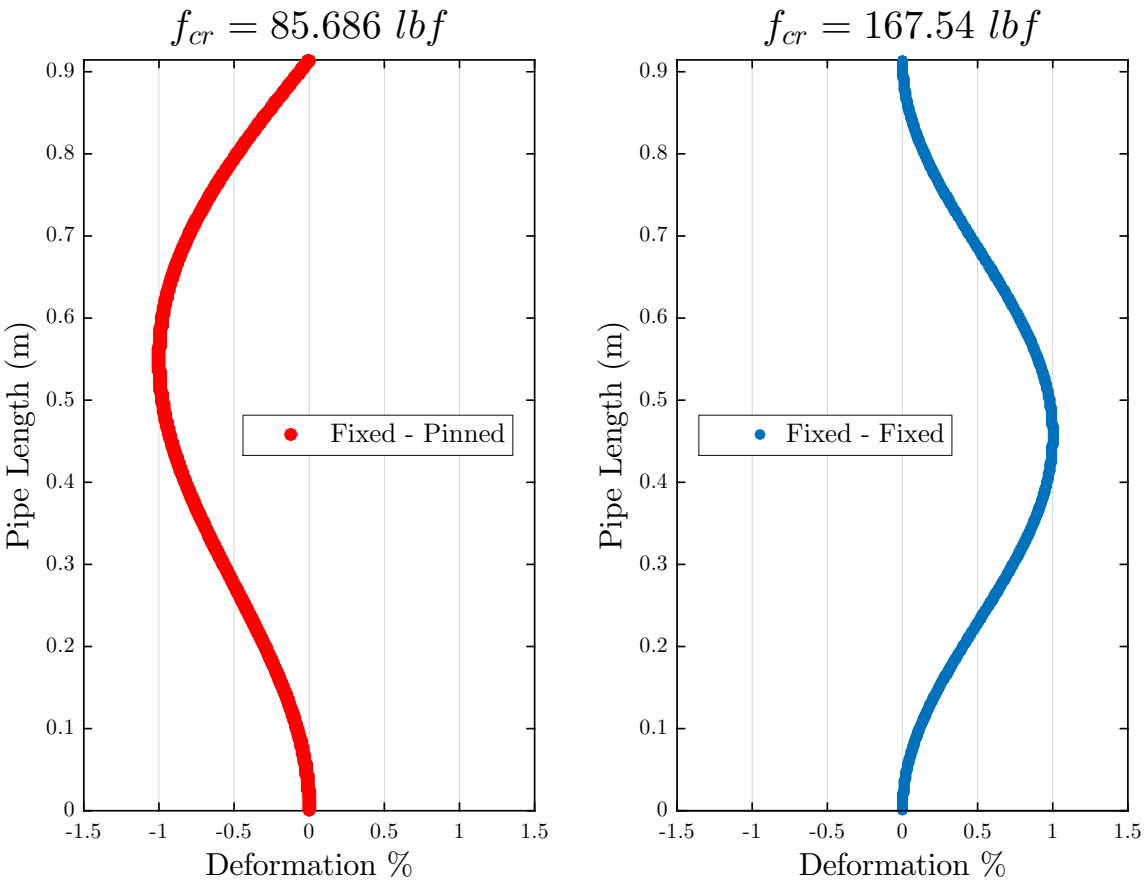

Figure 4.8: Euler's critical buckling force

axial force acting along the string, in addition to the rotational torque applied and bearings friction factor. Thus, the actual natural frequencies are overestimated.

An axially compressed circular cylinder is highly uniform and sensitive to lateral forces acting on it, if the pipe is in compression, the natural frequencies will be lower [77]. Also, if the pipe is surrounded by liquid, the fluid velocity, pressure and properties such as it's density, viscosity will affect the magnitude of the natural frequencies. Multiple research papers have modeled the response and attenuation under such scenarios. [78]. A simplified method to get representative results is

defining the motor speeds and computing the theoretical Euler's buckling natural frequency under compression stresses.

The American Petroleum Institute (API) defines critical speeds and resonances as follows[79]. Critical Speed, "A shaft rotational speed that corresponds to the peak of a non-critically damped (amplification factor > 2.5) rotor system resonance frequency. The frequency location of the critical speed is defined as the frequency of the peak vibration response as defined by a Bodé plot" and Resonance as "The manner in which a rotor vibrates when the frequency of a harmonic (periodic) forcing function coincides with a natural frequency of the rotor system".

The peak frequency on the Bode plot is around the damped natural frequency. A system is said to be resonant when the excitation frequency equals the damped natural frequency. A high damping system has no real peak and is said to be 'over damped' Lastly, the am- amplitude of oscillations continues to decrease along for all higher frequencies.

Structures can be seen as a sequence of discrete lumped masses approximations to approach a continuous mass distribution. The challenge is that there are multiple natural frequencies and for each rotational mass and discrete element of a system. Computing the overall natural frequencies as a continuously lumped mass analytically will yield only and estimate for a lumped mass model. FEA can be used to simulate and acquire more accurate behaviors.

Critical Buckling Force of Drill Pipe (f_{cr}) (lbf)	**Theoretical**	**Simulation**	**error %**
	85.6828 lbf	85.6859 lbf	0.00359 %

Natural Frequencies of Drill Pipe (f_n) (rad/sec)	**Theoretical**	**Simulation**	**error %**
1^{st}	45.7320	45.6999	-0.0716
2^{nd}	95.1226	95.3492	0.2382
3^{rd}	162.8060	163.0527	0.1515

Table 4.2: Numerical solution for the drill pipe's buckling critical load and natural frequencies

The calculations below are simple approximations to establish the natural frequency of rotational vibrations of hollow tubes in compression [78]. The natural frequency of a shaft equals the whirling speed. Whirl is due to resonant vibrations along the string when the drill string rotates at the same speed as one of the shafts natural frequencies. Modifying the speed and avoiding operating on a resonant frequency will eliminate excessive vibrations and mitigate the whirl dysfunction.

The natural frequency of a pipe is increased by an axial tension load and decreased by an axial compressive load.

$$\mathrm{F}\lambda_1 = \sqrt{\frac{\lambda_1^2 P}{\lambda_1^2 |\mathrm{Fcr}|} + 1}; (\lambda_1 = 3.9266;) (\lambda_2 = 7.06858;) (\lambda_3 = 10.2102;) (\lambda_4 = 13.3518;)$$

4.4 System Identification Procedure

The standard approach to control system design is to base the model on physical laws and restrictions to the corresponding physical parameters. This is called the classic or white box approach. Control systems are required to function based on noisy measurements and inaccurate instruments. Models that are set with adjustable parameters are called gray box models. In many control applications cases, linear models that do not completely represents a system based on an exact analytical solution to the relationship between the subprocesses involved, but approximate them are enough to acquire an acceptable level of controllability. These models are called black boxes model or method [80].

There are different model representations, for instance, transfer functions, state space, frequency response or differential equations that are used to represent a dynamic physical system. The level of parameterization or adjustable system parameters i.e. physical constants of each mass, its velocity, accelerations are based on what kind of model representation the designer chooses to use.

System identification modeling is the process of developing or improving an more accurate depiction of a physical system by analyzing it from actual measurements data. A mathematical model is always an approximation of real dynamic system. The properties and assumptions used in the development of many mathematical models vary because the full availability of observed data and limited knowledge of a given system prevent an exact mathematical representation of the system.

Furthermore, even if a great understanding of the system dynamics exists together with observable data to corroborate, a very complex model is often not desired. If an abstract representation of a process becomes too complicated, the control laws and models associated with it will also be complex. However, the actuators delays, limited bandwidth, and plant boundaries usually hinder the implementation of higher order systems and control algorithms. It is important to obtain experimentally verified models to utilize them for design improvements, performance evaluation, and cost reduction [81].

To acquire a fit between model output and observed data, an identification method, and a criterion function must be selected. The objective function is numerically solved to obtain a parameter estimation. A model validation step examines the accuracy of the fitted model to the real physical phenomena; the validation step is repeated until the model is considered appropriate. In practice, this becomes an iterative process until an accurate match can be drawn. The recommended practices to properly excite and acquire Inputs and Outputs data of a system are [82] [83] :

- Identifying a proper excitation signal. Using appropriate units, filters, sampling rates that relate to how the system will function in practice.
- Correct attachment of instrumentation calibration and positioning.
- Verifying that the output of the system correlates well with sampling rates set from the analytical model or identification algorithm.

- Adjust signal analog filters or averaging procedures for each signal.
- Minding those environmental variations such as temperature or vibrations that can introduce unwanted excitations to the system.
- Repeating several runs under slightly different parameters to obtain a pre-processed transfer function.

In this thesis, a closed loop controller was used to control both RPM and WOB accurately. The most important parameters in this design are the amount of Weight on Bit and the revolutions per minute that are used while drilling . Thus, especial attention was drawn into its analysis. The system was analyzed under static conditions, that is, without external disturbances acting on the motors. The magnitude of disturbances due to the drilling operation and polar inertias were regarded as random and harmonic perturbations.

The relationship between the input and output of the system is obtained using a modified pole-placement methodology that combines constraints on sensitivity functions. Acquired input and output data is imported into the MATLAB[84] workspace as a TimeSeries object, where a constructed model of the dynamic system was obtained by analyzing the input and output relationship in the time domain to identify the continuous or discrete time transfer function, process models, and state-space representations. A grey-box system identification for estimating the parameters of a defined model was used. The following workflow was used to generate the system response signals for post analysis:

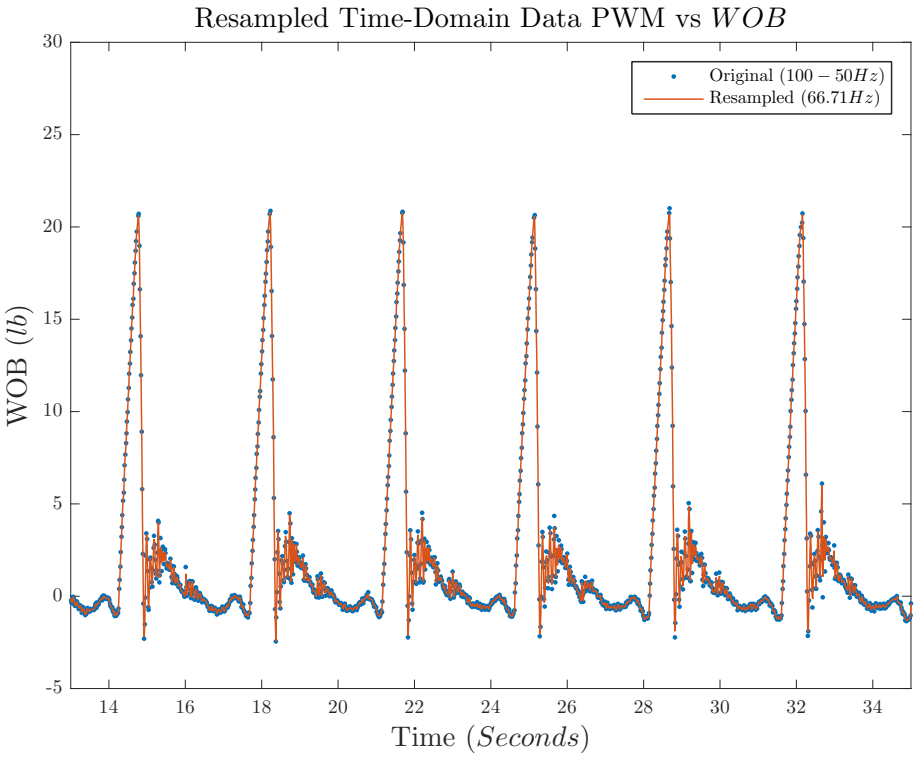

Figure 4.9: Resampled input PWM signal and WOB response

1. A calibration procedure was taken before and after each excitation runs to determine if our measured parameters were still accurate.
2. The sampling frequency was chosen based on the Nyquist theorem; which states that the minimum theoretical frequency rate at which an analog signal can be sampled without losing crucial information that limits the digital reproduction, is at least twice the original frequency. For instance, if a sine wave is oscillating ten times per second, this law dictates that a minimum sampling rate of twenty Hertz must be used to digitalize the signal. However, for practical purposes, a recommended sampling rate of at least eight times higher is recommended [85].

3. High frequency sampled raw data was acquired and saved using LabView through the NI cDAQ system.
4. The developed digital controller was meant to be implemented in a microcontroller; thus, data was also acquired through serial communication to determine the average processing and sampling time of the standalone loop.
5. Several tests were performed to assess the average sampling rate of the microcontroller both printing data and in stand-alone operation.
6. The excitation loop was programmed directly into the basic proportional controller and ran continuously until each test was finished.
7. Data was resampled and analyzed using the MATLAB® System Identification Toolbox. Example an input and output signal responses used to extract experiments and to determine the best reduced order transfer function is seen in Fig. 4.9.
8. Once an adequate signal was identified and used as the best response representation of the system, a higher order model was acquired.
9. The high-order transfer function obtained in step 8 was reduced to a second order one by decomposing the stable and unstable parts of the model and discarding the states that have low effects on the overall stable transfer function response to compute a lower order approximation.
10. Finally, the reduced order model was simulated in its closed loop form and a PID controller was tuned both experimentally and numerically.

4.5 PID Controller

Open-Loop vs Closed-Loop Control

An open loop system also referred as a feedforward controller does not rely on any sensors to determine the response to a given control input. A classic example can be a thermostat controlling an air conditioning system that cools a room just by switching it on and off depending on a threshold determined through the desired room temperature. The controller will send predefined saturated states (on/off) without confirming if the response is satisfactory. In a closed loop control scheme or feedback control system, the actual status of the room temperature will be verified, and the new room temperature will be used to compute the magnitude of the difference between the actual and desired room temperature to compute an adequate control signal to operate the air conditioning unit from 0 - 100 % capacity for example. In the realm of control systems theory, the algorithm used to calculate the control input or gain is referred as a controller, while the air conditioning unit used to regulate the room temperature would be referred as the plant.

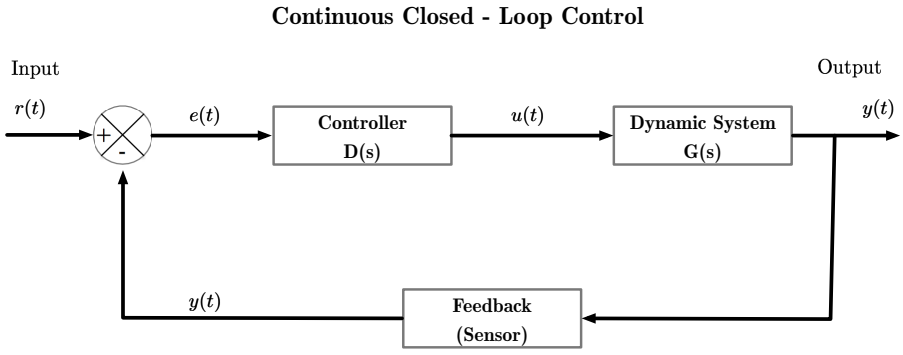

Figure 4.10: Continuous closed loop Control block diagram. Adapted from [86]

A Proportional Integrative Derivative controller calculates the error value between the desired set point and the measured output and calculates the required gain based on the proportional, integral, and derivative terms. The controller objective is to minimize the error over time by adjusting the control variable, which depending on the plant can be the input voltage of a motor or the amount of fluid injected to a hydraulic cylinder. The diagram representation of a PID controller is shown in Fig. 4.11.

In the Oil and Gas industry, this type of controllers are very commonly found from upstream to downstream operations. PID controllers are usually responsible for controlling pump pressures, flow rates and heating sources for chemical processes among others. In the drilling industry, these controllers are used by most 'auto-drillers' to control the drawworks and top drive motors [87].

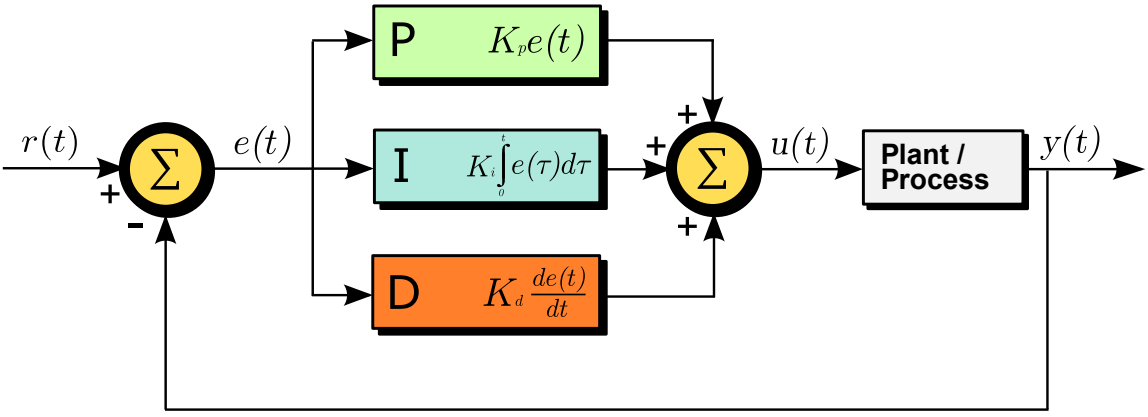

Figure 4.11: PID controller diagram. After [88]

From the block diagram representation of a PID controller shown in Fig. 4.11. The output of the system at time t ($u(t)$) can be derived as the sum of the three com-

puted parameters times the error where the proportional, integral, and derivative gains are defined by k_p, k_i, and k_d respectively:

$$u(t) = K_p e(t) + \frac{K_p}{T_i}\int_0^t e(\tau)d\tau + K_p T_d \frac{de(t)}{dt} \tag{4.22}$$

Micro-controller Driven PID Controller

The proposed PID controller was implemented in a micro-controller running at 84MHz. A micro-controller is a System on a Chip (SoC) integrated circuit containing a processor core, memory, and programmable inputs/outputs. Designed for embedded applications such as automatically controlled devices and control systems. Using a micro-controller reduces the size, costs and energy consumption compared to a design based on a microprocessor or a full sized computer. Modern consumer level micro-controllers are capable of archiving remarkable high operating speeds and efficiencies [4].

With the invention of computers, feedback references, and controller design began to be both acquired and implemented digitally. Thus, the continuous time analog signal is sampled and discretized, becoming a discrete representation of the original analog signal, this simplified control loop structure can be seen in Fig. 4.12 where T is the sampling time and kT the sampled element using an analog to digital converter A/D at time T.

The output of the discretized system ($u(t)$) can be derived in a similar fashion

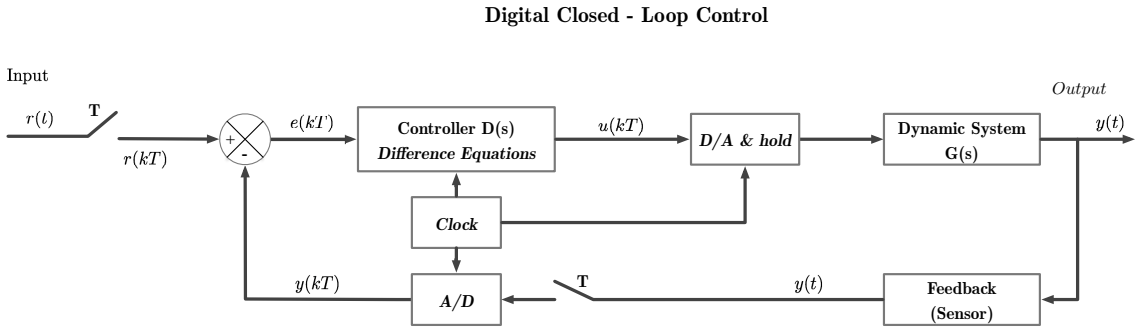

Figure 4.12: Discrete closed loop control block diagram. Adapted from [86]

as:

$$u(k) = K_p e(k) + K_i \sum_{0}^{k} e(k)\Delta t + K_d \frac{\Delta e(k)}{\Delta t} \tag{4.23}$$

Gears motors are more susceptible to overheating due to the amount of current being drawn to generate torque and the friction between internal gears; the input gain supplied should be kept between the maximum and minimum values specified by the manufacturer. The controllers incorporate this saturation point as with a PWM value that limits the amount of voltage supplied to the Gear motor. Furthermore, the algorithm also incorporates an *anti-windup* feature using a back-calculation Anti-windup method, to flush the PID Controller's integrator buffer when the controller hits the specified PWM saturation limits. This prevents the integral term from saturating and stops calculating the integral gain until the plant stabilizes to normal control margins.

Lastly, a gain - scheduled setup was defined for each PID controller defined in this thesis. This is, a controller whose gains are automatically adjusted as a function

of the operating condition, which in this case is determined by both the revolutions per minute and the amount of WOB that the controller is trying to follow. Gain scheduling is a common strategy to control systems whose dynamic conditions can change. The developed PIDs controller structures use a lookup table from which the P, I and D gains proved to be stable are drawn. Three gain parameters were chosen and defined as aggressive, moderate and conservative controller gains.

5 RESULTS

The drilling rig central operation room is seen in Fig. 5.1 from left to right the mechanical structure of the model rig can be seen, followed by the junction boxes where all the electronics and control circuits were isolated from external conditions. Four color-coded emergency switches are easily accessible that can shut down all power from the overall system or the supplied power to the motors. Next, the central driller's graphical user interface is seen at the central part of the picture where the drilling operation can be started, monitored, modified or stopped. Lastly, several Pason electronic drilling recorder and power systems are seen at the right end.

Figure 5.1: Drilling machine setup

A closer view of the GUI can be appreciated in Fig. 5.1. The main parameters built into the driller's GUI are the drilling revolutions per minute, the current WOB, drilling torque, and the calculated depth of cut. In addition, the magnitude of vibrations plotted in the frequency domain, the instantaneous power consumption of the rig, downhole data as well as the average rate of penetration and remote server connection status.

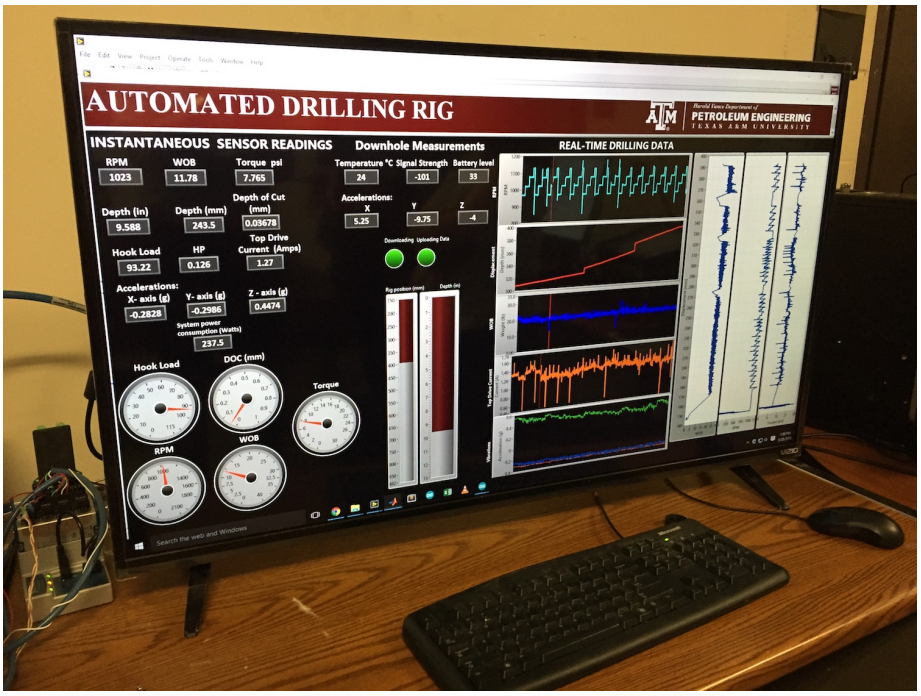

Figure 5.2: Driller's graphic user interface

5.1 Data Filtering

A practical example of the analog and digital methods used to condition instrumentation data is shown in Fig. 5.3. The signal on the left represents the raw sampled data from the displacement sensor used to measure depth, from which, several other derivatives variables were computed, such as the rate of penetration (ROP), Mechanical specific energy (MSE) and depth of cut (DOC). It is clearly visible that over the 30 seconds interval, raw data is filled with high amounts of noise coupled with an evident low-resolution sensor's digital to analog converter (DAC) which discretizes the signal, leading to wide voltage steps and gaps that translate into an even greater physical unit steps. Which renders the aforementioned signal useless for any real-time analysis or control loop.

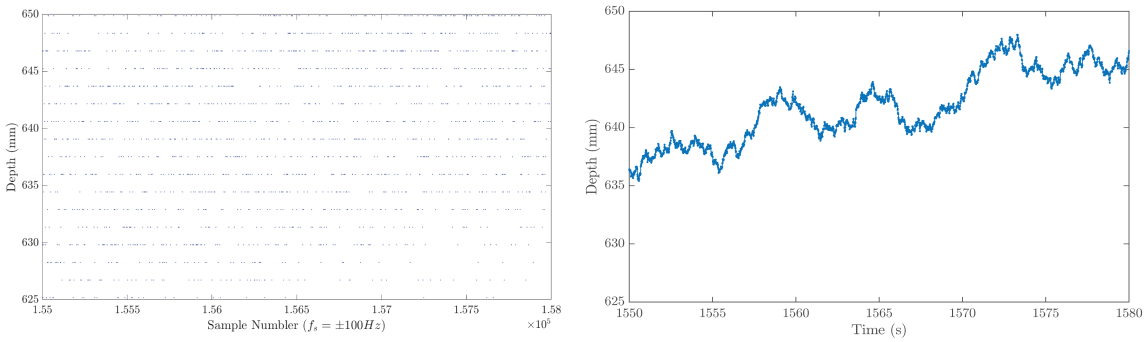

Figure 5.3: Noisy unfiltered displacement data vs filtered data

Analog techniques used to correct as much as possible this effect included the installation of ferrites claps along the main instrumentation signals cables, the design and implementation of low pass analog filters using operational amplifiers and

proper cable shielding. In addition, other digitally implemented signal conditioning methods were also incorporated. Specifically, a second order Butterworth filter, moving average, and using a lower effective sampling time. The same signal is seen on the right-hand side of the figure. From which, real measured values are clearly visible and identifiable, several relationships could be programmatically extracted from this conditioned sample and the algorithm was be able to determine that the rig was currently drilling at 0.334 mm/s or 3.94 ft/hr and using an average weight on bit of about 45 lbf and 700 revolutions per minute.

5.2 Controller Simulation

Second order continuous transfer functions were used to simulate the drawworks controller response. The identified transfer function and the theoretical DC motor Simulink model used for simulation purposes are shown in Fig. 5.4 and Fig. 5.5.

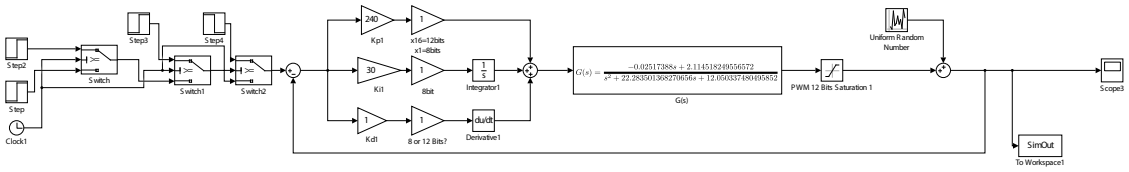

Figure 5.4: Simulink closed - loop identified transfer function simulation

In addition to the continuous time model, a discrete time parametrization was derived and simulated. However, its simulation accuracy was lower due to non-uniform sampling times found on the acquired tested response data. This happened

because the parsing and transmission of data values over the serial port take valuable processing ticks from the micro-controller, which makes the effective sampling time to vary and to be higher than the real running sampling time when running without printing data over the communication port. The aforementioned effect and other mechanical delays are inherently included in the identified continuous-time transfer function. Therefore, making its simulation more accurate.

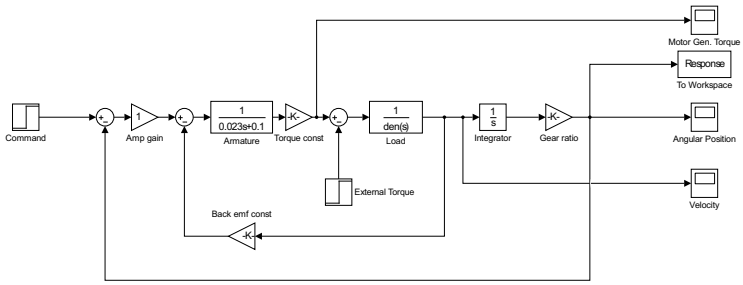

Figure 5.5: Simulink's geared DC motor simulation

The PID controllers were implemented digitally using a continuous average sampling time of 400,000 Hz and outputting the new motor gain every 10ms. A state space theoretical representation simulation was also carried, however, further experiments are needed to verify the accuracy of the control devices' performance parameters to properly adequate and fine tune the system. Nevertheless, the simulation of the identified transfer function as seen in Fig. 5.7 shows a strong match with the real system response under static conditions.

A gain-scheduled setup for the PID controller was chosen since it exhibited an improved response over holding constant P, I and D gains regardless of the magnitude of error in the applied weight on bit (WOB). Three scheduled gain sets

were established based on the amount of error between the reference point and the feedback WOB seen at a given time, going from 2%, 10%, and 50%, we referred to them as aggressive, neutral and conservative controller gains respectively. The algorithm used a look-up table to verify the limit criteria and modify the controller gains accordingly. The step response of the aggressive and conservative PID gains are shown in Fig. 5.6.

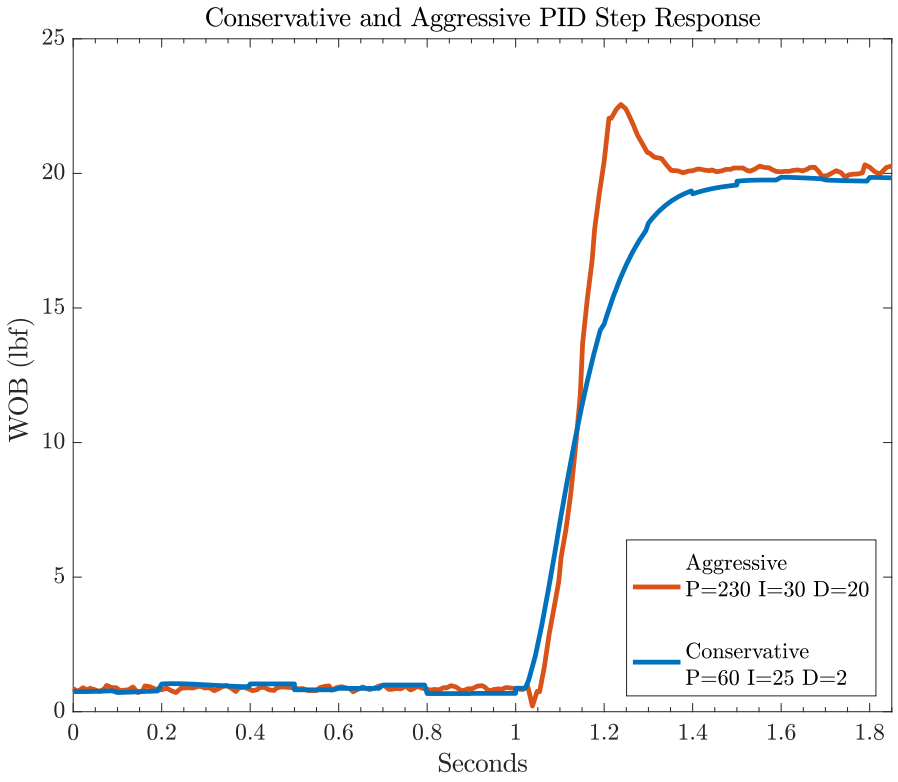

Figure 5.6: Conservative vs aggressive PID controller step response

The comparison between the simulated controller step response against the real system's step response is seen in Fig. 5.7. A good match is clearly seen for the response determined by the linear portion of the identified system; this is when the

drawworks line is in tension and more weight is applied to the bit by allowing the drawworks motor let the top drive assembly along the drilling string go. However, a small mismatch is observed when the motor has to drastically reduce the amount of weight supplied to the bit by pulling the drawworks line back. This is because a reduced second order linear transfer function is being simulated and non-linear factors such as friction losses; the drawworks line spring-like behavior and other elastic material properties are not considered.

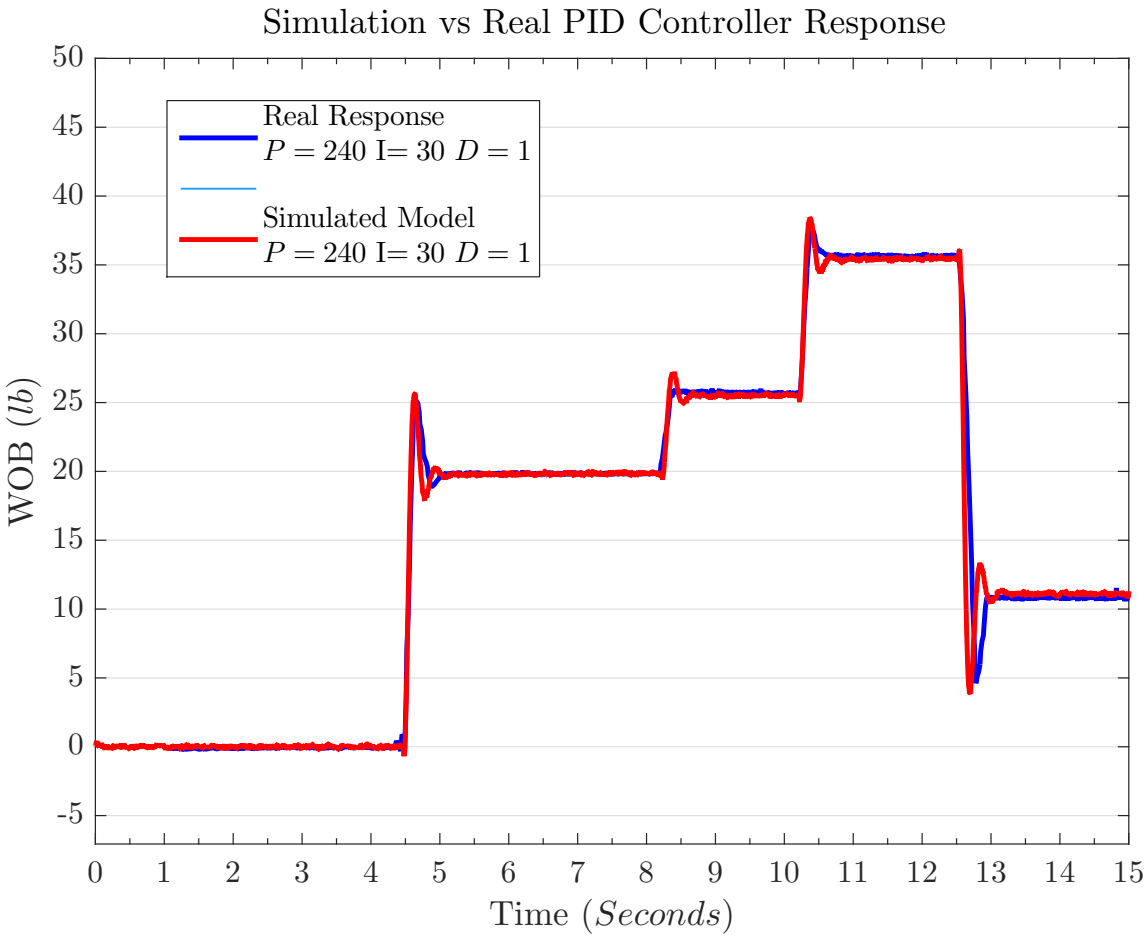

Figure 5.7: Closed loop PID controller simulated vs real step response

The step response under static conditions using a simple low performance on/off controller setup is seen in the left half of Fig. 5.8, the performance of this baseline controller never stabilizes at the given WOB set point, and the error magnitude is simply absurd at around 27%. This baseline control setup pales when comparing it to a similar step based test using the updated WOB scheduled-gain PID controller setup, where the settling time is less than 0.3 seconds and the controller never becomes unstable.

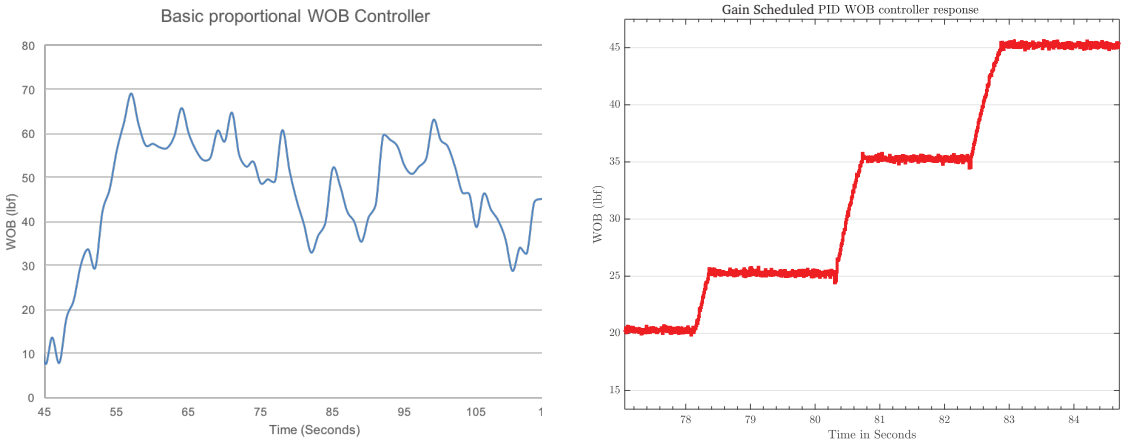

Figure 5.8: Gain-Scheduled WOB PID controller vs baseline performance

5.3 WOB Control Under Drilling Conditions

The displacement of the Top Drive can be used to measure the drill motion in the axial direction; however, this alone does not determine the drilling performance nor the applied WOB. A calibrated high precision Wheatstone bridge is used to measure the applied force at the bit, and the system is controlled using the improved PID controller. Fig. 5.9 shows the performance of the newly developed Gain-Scheduled PID control under dynamic drilling conditions. The signal shown is unaveraged and unfiltered. The test was performed using air gaps between the rock formation samples, and even while drilling through those unexpected conditions, the controller rejected such disturbances reapplying the desired weight on bit in and recovering and settling in less than half of a second.

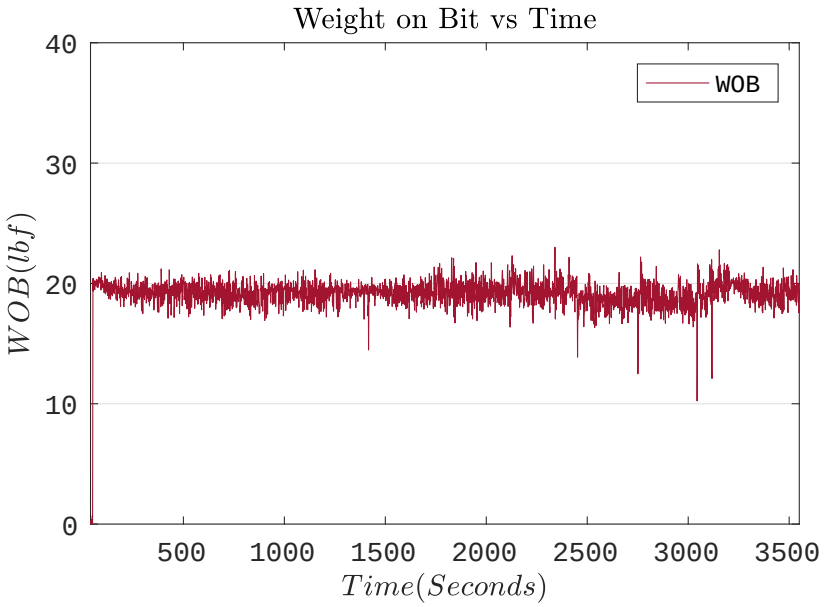

Figure 5.9: WOB control performance under dynamic drilling conditions

5.4 Whirl and Borehole Quality

A small misalignment or slight deviation in the axial displacement while rotating can create large normal and lateral forces that consequently create excessive vibrations. Which, can create problems such as whirl patterns and other bit dysfunctions that lead to poor drilling performance, excessive wear, and mechanical pipe failures [89]. Whirl-mitigation and control improvements are seen in borehole quality. A severely damaged hole is seen in Fig. 5.10 where borehole patterns that were caused by excessive bit whirl are clearly identifiable. In contrast, a straight, clean borehole is seen in Fig. 5.11 both tests were drilled into the same formation, under manual and automatic control. The patterns were completely eliminated using both type of bits with and without stabilizers, even when drilling hard formations like granite.

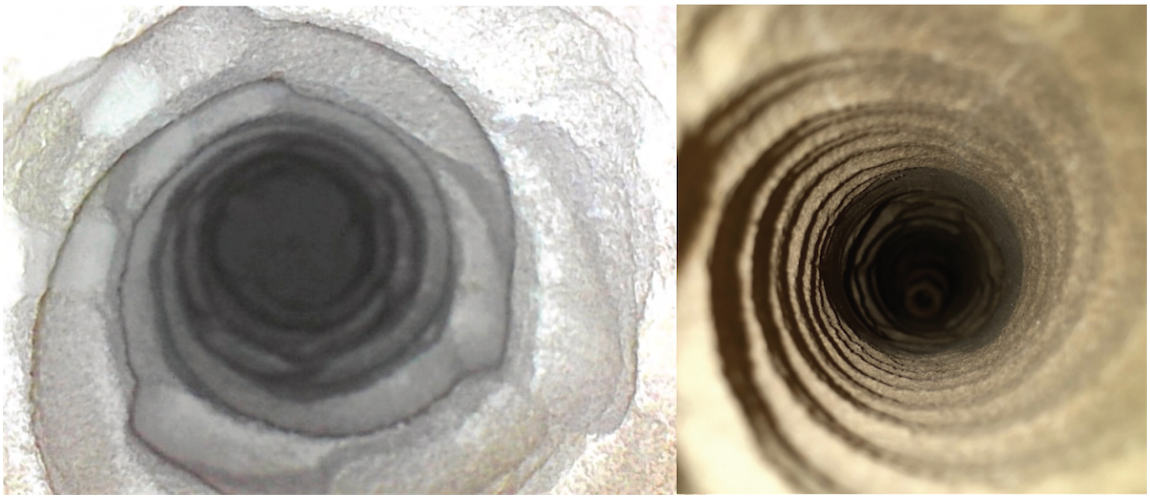

Figure 5.10: Borehole patterns caused by excessive bit whirl

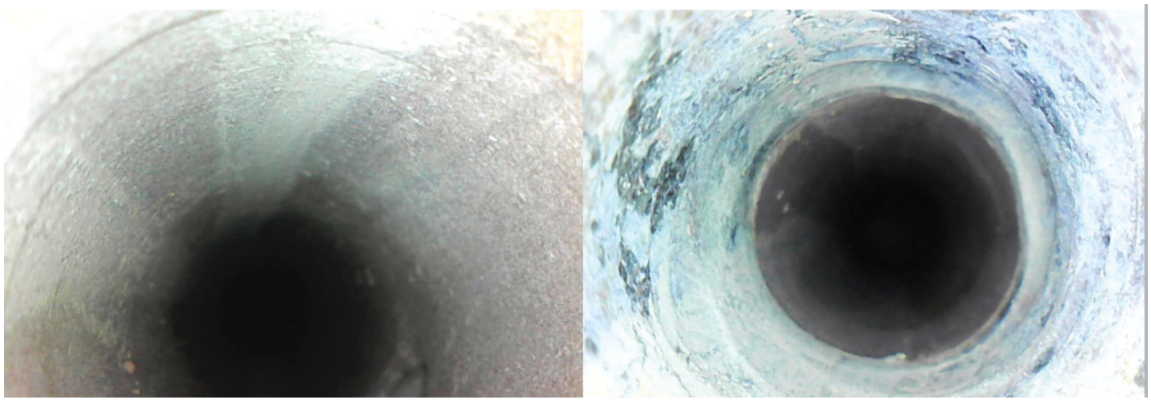

Figure 5.11: Borehole quality under sandstone and granite formations

Time and frequency domain analysis of the vibration data obtained from drilling tests showed a clear vibrational signature in the frequency domain when bit whirl was occurring. The data used for such analysis was sampled at a 1000 Hz, and a discrete fast Fourier transform was implemented to extract and identify such spikes in the magnitude of vibrations at a given frequency band. The power magnitude of vibration data in over the frequency domain corresponds to a function of the RPM, the number of cutters of the bit that is being used and the amount of WOB applied as shown Fig. 5.13 the magnitude of the vibrations was diminished by increasing the average WOB from 20 lbf to 50 lbf in such test. Improving the efficiency of the mechanical specific energy (MSE), the amount of DOC, and consequently, the average rate of penetration (ROP). The system is mainly a second order spring damper system, if vibrating in close to resonant frequency whirl will happen and the characteristic 2^{nd} order vibration signature will be clearly seen as shown in Fig. 5.13.

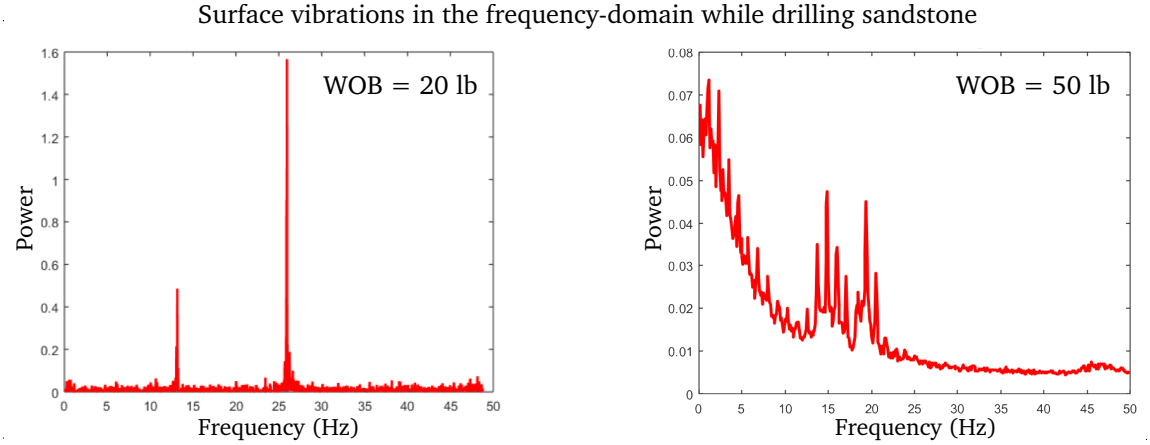

Figure 5.12: Frequency-domain drill-string vibrations with varying WOB

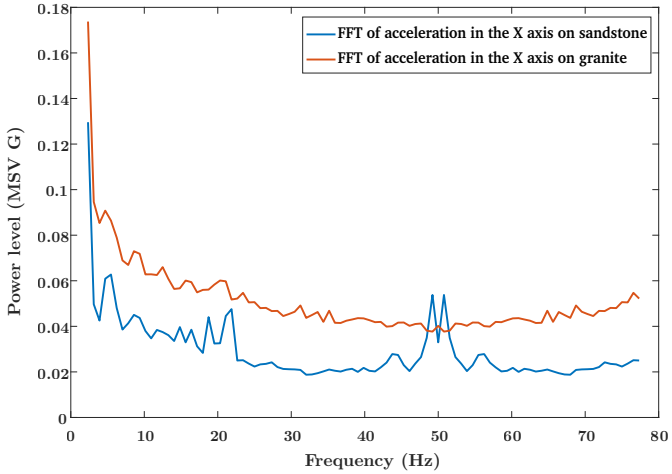

Figure 5.13: Frequency-domain vibrations while drilling sandstone and granite

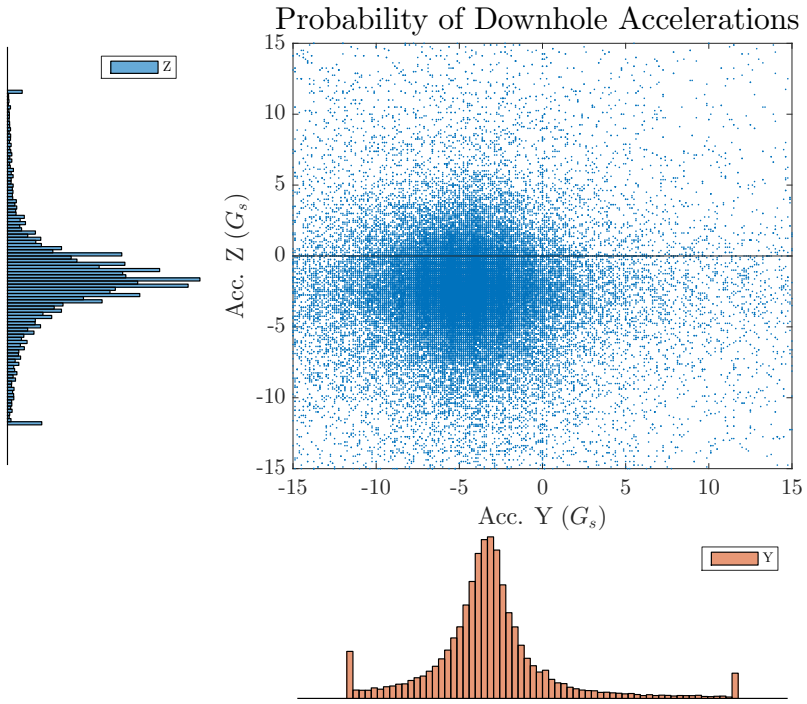

Figure 5.14: Probability of downhole accelerations

The probability of downhole vibrations was determined to be within a predetermined limits for a given bit, rpm, and formation. Further clustering analysis is needed to derive a real-time controller that takes into downhole vibrational data into consideration as seen in Fig. 5.14.

Furthermore, Fig. 5.15 shows the frequency domain of a drilling test performed mostly on sandstone and cement at around 680 RPM using a two cutters custom PDC bit at around 45lbf. The magnitude of vibrations in the 22.6 Hz band correspond to the actual drilling operation in which a clear pattern can be seen. Whirl was found to be happening at those times from the performed after analysis.

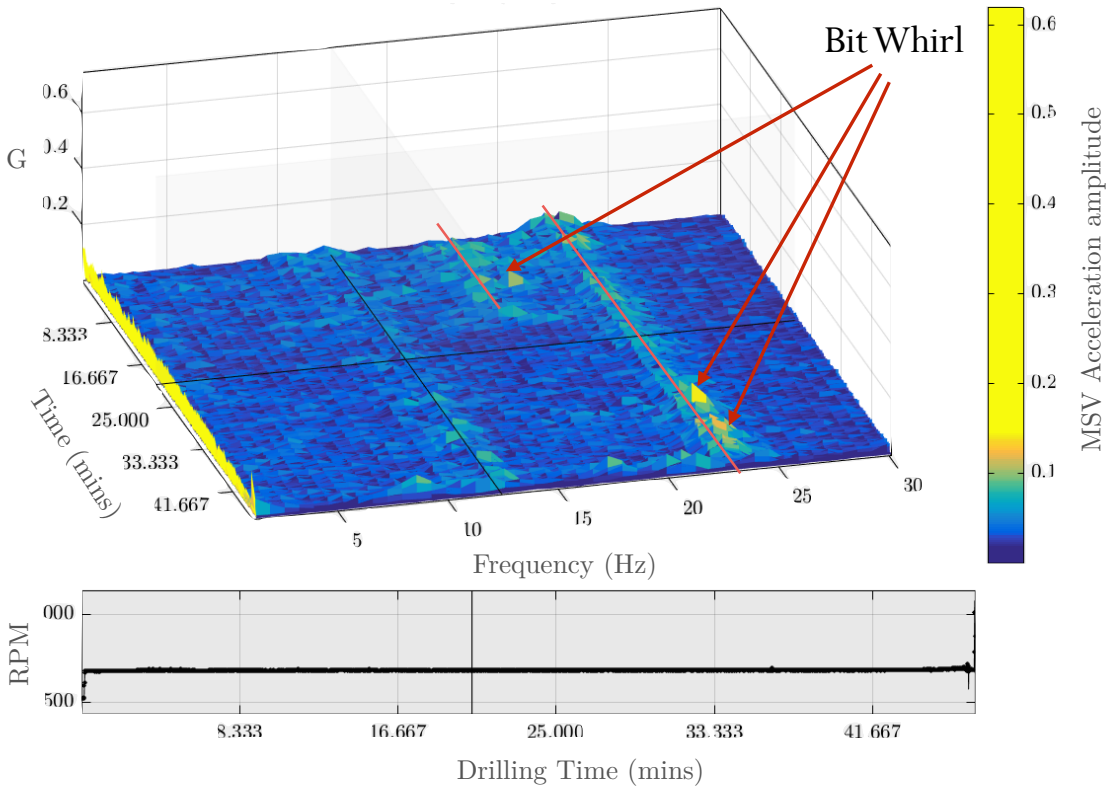

Figure 5.15: Frequency domain surface plot of bit whirl signatures

5.5 Determined ROP vs Drilling Parameters

The following plots show how the rate of penetration changes over different ranges of revolutions per minute and the applied weight on bit for different formation types. A proper fit function was derived from this data, to determine the expected ROP output and optimize its response.

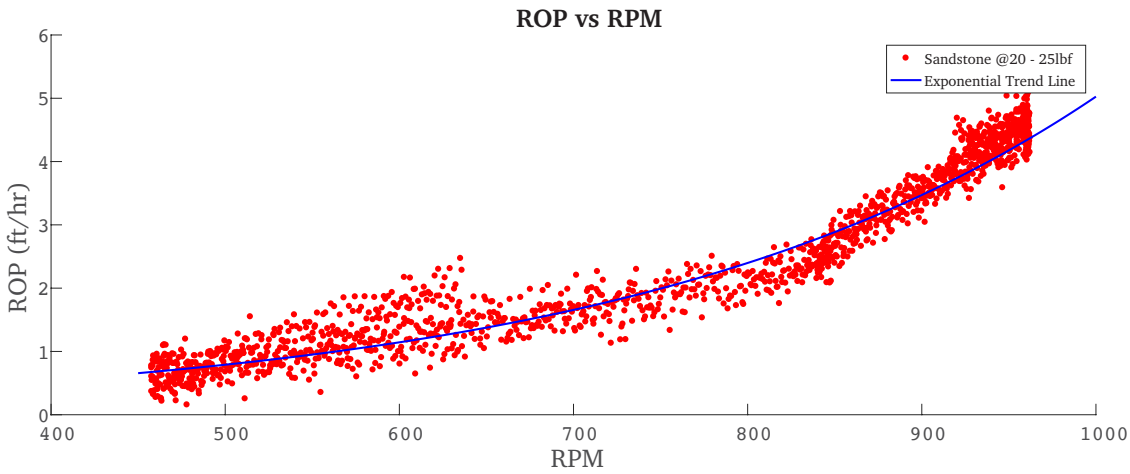

Figure 5.16: Rate of penetration vs revolutions per minute while drilling

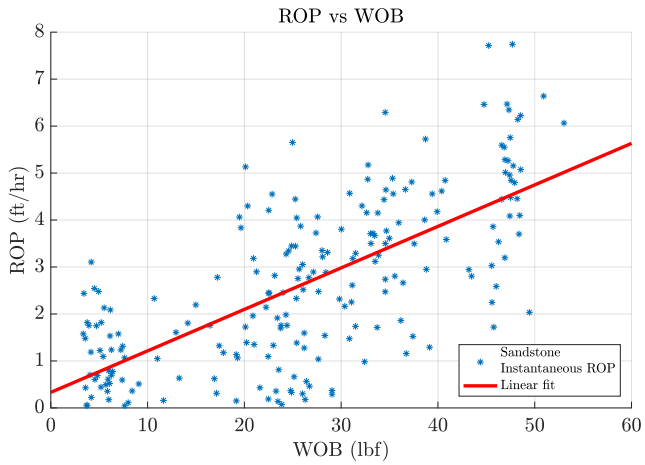

Figure 5.17: Rate of Penetration (ROP) vs Weight on Bit (WOB)

5.6 ROP Improvements

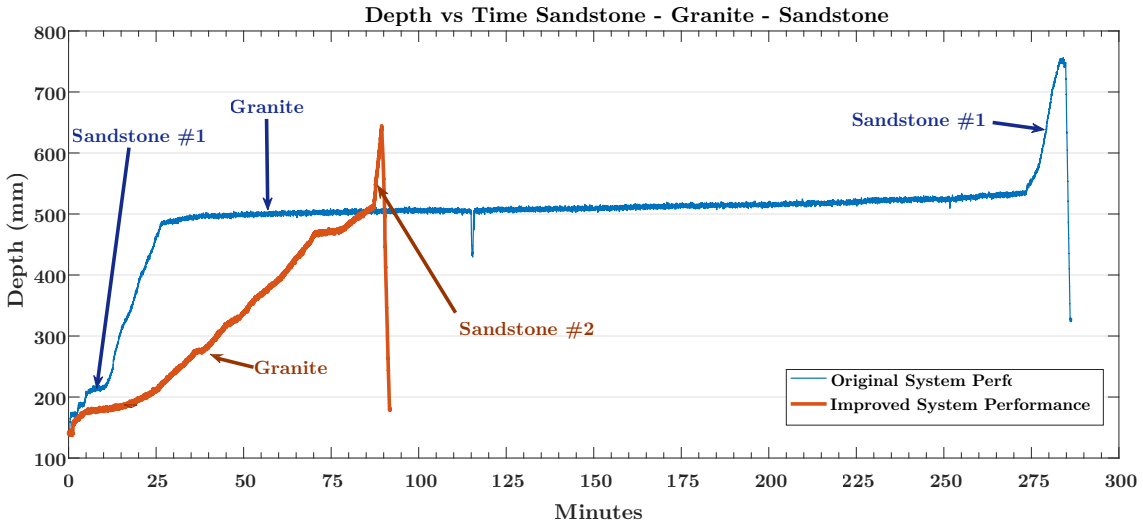

Figure 5.18: Rate of penetration improvement example while drilling sandstone and granite

This result is shown in Fig. 5.18 pictures a 320% Overall drilling performance gain in ROP while drilling the same interval the gain is more notable while drilling hard formations like granite.

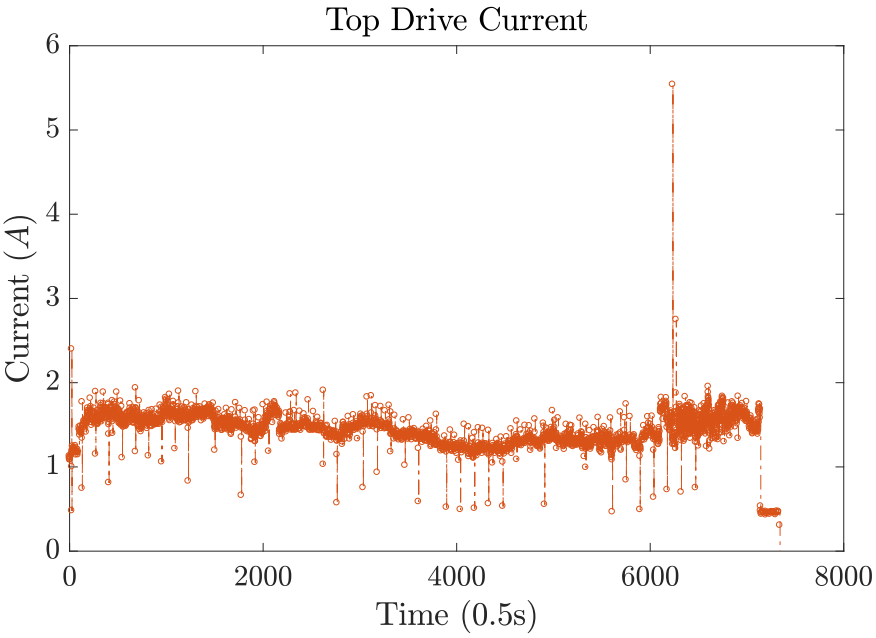

Figure 5.19: Top drive's current safety limit test. A current spike caused by a capsule failure triggered a safety response monitored by a stand alone micro-controller

6 CONCLUSIONS

A linear regression model was used to estimate the response for the rate of penetration (ROP) as a function of Revolutions per Minute and Weight on Bit to determine probable causes of potential dysfunctions while drilling. Using the known relationship that Mechanical Specific Energy changes depending on the overall drilling efficiency, which can be affected by bit dysfunctions happening in the wellbore. A step test method widely used in the drilling industry is used to estimate the efficiency of the drilling operation while optimizing its performance. Moreover, the causes of possible bit dysfunctions or inefficient drilling, conditions were determined using both, the mechanical specific energy (MSE) and the average rate of penetration (ROP) for a given formation interval and drilled section. The system operates, analyses and changes the necessary drilling parameters autonomously. Basic proportional-integral (PI) controllers work wonders for most drawworks or pumps drilling systems in the field but only if properly tuned. Most commercial data handling systems and auto drillers are not so smart today because they employ and rely on poorly conceived data and low sampling rates to generate an output that further increases the amount of error over the desired set-point without performing any higher level automated analysis like the one used in our experiments.

- Several rock formation samples were drilled using a 3/8”x 36” x 0.035” aluminum drill pipe with different PDC bits designs. The fragile pipe was used in order to increase the level of difficulty and control accuracy needed to avoid failure.
- Rock samples with different formations and dip angles were drilled to acquire and analyze data which helped to refine the control algorithm.
- Downhole readings were transmitted wirelessly and used on post analysis; future work involves determining a real-time feedback model controller based on downhole conditions.
- A closed loop gain scheduled PID controller was developed to consistently sample, filter and compute the draw works motor’s gain. Improving the WOB control performance under static conditions from a 150% to a 0.1% error response, and up to a 4% accuracy under dynamic drilling conditions.
- Time and frequency domain analysis of the drilling tests was carried, a clear signature was identified when bit whirl was occurring. A discrete Fast Fourier Transform was implemented on every data loop to detect and modify drilling variables accordingly.
- Up to a 320% Overall drilling performance gain in ROP was observed while drilling the same interval, even while drilling hard formations like granite as seen in Fig. 5.18.
- Whirl-mitigation and control improvements were also seen in borehole quality.

Patterns caused by excessive whirl were clearly identifiable. In contrast, a straight, much cleaner borehole was drilled when operating under automatic control.

6.1 Problems Encountered and Recommendations

Several wireless communication issues were faced while drilling due to an inadequate downhole antenna design; the metal capsule coupled with drilling fluid produced effects similar to a Faraday cage, which attenuated the downhole transmitted radio signals, dismissing the average sampling rate and increasing the amount of corrupted packages received by the client. Additionally, some downhole sensors were lost due to a poor liquid isolation within the downhole capsule. Furthermore, the derivative term in the PID controller was found to be troublesome due to the amount of noise in the signal, even after averaging and filtering. Lastly, vibrations induced electrical noise were seen even after placing dampening pads on the junction boxes.

Recommendations:

- Better data gathering, clustering, and analysis are needed to improve the optimization algorithm further. In order to implement more advanced controllers and high-level analysis such as unsupervised machine learning algorithms and self-adaptive controllers.
- The developed weight on bit, RPM and even pump controllers are accurate enough for any future drilling test. The focus should now go to the development of self-adaptive controllers and advanced machine learning methods based for example on the slope of depth of cut against the applied weight on bit or any other similar relationship for a given drilled interval.
- More manual control vs automatic control tests should be performed to assess the validity of the automated algorithm further.
- Common stick-slip mitigation systems are based on torsional speed changes, usually, without knowing the underlying physical causes, a per interval control algorithm such as the presented here could be proven advantageous in the field.

REFERENCES

[1] SPE, "SPE Drilling Systems Automation Technical Section site," 2016. Available: http://connect.spe.org/dsats/home

[2] R. Bromell, "Automation in Drilling," *Journal of Petroleum Technology*, 1967. Available: http://dx.doi.org/10.2118/1842-MS

[3] O. Bello, C. Teodoriu, T. Yaqoob, J. Oppelt, J. Holzmann, and A. Obiwanne, "Application of Artificial Intelligence Techniques in Drilling System Design and Operations: A State of the Art Review and Future Research Pathways," 2016. Available: http://dx.doi.org/10.2118/184320-MS

[4] J. Koomey, S. Berard, M. Sanchez, and H. Wong, "Implications of Historical Trends in the Electrical Efficiency of Computing," *IEEE Annals Hist. Comput.*, vol. 33, no. 3, pp. 46–54, mar 2011. Available: http://dx.doi.org/10.1109/MAHC.2010.28

[5] U. E. I. Administration, "Trends in U.S. Oil and Natural Gas Upstream Costs," *U.S. Energy Information Administration*, March 2016. Available: http://www.eia.gov/analysis/studies/drilling/pdf/upstream.pdf

[6] A. W. Eustes, "The Evolution of Automation in Drilling," *SPE Annual Technical Conference and Exhibition*, 2007. Available: http://dx.doi.org/10.2118/111125-MS

[7] H. W, "System of control for pill-well or other earth drilling," Mar. 29 1927, US Patent 1,622,784. Available: https://www.google.com/patents/US1622784

[8] H. Kverneland, A. Austefjord, A. Kyllingstad, and M. M. Moe, "Utilizing Permanent Magnet Motor Technology on Larger Drilling Equipment for Improved Safety and Better Control," 2006. Available: http://dx.doi.org/10.2118/99078-MS

[9] F. Young, "Computerized Drilling Control," *Journal of Petroleum Technology*, vol. 21, no. 04, pp. 483–496, apr 1969. Available: http://dx.doi.org/10.2118/2241-PA

[10] *The DDP-16, first commercial 16-bit minicomputer. Technical Manual 1968.* Available: http://www.ddp116.org/products/ddp116/ddp116.pdf

[11] *Atmel SMART ARM-based MCU 32-bit ARM-Cortex-M3 processor datasheet.* Available: https://goo.gl/R8goIt

[12] H. Fujita, M. Sato, N. Shiraishi, Y. Wakiya, and S. Tanaka, "Development of Automated Offshore Drilling System," 1990. Available: http://dx.doi.org/10.4043/6229-MS

[13] R. Stone and S. Tian, "Sometimes Neglected Hydraulic Parameters of Underbalanced and Managed-Pressure Drilling," 2008. Available: http://dx.doi.org/10.2118/114667-MS

[14] M. Mæland, "Managed Pressure Drilling: The Solaris Prospect-HPHT Exploration well," *Thesis*, 2013.

[15] D. E. et al., "Managed Pressure Drilling Erases the Lines," *Oilfield Review 23, no. 1.*, 2011. Available: https://www.slb.com/~/media/Files/resources/oilfield_review/ors11/spr11/managed_pressure.pdf

[16] Malyszkz, "Kelly Rig," 2011, [Online; accessed Aug 27, 2016]. Available: https://commons.wikimedia.org/wiki/File:Oil_Rig_NT8.svg

[17] D. Boutwell, "Top drive interlock," Feb. 8 2011, uS Patent 7,882,902. Available: https://www.google.com/patents/US7882902romr

[18] NOV, "Top Drive Solutions," Online, 2015. Available: https://www.nov.com/WorkArea/DownloadAsset.aspx?id=12017

[19] A. Kyllingstad and P. J. Nessjøen, "A New Stick-Slip Prevention System," 2009. Available: http://dx.doi.org/10.2118/119660-MS

[20] P. NESSJOEN and Å. KYLLINGSTAD, "Method and apparatus for reducing stick-slip," Jan. 23 2013, eP Patent App. EP20,120,188,975. Available: https://www.google.com/patents/EP2549055A2?cl=en

[21] A. Kyllingstad and P. J. Nessjoen, "Hardware-in-the-Loop Simulations Used as a Cost-Efficient Tool for Developing an Advanced Stick-Slip Prevention System," *IADC / SPE Drilling Conference and Exhibition*, 2010. Available: http://dx.doi.org/10.2118/128223-MS

[22] B. I. Saldivar Marquez, Martha Belem and H. Mounier, *Analysis and Control of Oilwell Drilling Vibrations : A Time-Delay Systems Approach*. ProQuest ebrary: Springer, 2015.

[23] S. K. Vogel and A. P. Creegan, "Case Study for Real Time Stick/Slip Mitigation to Improve Drilling Performance," 2016. Available: http://dx.doi.org/10.2118/178176-MS

[24] J. D. Macpherson, J. P. de Wardt, F. Florence, C. Chapman, M. Zamora, M. Laing, and F. Iversen, *Drilling-Systems Automation: Current State, Initiatives, and Potential Impact*. Society of Petroleum Engineers (SPE), dec 2013, vol. 28, no. 04. Available: http://dx.doi.org/10.2118/166263-PA

[25] G. LV, "Technology Outlook 2025: Energy," http://to2025.dnvgl.com/energy/, April 2016. Available: http://to2025.dnvgl.com/energy/

[26] BP, "BP Technology Outlook," Article, 2015. Available: http://www.bp.com/content/dam/bp/pdf/technology/bp-technology-outlook.pdf

[27] "RDS launches new robotic pipe handler and signs contract for first delivery," Online, July 2016. Available: http://www.rds.no/news-/rds-launches-new-robotic-pipe-handler-and-signs-contract-for-first-delivery

[28] J. Dunlop, R. Isangulov, W. D. Aldred, H. A. Sanchez, J. L. S. Flores, J. A. Herdoiza, J. Belaskie, and C. Luppensenti, "Increased Rate of Penetration Through Automation," 2011. Available: http://dx.doi.org/10.2118/139897-MS

[29] E. Abrahamsen, R. Bergerud, R. Kluge, and M. King, "Breakthrough in Drilling Automation Saves Rig Time and Safeguards Against Human Error," 2015. Available: http://dx.doi.org/10.2118/177825-MS

[30] W. R. Nelson, "Improving Safety of Deepwater Drilling Through Advanced Instrumentation, Diagnostics, and Automation for BOP Control Systems," 2016. Available: http://dx.doi.org/10.4043/27188-MS

[31] J. P. de Wardt, J. D. Macpherson, M. Zamora, B. Dow, S. Hbaieb, R. A. Macmillan, M. L. Laing, A. M. DiFiore, C. E. Inabinett, and M. W. Anderson, "Drilling Systems Automation Roadmap - The Means to Accelerate Adoption," 2015. Available: http://dx.doi.org/10.2118/173010-MS

[32] J. de Wardt, "Drilling Systems Automation (DSA) Roadmap - Phase II, Stage I full report," Online, October 2015. Available: http://www.iadc.org/wp-content/uploads/2014/04/John-de-Wardt-DSA-Roadmap-Oct-2015.pdf

[33] J. P. de Wardt, "Industry Analogies for Successful Implementation of Drilling-Systems Automation and Real-Time Operating Centers," *SPE Drilling & Completion*, vol. 29, no. 01, pp. 22–27, mar 2014. Available: http://dx.doi.org/10.2118/163412-PA

[34] J. P. de Wardt, M. Behounek, C. Chapman, and D. Putra, "Drilling Systems Automation - Preparing for the Big Jump Forward," 2013. Available: http://dx.doi.org/10.2118/163422-MS

[35] W. G. Lesso, M. Ignova, F. Zeineddine, J. M. Burks, and J. B. Welch, "Testing the Combination of High Frequency Surface and Downhole Drilling Mechanics and Dynamics Data Under a Variety of Drilling Conditions." 2011. Available: http://dx.doi.org/10.2118/140347-MS

[36] M. Behounek, "Operator's Group on Drilling Data Quality (OGDDQ)," *Sensors to Solutions SPE Workshop*, 1-3 September. 2015.

[37] N. Zenero, S. Koneti, and W. Schnieder, "Iron Roughneck Make Up Torque–Its Not What You Think!" 2016. Available: http://dx.doi.org/10.2118/178776-MS

[38] K. Ogata, *Modern Control Engineering*, 4th ed. Upper Saddle River, NJ, USA: Prentice Hall PTR, 2001.

[39] P. Pournazari, P. Ashok, E. van Oort, S. Unrau, and S. Lai, "Enhanced Kick Detection with Low-Cost Rig Sensors Through Automated Pattern Recognition and Real-Time Sensor Calibration," 2015. Available: http://dx.doi.org/10.2118/176790-MS

[40] H. P. Lohne, J. E. Gravdal, E. W. Dvergsnes, G. H. Nygaard, and E. H. Vefring, "Automatic Calibration of Real-Time Computer Models in Intelligent Drilling Control Systems - Results From a North Sea Field Trial," 2008. Available: http://dx.doi.org/10.2523/12707-MS

[41] E. Cayeux, B. Daireaux, E. W. Dvergsnes, and F. Florence, "Toward Drilling Automation: On the Necessity of Using Sensors That Relate to Physical Models," *SPE Drilling & Completion*, vol. 29, no. 02, pp. 236–255, jun 2014. Available: http://dx.doi.org/10.2118/163440-PA

[42] M. Behounek, "Operator's Group on Drilling Data Quality (OGDDQ)," in *Presentation, Sensors to Solutions SPE Workshop*. SPE DSATS, September. 2015.

[43] F. Florence, C. Chapman, J. Macpherson, and M. Cavanaugh, "Implementation of Drilling Systems Automation - Halifax Workshop Summary: Industry Standards, Business Models and Next Steps," 2015. Available: http://dx.doi.org/10.2118/174779-MS

[44] Ø. Andersen, "Using RealTime Data for Well Design Optimization, Not Just Drilling Optimization," 2016. Available: http://dx.doi.org/10.2118/181027-MS

[45] C. Klotz, P. R. Bond, I. Wassermann, and S. Priegnitz, "A New Mud Pulse Telemetry System for Enhanced MWD/LWD Applications," vol. l, 2008. Available: http://dx.doi.org/10.2118/112683-MS

[46] J. R. Bailey, C. C. Elsborg, R. W. James, P. E. Pastusek, M. T. Prim, and W. W. Watson, "Design Evolution of Drilling Tools to Mitigate Vibrations," 2013. Available: http://dx.doi.org/10.2118/163503-MS

[47] J. Fay, H. Fay, and A. Couturier, "Wired Pipes for a High-Data-Rate MWD System," 1992. Available: http://dx.doi.org/10.2118/24971-MS

[48] C. McCartney, S. Allen, M. Hernandez, D. MacFarlane, A. Baksh, and M. E. Reeves, "Step-Change Improvements With Wired-Pipe Telemetry," 2009. Available: http://dx.doi.org/10.2118/119570-MS

[49] A. Wilson, "Wired-Drillpipe Field Trials Reveal Potential Benefits Over Traditional Pipe," *Journal of Petroleum Technology*, vol. 65, no. 06, pp. 105–107, jun 2013. Available: http://dx.doi.org/10.2118/0613-0105-JPT

[50] M. J. Manning, J. D. Macpherson, D. E. Taylor, N. Baksh, C. Peveto, L. Farnsworth, and S. R. Lemke, "Wired Pipe-Enabled Logging While Drilling Applications," vol. d, 2008. Available: http://dx.doi.org/10.2523/12504-MS

[51] A. K. Vajargah, G. Sullivan, and E. van Oort, "Automated Fluid Rheology and ECD Management," 2016. Available: http://dx.doi.org/10.2118/180331-MS

[52] S. T. Edwards, C. J. Coley, N. A. Whitley, R. G. Keck, V. Ramnath, T. Foster, K. Coghill, and M. Honey, "A Summary Of Wired Drill Pipe (IntelliServ Networked Drillstring) Field Trials And Deployment In Bp," 2013. Available: http://dx.doi.org/10.2118/163560-MS

[53] R. A. Shishavan, C. Hubbell, H. D. Perez, J. D. Hedengren, D. S. Pixton, and A. P. Pink, "Multivariate Control for Managed-Pressure-Drilling Systems by Use of High-Speed Telemetry," *SPE Journal*, vol. 21, no. 02, pp. 459–470, apr 2016. Available: http://dx.doi.org/10.2118/170962-PA

[54] J. Brett, T. Warren, and D. Wait, "Field Experiences With Computer-Controlled Drilling," 1990. Available: http://dx.doi.org/10.2118/20107-MS

[55] Y. Lu, K. Morris, and S. Frechette, "Current Standards Landscape for Smart Manufacturing Systems," *U.S. National Institute of Standards and Technology*, feb 2016. Available: http://dx.doi.org/10.6028/NIST.IR.8107

[56] J. Yates and C. N. Murphy, "Coordinating International Standards: The Formation of the ISO," *SSRN Electronic Journal*, 2007. Available: http://dx.doi.org/10.2139/ssrn.962455

[57] M. R. ENDSLEY, "Level of automation effects on performance, situation awareness and workload in a dynamic control task," *Ergonomics*, vol. 42, no. 3, pp. 462–492, mar 1999. Available: http://dx.doi.org/10.1080/001401399185595

[58] A. Vera, "Integration of Human and Machine Intelligence: toward performance in non-deterministic environments," Presentation at the SPE DSATS/IADC ART Symposium: Human Integration with Automation and Machine Intelligence, 29 February 2016.

[59] R. Parasuraman, T. B. Sheridan, and C. D. Wickens, "A model for types and levels of human interaction with automation," *IEEE Transactions on systems, man, and cybernetics-Part A: Systems and Humans*, vol. 30, no. 3, pp. 286–297, 2000.

[60] J. Thorogood, W. D. Aldred, F. Florence, and F. Iversen, "Drilling Automation: Technologies, Terminology, and Parallels With Other Industries," *SPE Drilling & Completion*, vol. 25, no. 04, pp. 419–425, dec 2010. Available: http://dx.doi.org/10.2118/119884-PA

[61] N. Vishnumolakala, "Automatic Control and Optimization of Drilling Operations," Master's thesis, Texas A & M University., 2015. Available: http://hdl.handle.net/1969.1/156284.

[62] D. Society of Petroleum Engineers (SPE). (2016) The Drillbotics International Competition. Available: http://www.drillbotics.com

[63] V. A. Bavadiya, M. J. Aljubran, J. M. Kibe, S. M. Christy, H. N. Le, R. Ahmed, and F. Florence, "Design, Construction and Operation of an Automated Drilling Rig for the DSATS University Competition," 2015. Available: http://dx.doi.org/10.2118/174920-MS

[64] C. W. De Silva, *Sensors and Actuators: Engineering System Instrumentation*. CRC Press, 2015.

[65] F.Dupriest, "High Performance Drilling Practices," Texas A& M University, PETE Lecture., Spring 2016.

[66] R. Teale, "The concept of specific energy in rock drilling," in *International Journal of Rock Mechanics and Mining Sciences & Geomechanics Abstracts*, vol. 2, no. 1. Elsevier, 1965, pp. 57–73.

[67] F. E. Dupriest and W. L. Koederitz, "Maximizing Drill Rates with Real-Time Surveillance of Mechanical Specific Energy," 2005. Available: http://dx.doi.org/10.2118/92194-MS

[68] Pason EDR Mechanical Specific Energy Traces Online [http://www.pasonusa.com/rig-site/electronic-drilling-recorder-edr/], 2016.

[69] J. Moura, "What is signal processing?[President's Message]," *IEEE Signal Processing Magazine*, vol. 26, no. 6, pp. 6–6, 2009.

[70] S. M. Kuo, B. H. Lee, and W. Tian, *Real-time digital signal processing: fundamentals, implementations and applications*. John Wiley & Sons, 2013.

[71] E. Z. Losoya, "Data Acquisition System Diagram," WikiCommons [https://en.wikipedia.org/wiki/File:DigitalDAQv2.pdf], Oct. 2016.

[72] W. Kester, "Basic DAC Architectures I: String DACs and Thermometer (Fully Decoded) DACs," Analog Devices Online [http://www.analog.com/media/en/training-seminars/tutorials/MT-014.pdf] Accessed:, Oct. 2016.

[73] "National Instruments," Online http://www.ni.com/en-us.html.

[74] S. M. Han, H. Benaroya, and T. Wei, "Dynamics Of Transversely Vibrating Beams Using Four Engineering Theories," *Journal of Sound and Vibration*, vol. 225, no. 5, pp. 935 – 988, 1999. Available: http://www.sciencedirect.com/science/article/pii/S0022460X99922575

[75] S. S. Kolukula, "Natural Frequencies & Buckling Loads of Columns Using Finite Element Method," MATLAB Central File Exchange, Retrieved Oct 1, 2016., Sept. 2011.

[76] C. Krishnamoorthy, *Finite Element Analysis: Theory and Programming*. Tata McGraw-Hill, 1995. Available: https://books.google.com/books?id=M0cK4Tocx9MC

[77] E. Swanson, C. D. Powell, and S. Weissman, "A practical review of rotating machinery critical speeds and modes," *Sound and vibration*, vol. 39, no. 5, pp. 16–17, 2005.

[78] A. Farshidianfar and P. Oliazadeh, "Free Vibration Analysis of Circular Cylindrical Shells: Comparison of Different Shell Theories," *International Journal of Mechanics and Applications*, vol. 2, no. 5, pp. 74–80, dec 2012. Available: http://dx.doi.org/10.5923/j.mechanics.20120205.04

[79] API, "API Standard Paragraphs Rotordynamic Tutorial: Lateral Critical Speeds, Unbalance Response, Stability, Train Torsionals, and Rotor Balancing." *American Petroleum Institute*, August 2005, no. RP 684.

[80] L. Liung, *System identification-Theory for the user 2nd ed*, 1999.

[81] K. Alvin, A. Robertson, G. Reich, and K. Park, "Structural system identification: from reality to models," *Computers & structures*, vol. 81, no. 12, pp. 1149–1176, 2003.

[82] R. S. Sánchez-Peña, J. Q. Casín, and V. P. Cayuela, *Identification and control: the gap between theory and practice*. Springer Science & Business Media, 2007.

[83] K. C. Park, "OSE801 Engineering System Identification," Lecture Fall 2012, Retrieved Oct. 2016.

[84] Mathworks, "MATLAB," Available: https://goo.gl/yYI1z7, 2016.

[85] J. Leis, *Digital Signal Processing Using MATLAB for Students and Researchers*. Wiley, 2011. Available: https://books.google.com/books?id=Qtd-e1NtZVkC

[86] R. C. Dorf and R. H. Bishop, "Modern control systems," 1998.

[87] P. Pastusek, M. Owens, D. Barrette, V. Wilkins, A. Bolzan, J. Ryan, K. Akyabi, M. Reichle, and D. Pais, "Drill Rig Control Systems: Debugging, Tuning, and Long Term Needs," 2016. Available: http://dx.doi.org/10.2118/181415-MS

[88] A. Urquizo, "PID Controller Diagram," Online [https://commons.wikimedia.org/wiki/File:PID.svg], Accesed Oct. 2016.

[89] F. E. Dupriest, W. C. Elks, S. Ottesen, P. E. Pastusek, J. R. Zook, and C. R. Aphale, "Borehole-Quality Design and Practices To Maximize Drill-Rate Performance," *SPE Drilling & Completion*, vol. 26, no. 02, pp. 303–316, jun 2011. Available: http://dx.doi.org/10.2118/134580-PA